Adjoint Error Estimation for Elastohydrodynamic Lubrication

by

Daniel Edward Hart

Submitted in accordance with the requirements for the degree of Doctor of Philosophy.

The University of Leeds
School of Computing

January 2008

The candidate confirms that the work submitted is his own, except where work which has formed part of jointly-authored publications has been included. The contribution of the candidate and the other authors to this work has been explicitly indicated overleaf. The candidate confirms that appropriate credit has been given within the thesis where reference has been made to the work of others.

Declarations

Some parts of the work presented in this thesis have been published in the following articles which are reproduced in the appendix to this work.

Chapter 4 contains material also published as part of:

Goodyer, C E; Fairlie, R; Hart, D E; Berzins, M; Scales, L E. , "Calculation of friction in steady-state and transient EHL simulations" in: Lubrecht, A. and Dalmaz, G. (editors) Transient Processes in Tribology: Proceedings of the 30th Leeds-Lyon Symposium on Tribology Elsevier Science (2004) 579–590

This material is the candidate's work with the other authors contributing the rest of the paper.

Chapter 5 contains material also published as part of the following two papers:

Hart, D E; Goodyer, C E; Berzins, M; Jimack, P K; Scales, L E. , "Adjoint error estimation for EHL-like models", *International Journal for Numerical Methods in Fluids*, 47 (2005) 1069–1075

Hart, D E; Goodyer, C E; Berzins, M; Jimack, P K; Scales, L E. , "Adjoint error estimation and spatial adaptivity for EHL-like models", IUTAM Symposium on Elastohydrodynamics and Micro-elastohydrodynamics, Springer, (2006) 47–58

All material in these papers is the candidate's own work under the supervision of the co-authors.

Abstract

In this thesis, adjoint error estimation techniques are applied to complex elastohydrodynamic lubrication (EHL) problems. A functional is introduced, namely the friction, and justification is provided as to why this quantity, and hence its accuracy, is important. An iterative approach has been taken to develop understanding of the mechanisms at work. A series of successively complex cases are proposed, each with adjoint error estimation techniques applied to them. The first step is built up from a model free boundary problem, where the cavitation condition is captured correctly using a sliding mesh. The next problem tackled is a hydrodynamic problem, where non-linear viscosity and density are introduced. Finally, a full EHL line contact problem is introduced, where the surface deforms elastically under pressure. For each case presented, an estimate of a finer mesh friction, calculated from solutions obtained only on a coarse mesh, is corrected according to the adjoint error estimation technique. At each stage, care is taken to ensure that the error estimate is computed accurately when compared against the measured error in the friction.

Non-uniform meshes are introduced for the model free boundary problem. These non-uniform meshes are shown to give the same excellent predictions of the error as uniform meshes. Adaptive refinement is undertaken, with the mesh being refined using the adjoint error estimate. Results for this are presented for both the model free-boundary problem and the full EHL problem. This is shown to enable the accurate calculation of friction values using an order of magnitude fewer mesh points than with a uniform mesh.

Throughout this thesis, standard numerical techniques for calculating EHL solutions have been used. That is, regular mesh finite difference approximations have been used to discretise the problem, with multigrid used to efficiently solve the equations, and spatial adaptivity added through multigrid patches. The adjoint problems have been solved using standard linear algebra packages.

Acknowledgements

In alphabetical order, I would like to thank all four of my supervisors, Professor Martin Berzins, Dr. Christopher Goodyer, Professor Peter Jimack, and Professor Laurence Scales, whose help, advice, patience and support I have not only needed, but appreciated immensely. I'd also like to thank Dr. Roger Fairlie, Dr. Hang Leung, and Dr. Mark Walkley for much the same, sharing their knowledge, giving advice, and helping me to keep the faith. Since Eleanore Boullier has put up with the worse of the mood swings and erratic working hours, it's only fitting that she comes next on the bill, along with my mum, dad, and brother. Without their combined support, I'd never have made it even close to this far.

This work was funded through an EPSRC CASE studentship with Shell Global Solutions.

Contents

List of Figures

List of Tables

Chapter 1

Introduction

Friction is the resisting force which acts when one body moves over or through another. Clearly friction is essential whenever traction is required, for example to avoid slipping when walking. In this case, relative motion of the two surfaces is undesirable. However, a machine like a car has many moving parts which are frequently in relative motion as part of its normal operation. Any work which is required to overcome friction in order to achieve or maintain relative movement will be a waste. In addition to the energy wasted overcoming friction, a further source of waste is that caused by the wear of the surfaces which are in contact.

An excellent introduction to some of the different aspects of friction and wear can be found in [84]. An indication of the magnitude of the problem presented by friction and wear is given by Taylor [68], who says "According to some analysts, however, the direct costs of friction and wear can account for nearly 10% of the gross national product (GNP) in many industrial nations". The effective use of a lubricant, defined by [85] as "Any substance interposed between two surfaces in relative motion for the purpose of reducing the friction and/or the wear between them", is clearly key in mitigating this waste. Taylor goes on to say "Moreover, they estimate that cost savings of up to 1% of the GNP could be achieved simply by using the right lubricant for the job". Apart from the clear economic incentive to reduce the amount of this waste (the GDP of Britain in 2006 was approximately $1.9trillion), there is also the environmental impact. Bovington [7] says

"The main driving force behind changes in automotive design and in lubricant requirements is the need to reduce levels of gaseous emission levels, conserve hydrocarbon fuels and maintain emission levels over extended periods. Minimisation of lubricant-related friction and wear is a key contribution to the achievement of these targets."

There are four categories of lubrication problem: hydrodynamic, boundary, mixed and elastohydrodynamic (EHL). Hydrodynamic lubrication, or fluid film lubrication, is where there is a full fluid film that is maintained between the surfaces by the pressure generated though the relative motion of the surfaces. Boundary lubrication is the case where the film breaks down, potentially due to increased load or decreased speed, and there is significant contact between the surfaces. Mixed lubrication is a mixture of hydrodynamic and boundary lubrication, where the surfaces may contact, but not regularly. The main focus of this work is the fourth type of problem, EHL, however hydrodynamic lubrication is also introduced in Chapter 6 as an intermediate step between a model free-boundary problem in Chapter 5 and the full EHL problem of Chapter 7. Elastohydrodynamic lubrication (EHL) is the study of elastically deforming lubricated surfaces. This occurs in a wide range of situations, from so called "soft EHL" in human hip joints [40], to "hard EHL" in roller bearings etc. [63]. In this work, reference is largely made to the latter, where the lubricant is likely to be a mineral oil, with the lubricated surfaces typically made of steel. EHL occurs where the contacting elements are non-conformal (the area over which they would contact unlubricated is small) and the loads applied to the components are large compared to the elastic modulus of the contacting materials, generating very large pressures within the contact region. In such circumstances, one might reasonably expect the lubricant to be squeezed from within the contact area, leaving the surfaces unlubricated. However, due to the pressure exerted on the lubricant, its rheology changes significantly, and "becomes glass-like and behaves more like a solid than a liquid" [68]. This massive increase in viscosity and the adhesion of the lubricant to the surfaces ensures that a fluid film is maintained. This leaves the load to be borne by the elastic deformation of the steel components.

One factor which makes this lubrication regime so effective in preventing direct contact, and hence wear, of the surfaces is that the thickness of the lubricant film is remarkably insensitive to increases in the loading of the contact [66]. This is because it is easier to further deform the steel components than to compress the lubricant film.

The topic of this thesis is computational simulation of EHL with a view to estimating the friction in a contact. As explained in the next section, friction is an important quantity which can be computed from an EHL solution. This will require a discussion of both the

mathematical and numerical models and also the need to estimate the error in the friction calculation. This will be achieved through the use of a discrete adjoint approach [77].

The motivation for this work stems from a key goal of lubrication engineers: the design of lubricants and machine elements. In order to design anything, there must first be a goal which is the principal aim of the design, and in order to assess whether this goal, or even progress toward the goal, has been achieved, a way of measuring the success of a particular solution is necessary. As mentioned, one measure frequently calculated in EHL simulations is the friction within the contact. It is the calculation of this key quantity that will be the driving motivation throughout this thesis.

Chapter 2 provides further background and an introduction to EHL, starting with a brief history, the full numerical problem and an overview of popular solution methods employed, including multigrid and multi-level multi-integration. Chapter 3 follows a similar course, although this time introducing the use of a discrete adjoint for the purposes of error estimation. A brief history, and some background theory is provided, after which, Chapter 4 presents some work on the accurate calculation of the friction for a typical EHL problem. Chapter 5 then focuses on application of the adjoint ideas introduced in Chapter 3 to the solution of a model free boundary problem, which is designed to represent a much simplified EHL problem. Results are presented that allow for the free boundary to be included into the adjoint formulation, and hence the accuracy of the method in predicting the error in a derived quantity, similar in formulation to the friction introduced in Chapter 4, is investigated. Results are also shown for simplistic spatial mesh adaptation, based on the information gleaned from the adjoint error estimation process. This process is demonstrated to still give excellent predictions of the error in the friction. In Chapter 6, the problem being solved moves a step closer to the full EHL case. The addition of both non-linear viscosity and non-linear density moves the idea from a rather simple model free boundary problem to a model of the hydrodynamic lubrication regime. Two different formulations of the residual equations are investigated, leading to two different adjoint systems to be solved. Results for both are presented, with justification for the choice that is taken forward to the next chapter. Results are presented to show that the error predictions for both adjoint systems are good for this new non-linear problem. Chapter 7 introduces adjoint error estimation as applied to the full EHL problem. Results are presented for rolling and sliding friction on uniform meshes for a series of loads, all showing the excellent inter-grid friction error estimates. Following this, spatial mesh adaptation is introduced and used to get non-uniform mesh solutions for both the forward and adjoint problems. Again, results are presented showing the accuracy of the estimation of the fric-

tion error. The potential benefits of using this error estimate to drive local mesh adaptivity are also demonstrated. Finally, Chapter 8 discusses the results presented, and discusses areas where future research is likely to be fruitful.

Chapter 2

Background to EHL

In this chapter, elastohydrodynamic lubrication (EHL) is introduced. First the problem will be defined before moving on to provide an overview of some of the most significant other work in the area.

2.1 Governing equations

As the name suggests, the EHL equations are based upon a lubrication approximation applied to the Stokes flow of an incompressible fluid. This approximation serves to reduce the dimension of the model from three to two by assuming flow in the direction perpendicular to the contact is negligible. Two further simplifications will be made throughout this thesis: firstly, the dimension of the problem will be reduced further by only considering the line contact problem (in which end effects are assumed to be negligible); and secondly, only steady-state problems will be considered.

Before introducing the equations describing the problem the quantities involved, and the variables representing them, are established. In the full EHL point contact problem there are three independent variables. The distance through the computational domain is given by x, the distance perpendicular given by y, with the centre of the contact located at $(x,y) = 0$. The time the contact has been running for is given by t. Since the work in this

thesis is entirely concerned with steady-state line contact EHL, y and t will be introduced only briefly before being simplified out.

The pressure p is the hydrodynamic lubricant pressure, and is assumed to be constant through the thickness of the lubricant film, h. The lubricant viscosity is denoted by η and the lubricant density by ρ. The flows that are simulated represent a lubricating fluid squeezed between two contacting surfaces in relative motion to each other (see Figure 2.1). The speeds of the two surfaces are given by u_a and u_b, with the entrainment velocity, essentially the speed at which lubricant is pulled into the contact, $u_s = u_a + u_b$. There is also an applied load, perpendicular to the contact, which is denoted by L.

2.1.1 Reynolds equation

The main equation solved is the Reynolds equation (2.1). This can be derived from the Navier-Stokes equations using two simplifying steps. The first is to assume that the mass-inertia terms are negligible compared to the viscous terms. The second is to assume that the gap between the surfaces is narrow, and hence variation in the z-direction is negligible compared to the x and y directions. These steps eventually lead to equation (2.1). A more comprehensive derivation can be found in [61].

In dimensional form, for flow parallel to the x-axis, the Reynolds equation is given by

$$\frac{\partial}{\partial x}\left(\frac{\rho h^3}{\eta}\frac{\partial p}{\partial x}\right)+\frac{\partial}{\partial y}\left(\frac{\rho h^3}{\eta}\frac{\partial p}{\partial y}\right)-6u_s\frac{\partial(\rho h)}{\partial x}-12\frac{\partial(\rho h)}{\partial t}=0. \tag{2.1}$$

This describes a point contact situation, arising from contact between two spheres. For a 1D line contact, the bodies considered are infinitely long rollers, rather than spheres (see Figure 2.1). In this case there is no variation in the y-direction, due to symmetry. In addition, the edge effects can be ignored, so the second term from equation (2.1) can be eliminated. Further to this, all the work in this thesis refers to "steady state" EHL, where there are no transient effects. This means that the final term in equation (2.1), the time dependent "squeeze term" can be neglected to give equation (2.2):

$$\frac{\partial}{\partial x}\left(\frac{\rho h^3}{\eta}\frac{\partial p}{\partial x}\right)-6u_s\frac{\partial(\rho h)}{\partial x}=0. \tag{2.2}$$

For a given film thickness, fluid viscosity and density, this differential equation can be solved to give the hydrodynamic pressure in the fluid. The first term describes the Poiseuille flow, or laminar flow, of the lubricant. The second term is called the wedge term, or Cou-

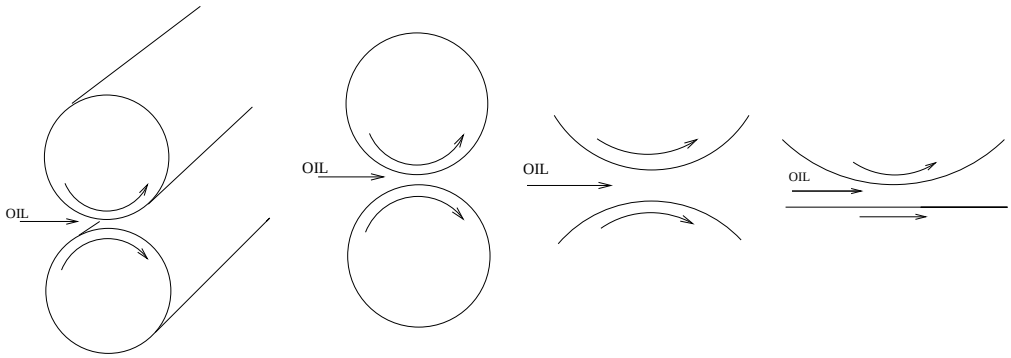

Figure 2.1: Simplification steps to get 1D line contact geometry

ette flow term, and these are the two different pressure generation mechanisms within the EHL contact.

EHL is a challenging problem to solve numerically. However, it is especially difficult to solve at high loads due to the huge change in character of the Reynolds equation through the contact. In the inlet region, the Poiseuille term dominates and hence the problem is largely elliptic in nature. However, moving into the contact region, the wedge term dominates making the problem more hyperbolic. Essentially, the dominant term changes from being the Poiseuille flow outside the contact area (diffusive terms), to the wedge term when inside the contact region (advective-like term). The reason for this is expanded upon in Section 2.4. It is the dominance of this term which makes the film thickness and pressure solutions highly sensitive to changes in either one or the other. With increasing loading, the pressure becomes increasingly sensitive to changes in the film thickness. This is because the lubricant becomes very dense and viscous, meaning an increasingly large increase in pressure is required to further reduce the film thickness.

2.1.2 Film thickness

The next equation described in the context of EHL is the film-thickness equation. This arises due to linear elastic deformation that occurs in the contacting elements due to the very high pressures that they experience at their surface. Mathematically, this deformation may be added to the undeformed contact geometry (assumed to be parabolic) to yield the film thickness:

$$h(x,p) = h_0 + \frac{x^2}{2R_x} + \frac{4}{\pi E'} \int_{-\infty}^{\infty} \ln \left| \frac{x-x'}{x_0} \right| p(x') \mathrm{d}x'. \tag{2.3}$$

The above equation is made up of three parts which between them, given a pressure profile p, specifies the fluid film thickness. The first term, h_0, gives the separation of the

undeformed surfaces. The second term gives the undeformed geometry of the contacts, and is derived according to Figure 2.1. The starting point is with two infinitely long rollers contacting along a line (hence line contact). Due to symmetry and the ability to avoid edge effects, these infinitely long 3D cylinders can be reduced to two 2D discs. Both of the discs can then be approximated accurately as parabolas, with radius of curvature R_{x1} and R_{x2}. This approximation is possible due to the fact that the film thickness and the contact width are both small compared to the radius of curvature in the contact region. Beginning with the equation for a circle centred on the z-axis a distance R above the x-axis

$$(z-R)^2+x^2=R^2,$$

expanding the first term yields

$$z^2-2Rz+R^2+x^2=R^2.$$

After cancelling the R^2 terms, it is noted that since z is small, the z^2 term may be neglected and so, re-arranging for z, the expression becomes

$$z=\frac{x^2}{2R}.$$

Finally, the two parabolas, with radii of curvature R_{x1} and R_{x2}, can be reduced to a plane and a parabola of equivalent radius R_x using

$$\frac{1}{R_x}=\frac{1}{R_{x1}}+\frac{1}{R_{x2}}.$$

This reduces the problem to one-dimension. The final term in equation (2.3) defines the elastic deformation at a given point in space due to a pressure distribution, given by linear elastic theory. More details of this can be found in [36, 41]. This final part is one of the reasons that makes this problem especially difficult to solve numerically, since even pressure applied at some distance can have a significant effect on the local deformation. Altogether this gives the deformed geometry of the contact, and hence the lubricant film thickness.

2.1.3 Force balance

The final, and most straightforward, of the EHL equations is the force balance equation:

$$\int_{-\infty}^{\infty} p(x)\mathrm{d}x = L. \tag{2.4}$$

This simply states that the total pressure generated in the fluid film must equal the applied load, L. Whilst it not immediately obvious, it is this equation which is used in the numerical simulation to determine the correct separation of the bodies (H_0). This connection is described in Section 2.4.2.

2.1.4 Viscosity

The lubricating film is non-Newtonian and consequently its viscosity is highly dependent upon the pressure. Two different models for viscosity are considered in this work but in both cases the viscosity varies exponentially with increasing pressure. This ultimately results in a glass-like behaviour of the lubricant in the high pressure contact region [1,89]. The two models that are considered in this work are the Roelands equation [62]

$$\eta(p) = \eta_0 e^{\left(\frac{\alpha p_0}{z}\left[-1+\left(1+\frac{p}{p_0}\right)^z\right]\right)}, \tag{2.5}$$

and the Barus equation [2]

$$\eta(p) = \eta_0 e^{\alpha p}, \tag{2.6}$$

where p_0 is the pressure viscosity coefficient, z is the viscosity index, α is the pressure-viscosity index and η_0 is the viscosity at ambient pressure. Although we initially consider the algebraically simpler form (2.6), it is fair to say that (2.5) is more widely adopted in practice (and is considered later in this work). This is because, whilst the viscosity clearly increases exponentially for both models, when the pressure gets very large a simple exponential relationship, such as that given by the Barus equation, tends to significantly overestimate the viscosity.

2.1.5 Density

Finally, it is necessary to introduce a density-pressure relationship to the system of equations. The density, equation (2.7), is based on empirical observation. The model used

here is the standard model of Dowson and Higginson [17], and is generally of less importance (in the sense that the model is less sensitive to the precise choice of density-pressure relation) than the more highly non-linear viscosity

$$\rho(p) = \rho_0 \frac{0.59 \times 10^9 + 1.34p}{0.59 \times 10^9 + p}, \tag{2.7}$$

where ρ_0 is the density at ambient pressure.

2.2 Non-dimensionalisation

In this section, we provide a description of the standard approach that is used for the non-dimensionalisation of the EHL equations. This is followed by a summary of the non-dimensional equations themselves. Non-dimensionalisation is simply the process of removing the dimensionality from the variables within the equations involved. It is useful in that different physical problems may have the same underlying mathematical formulation. This means that non-dimensional parameters which have similar effects on the solution can be grouped together, reducing the dimension of the parameter space. For example, if doubling the surface speed has the same effect on an EHL solution as halving the load, there is no need to solve two separate EHL cases.

At the same time that non-dimensionalisation occurs, the variables are often scaled to have a value somewhere around 1. This is achieved by dividing through by characteristic solution values. By doing this, rounding errors in the ensuing numerical calculations can be reduced.

The non-dimensionalisation used here is based on Hertz's theory for a dry contact [36]. Introducing the maximum Hertzian pressure, p_h, as

$$p_h = \frac{2L}{\pi b} \tag{2.8}$$

where b is the Hertzian radius, describing the half width of a contact with reduced modulus of elasticity E', given by

$$b = \sqrt{\frac{8LR_x}{\pi E'}}, \tag{2.9}$$

and the non-dimensional variables

$$X = \frac{x}{b}, \qquad P = \frac{p}{p_h}, \qquad H = \frac{hR_x}{b^2} \tag{2.10}$$

$$\overline{\eta} = \frac{\eta}{\eta_0}, \qquad \overline{\rho} = \frac{\rho}{\rho_0}, \tag{2.11}$$

it is possible to rewrite equations (2.2) to (2.7) as the following non-dimensional equation set. After substitution of the above variables, and with appropriate use of the chain rule, the Reynolds equation can be rewritten as

$$\frac{\partial}{\partial X}\left(\varepsilon\frac{\partial P}{\partial X}\right) - \frac{\partial(\overline{\rho}H)}{\partial X} = 0 \tag{2.12}$$

where

$$\varepsilon = \frac{\overline{\rho}H^3}{\overline{\eta}\lambda}$$

and

$$\lambda = \frac{6\eta_0 u_s R_x^2}{b^3 p_h}$$

are both non-dimensional parameters. Similarly, the film thickness equation can be written as

$$H(X,P) = H_0 + \frac{X^2}{2} + \frac{1}{\pi}\int_{-\infty}^{\infty} \ln\left|X - X'\right| P(X')\mathrm{d}X', \tag{2.13}$$

with the force balance equation given by

$$\int_{-\infty}^{\infty} P(X)dX = \frac{\pi}{2}. \tag{2.14}$$

The remaining constitutive equations for viscosity and density become

$$\overline{\eta}(P) = e^{\left(\frac{\alpha p_0}{z}\left[-1+\left(1+\frac{Pp_h}{p_0}\right)^z\right]\right)} \tag{2.15}$$

for Roelands viscosity, with Barus viscosity as

$$\overline{\eta} = e^{\overline{\alpha}P}, \tag{2.16}$$

and density as

$$\overline{\rho}(P) = \frac{0.59\times10^9 + 1.34Pp_h}{0.59\times10^9 + Pp_h}. \tag{2.17}$$

2.3 Discretisation

Finite difference approximations have long been used and are generally well understood. They can be easily derived through Taylor series expansions, and form a straightforward way of discretising differential equations. For more information on finite difference methods, a comprehensive text is [67]. Here, the basic stencils used in this work are derived. Before this, however, we note that the first step in the discretisation process is to replace the infinite domain by a finite domain $[X_{in}, X_c]$. Here, X_{in} is taken to be far upstream of the contact and X_c is chosen to be downstream of the contact. Further discussion of the choice of X_c will appear later in the thesis. We can now discretise the spatial domain with a uniform grid of n points with mesh size Δx

The Taylor series expansion of a function $f(x-\Delta x)$ is given by

$$f(x-\Delta x) = f(x) - \Delta x f'(x) + \frac{(\Delta x)^2}{2!} f''(x) - \ldots. \tag{2.18}$$

Combining all terms in the series after the second into one error term, where ξ is some unknown point in $[x-\Delta x, x]$, yields

$$f(x-\Delta x) = f(x) - \Delta x f'(x) + \frac{(\Delta x)^2}{2!} f''(\xi) \tag{2.19}$$

which is easily re-arranged to form the first order backwards difference formula

$$f'(x) = \frac{f(x) - f(x-\Delta x)}{\Delta x} + \frac{\Delta x}{2!} f''(\xi). \tag{2.20}$$

The last term, which is not used in the calculations, is the error term due to the truncation of the series, and shows this approximation to be $O(\Delta x)$, or first order accurate.

To derive the second order backwards difference, the two expansions required are

$$f(x-\Delta x) = f(x) - \Delta x f'(x) + \frac{(\Delta x)^2}{2!} f''(x) - \frac{(\Delta x)^3}{3!} f'''(\xi_1) \tag{2.21}$$

and

$$f(x-2\Delta x) = f(x) - 2\Delta x f'(x) + \frac{(2\Delta x)^2}{2!} f''(x) - \frac{(2\Delta x)^3}{3!} f'''(\xi_2), \tag{2.22}$$

where $\xi_1 \in [x-\Delta x, x]$ and $\xi_2 \in [x-2\Delta x, x]$. Subtracting four times equation (2.21) from

equation (2.22) gives

$$f(x-2\Delta x)-4f(x-\Delta x)=-3f(x)+2\Delta x f'(x)-4\frac{(\Delta x)^3}{3!}f'''(\xi_1)-\frac{(2\Delta x)^3}{3!}f'''(\xi_2). \tag{2.23}$$

Rearranging for $f'(x)$ yields the second order backwards formula, shown as

$$f'(x)=\frac{3f(x)-4f(x-\Delta x)+f(x-2\Delta x)}{2\Delta x}+(\Delta x)^2\left(4\frac{1}{3!}f'''(\xi_1)+\frac{8}{3!}f'''(\xi_2)\right). \tag{2.24}$$

In this case the error term is multiplied by $(\Delta x)^2$, and so the formula is second order accurate.

Having derived these two backwards difference formulae, it is possible to decide on one with which to discretise the wedge term in the Reynolds equation. For the work presented throughout this thesis, the first order backwards difference will be used. The main reason for this choice is primarily historical, since the first order difference has been demonstrated to be stable under a far greater range of problem cases than the second order one [55], leading to a more robust solver. Although transient cases are not discussed, were there to be a case where the direction of flow reversed, the discretisation would need to change to a forward difference formula. The second order backward difference is used in the cavitation boundary derivative used from Chapter 5 onwards. This is because, with the right-hand boundary fixed with $P=0$, the first order backwards difference would require that the first grid point inside the boundary would also be zero in order that the derivative be zero, effectively fixing the cavitation point in the wrong place.

Finally, the second order central difference approximation to f'' is derived as follows. First, the Taylor series is expanded up the 5th term for both forward

$$f(x+\Delta x)=f(x)+\Delta x f'(x)+\frac{(\Delta x)^2}{2!}f''(x)+\frac{(\Delta x)^3}{3!}f'''(x)+\frac{(\Delta x)^4}{4!}f^{(4)}(\xi_3), \tag{2.25}$$

and backward differences

$$f(x-\Delta x)=f(x)-\Delta x f'(x)+\frac{(\Delta x)^2}{2!}f''(x)-\frac{(\Delta x)^3}{3!}f'''(x)+\frac{(\Delta x)^4}{4!}f^{(4)}(\xi_4), \tag{2.26}$$

where $\xi_3\in[x-2\Delta x,x]$ and $\xi_4\in[x-2\Delta x,x]$. Adding equations (2.25) and (2.26) gives

$$f(x+\Delta x)+f(x-\Delta x)=2f(x)+2\frac{(\Delta x)^2}{2!}f''(x)+\frac{(\Delta x)^4}{4!}f^{(4)}(\xi_3)+\frac{(\Delta x)^4}{4!}f^{(4)}(\xi_4). \tag{2.27}$$

This can then be rearranged to give

$$f''(x) = \frac{f(x+\Delta x) - 2f(x) + f(x-\Delta x)}{(\Delta x)^2} + (\Delta x)^2 \left(\frac{1}{4!} f^{(4)}(\xi_3) + \frac{1}{4!} f^{(4)}(\xi_4) \right). \quad (2.28)$$

Looking at the multiplier in the error term, this is clearly also second order accurate. This stencil is used to discretise the second order Poiseuille term in the Reynolds equation.

Discretisation of the film thickness and the force balance equations is relatively straightforward, being based on standard quadrature formulae. For example, (2.13) is approximated at a grid point *i* by

$$H_i = H_0 + \frac{X_i^2}{2} + \frac{1}{\pi} \sum_{j=0}^{n-1} K_{ij} P_j. \quad (2.29)$$

When it is assumed that a finite difference mesh of n equally spaced points is used, the dense matrix K may be precomputed.

2.4 Solution method

In this section, the solution procedure used within the 'Carmehl' [71] industrial EHL solver is described. This is the code that is used to generate the forward solutions for Chapters 4 and 7. A modified version is also used to generate the solutions in Chapter 6. A detailed overview is therefore justified. For more specific details than contained here, the reader should consult [26].

2.4.1 Single grid solution

The basic iterative solution procedure on a single grid is outlined first. For given solution profiles of H, $\overline{\eta}$, and $\overline{\rho}$, and a latest solution profile for pressure, P, the first step is to solve the Reynolds equation. This is calculated using several iterations of an approximate Newton solve:

$$\tilde{J}\Delta P = -R. \quad (2.30)$$

where $\tilde{J}$ is the approximate Jacobian, and ΔP is the correction to the pressure. In this work a penta-diagonal Jacobian approximation is sufficient.

The Nurgat Jacobi line scheme [55], which is used throughout in solving for this

equation, distinguishes between the contact and non-contact region of the solution. It does this based on the size of ε, where $\varepsilon = \frac{H^3\overline{\rho}}{\lambda\overline{\eta}}$ as in the above formulation of Reynolds equation (2.12). Outside the contact region, where H is large and $\overline{\eta}$ is small, ε is large. Conversely, moving into the contact region, H becomes small and $\overline{\eta}$ becomes very large, so ε becomes very small. This is the reason why the Reynolds equation behaves so differently in the two different regions, as the equation is dominated by the different terms. This is reflected in the solver since, after each Newton solve, the correction calculated is used to update the pressure profile only at those points outside the contact region. The points inside the contact region are then updated after the last solve. In each case, an under-relaxation factor is applied. In this work, typically values of under-relaxation used are 0.15 for the points outside the contact, and 0.1 for those inside the contact region.

A number of iterations of this procedure would result in the exact solution for P for the values of H, $\overline{\eta}$, and $\overline{\rho}$ given. However, since these values themselves are all dependent on P, there would be little point in solving P exactly at this stage. So following each pressure update, H, η, and ρ are recalculated. This process is repeated until the pressure solved for, along with the values of H, $\overline{\eta}$, and $\overline{\rho}$, calculated from it, give sufficiently small values for the Reynolds residual equations. In this case, that is after the RMS (root mean square) value of the residuals is below 10^{-10} in size.

In the context of describing the FAS Multigrid algorithm below, this whole process from Newton-Iteration through to recalculation of H, $\overline{\eta}$, and $\overline{\rho}$ and hence the Reynolds residuals will be referred to as one “smooth”, and is summarised in Figure 2.2.

2.4.2 Force balance (H_0) update

The final addition to the single grid solution process is the way in which the force balance equation is satisfied. During the process of solving for P, H, $\overline{\eta}$, and $\overline{\rho}$ outlined above, there is no guarantee that the integral of the pressure over the computational domain will remain equal to the load (i.e. force balance may be violated). For this reason, it is necessary to alter H_0 (the separation of the undeformed solids) during the course of the process so that once a solution is found, it also satisfies the force balance equation. By integrating over the domain, it is possible to ascertain how close to the correct non-dimensional load of $\frac{\pi}{2}$ the sum of pressures is. By recognising that increasing the separation of the surfaces decreases the total pressure in the domain, it follows that if the sum of pressures is too large, the surfaces are too close and so H_0 must be made larger. Equally, if the sum is too small, the surfaces are too far apart and H_0 should be made smaller. However, since all

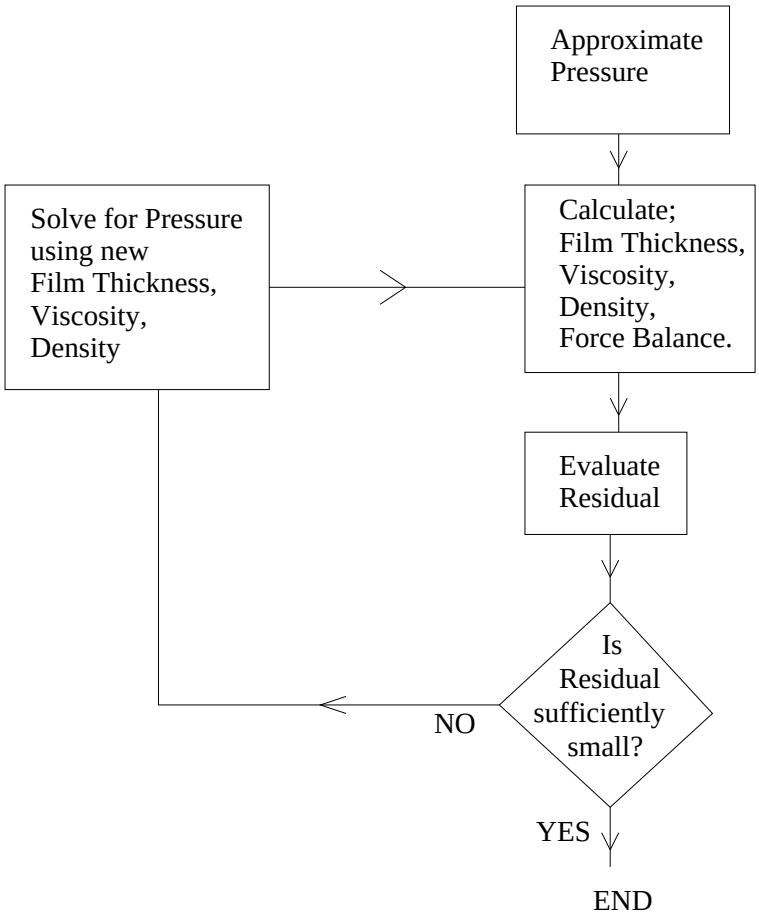

Figure 2.2: High level EHL numerical solution algorithm

of the H values are affected by a change in H_0, which then has a corresponding effect on the P solution, there is no simple relationship which describes the relationship between H_0 and the sum of pressures. Hence, the standard update formula used to achieve this is given by

$$H_0 \leftarrow H_0 - \omega \left(\frac{\pi}{2} - \sum_{i=0}^{n-2} \frac{P_i + P_{i+1}}{2} \Delta X \right), \tag{2.31}$$

where ω is some under-relaxation factor (typically somewhere between 0.05 and 0.2 in this work). This is not necessarily updated every time that a smooth is performed.

2.4.3 FAS multigrid

In order to speed up the convergence of the Reynolds solution, multigrid is used. Multigrid is so-called because of the sequence of meshes the solution is solved on. The basic principle is that errors in a solution can be removed on a series of grids. The errors of comparable wavelength to a particular grid can be efficiently reduced before restriction to a coarser mesh, where the errors of a different wavelength can be reduced. This requires a smoother which can efficiently reduce the components of the error which are high frequency compared to the resolution of the mesh. The first application of multigrid to EHL was by Lubrecht [50].

Standard texts by Briggs [11] and Trottenberg *et al.* [70] provide full technical details. Multigrid as applied to EHL is well presented in both of [26, 83], but a brief overview is presented below.

In this work we use FAS (Full Approximation Scheme) multigrid because this is able to be applied to non-linear systems. The basic idea is to modify the right-hand side of the equation system on the coarser grid to be equivalent to that solved for on the finer grid. In this example, only two grids will be used, but it is straightforward to extend to multiple levels. Once the actual system of solutions has been explained, the restriction and prolongation operators used in this work (I_h^H and I_H^h) will be prescribed.

Consider a non-linear system

$$Lu = f, \tag{2.32}$$

where L is a non-linear operator, f is the right-hand side function, and u is the solution to be approximated. For a fine mesh with spacing h, the discrete system can be written as

$$L^h u^h = f^h. \tag{2.33}$$

The residual equation can then be written as

$$r^h = f^h - L^h \tilde{u}^h, \tag{2.34}$$

where $\tilde{u}^h$ is an approximate solution obtained by a small number of smooths using the selected iterative scheme. By defining the error equation to be

$$e^h = u^h - \tilde{u}^h, \tag{2.35}$$

and after re-arranging (2.34) for f^h, substitution into (2.33) of (2.34) and (2.35) yields

$$L^h(e^h + \tilde{u}^h) = L^h \tilde{u}^h + r^h. \tag{2.36}$$

On the coarse grid, with mesh spacing H, where $H = 2h$, this can be approximated by

$$L^H \tilde{u}^H = f^H \tag{2.37}$$

where $\tilde{u}^H$ is the coarse grid solution variable given by

$$\tilde{u}^H = I_h^H(e^h + \tilde{u}^h) = e^H + I_h^H(\tilde{u}^h). \tag{2.38}$$

The FAS right-hand side is

$$f^H = I_h^H(L^h \tilde{u}^h + r^h) = I_h^H(L^h \tilde{u}^h) + I_h^H(r^h). \tag{2.39}$$

It can be shown [83] that both L^H and $I_h^H(L^h)$ can be used as an approximation to the fine grid system, and since it is more straightforward to form the non-linear operator on the coarse grid, that is what is used. The FAS right-hand side becomes

$$f^H = L^H(I_h^H(\tilde{u}^h)) + I_h^H(r^h). \tag{2.40}$$

There are now two clear parts to this right-hand side. The first term, $L^H(I_h^H(\tilde{u}^h))$, is the part which adjusts the coarse grid system to be equivalent to the fine grid system. This is really just the coarse grid right-hand side, plus the residual gained when putting the fine grid solution into the coarse grid system. The second term $I_h^H(r^h)$ is the residual from the fine grid after restriction to the coarse mesh. So the other way to think of the FAS right-hand side is as the coarse grid right-hand side function, adjusted by two different residuals. These are the coarsened fine grid residuals, and the coarse grid residuals computed from

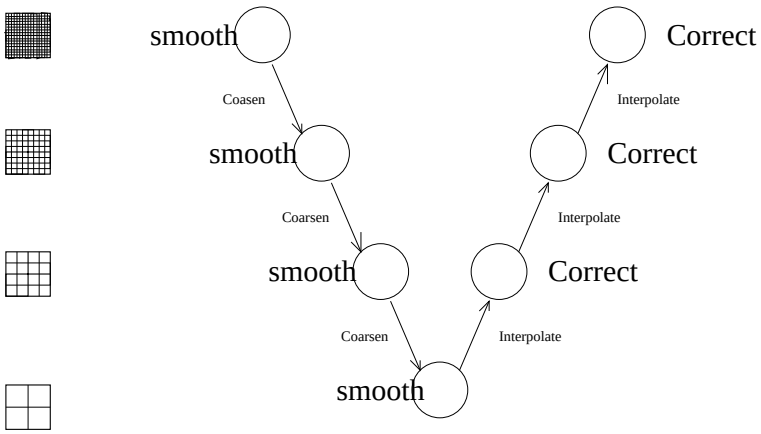

Figure 2.3: Schematic of a multigrid V-cycle

the coarsened fine grid solution.

Having formulated this system, it can be solved more cheaply than the fine grid version. In practice, this system would be restricted to a yet coarser mesh for recursive solution down to a coarsest level.

Once the coarse grid solution is solved, the coarse grid variable $\tilde{u}^H$ can then be used to update the fine grid solution $\tilde{u}^h$ according to

$$\tilde{u}^h = \tilde{u}^h + I_H^h(\tilde{u}^H - I_h^H \tilde{u}^h). \tag{2.41}$$

After this, the solution is again smoothed on the fine grid.

Having described the solution process, a note on the inter-grid transfer operators is required. For reasons of stability and robustness, the restriction operator in this work uses injection. That is, when coarsening a solution from a fine grid to a coarse one, the coincident points on the fine grid are used to give the values on the coarse grid. In some circumstances, injection may not represent fine grid errors accurately on the coarse grid, leading to degraded solution convergence, but that is not an issue here since the error is generally well smoothed on the fine grid before restriction takes place. The prolongation used is equivalent to linear interpolation. This may introduce a small amount of high frequency errors, but again, this is not an issue as high frequency errors can be removed efficiently on the fine mesh. A more detailed discussion on inter-grid transfer operators can be found in [70]. The whole process is summarised for one V-cycle in Figure 2.3.

In Chapter 7, the goal is to solve EHL problems adaptively. This requires the problem to be discretised on a non-uniform grid. Fortunately, the MLAT scheme [70] can be used

in conjunction with FAS multigrid. This is where the problem is posed on a series of uniform meshes, and solved using multigrid, but "patches" of refinement are used where additional refinement is required. The solution is computed as normal on the coarse grid, before the region inside the patch is interpolated to the fine grid. The end points of this patch are then set to be Dirichlet boundary points on the finest mesh, and the solution can continue. As with normal multigrid, this would typically happen over a number of levels with patches of different sizes on different levels.

There are various types of multigrid which are more applicable in certain other situations. Linear multigrid is a technique for solving a system of linear equations. On each level of the multigrid solve, it is the error equation which is solved for, rather than the solution adjusted for the difference between the grids. This is only possible because of the linear nature of the problem [11].

Algebraic multigrid uses a series of coarser approximations to the original system matrix, but doesn't require an underlying hierarchy of grids [11], whereas P-multigrid uses polynomials of different orders to achieve faster convergence [24].

2.4.4 Multilevel multi-integration

Multilevel multi-integration (MLMI) [8] is a powerful tool for reducing the time taken during the film thickness calculation. With the deformation at every point influenced by the pressure at all points, the calculation time will clearly be $O(n^2)$ for a grid of n points, since equation (2.29) will be calculated n times and requires $O(n)$ operations. MLMI exploits the smooth nature of the deformation kernel away from the central singularity, by summing for the local deformation first on the coarsest grid, and then correcting in local patches near the singularity on the finer grids. This reduces the complexity to $O(n \log n)$, a huge saving.

By starting off on the finest grid, the pressure values are restricted using high order operators onto coarser and coarser grids, until the coarsest level is reached. There, the local deformation is calculated using the whole mesh. The local deformation values for each point on the grid are then prolonged back up to the next coarsest grid using high order interpolation. Here, the effect of the pressures within a few mesh points of the singularity $X' = X$ is calculated for the more accurate kernel on that level. Since that small region has influenced the deflection twice, the coarse grid effects are removed, on that area only, and the process is repeated until the finest level is reached.

This effectively means that the summation is performed on a different adaptive mesh for each point, even though the underlying structure is actually a uniform mesh everywhere. It should be noted however that we do not make use of MLMI in this work since it requires uniform refinement of the grids at each level. Since our ultimate goal (achieved in Chapter 7) is to apply local mesh refinement for the EHL problem, developing a new variant of MLMI for such grids is beyond the scope of this work.

2.5 A brief history of EHL modelling

EHL was born out of the realisation that both a viscosity-pressure dependence in the lubricant and an elastic deformation of the contacting body are necessary to explain satisfactorily the lubricant film thickness of certain non-conforming contacts. In other words, before then, hydrodynamic lubrication had been augmented with both effects individually, and while both increased the film thickness, neither increased it sufficiently to be validated by the practically observed life of bearings. There have been several excellent reviews into the history of EHL, including [15], [16], and [39], and it would serve little purpose to recreate them in full. However a brief overview of particular areas of relevance to this thesis follows.

2.5.1 Overview of numerical methods for EHL problems

Since the first numerical solution of both the elastic equation and the Reynolds equation by Petrusevich [57] in 1951, a number of different numerical methods have been developed for the solution of EHL. The first extensive set of solutions was calculated by Dowson and Higginson [17], using an inverse approach. This inverse approach involves solving the Reynolds equation for the film thickness, in addition to using the more standard film thickness equation, (2.3), and the difference between these film thicknesses is used to correct the pressure. This approach allows for the solution of extremely highly loaded cases, but is unstable at low loads.

The standard way of solving EHL numerically is detailed by Venner and Lubrecht [83], and summarised here in Section 2.4. That is, using finite difference discretisations on regular uniform meshes. This is accelerated by the use of the multilevel techniques of multigrid and multilevel multi-integration.

There is also a need for a different solver to be used outside of the contact region [80]. In the contact region Venner uses a distributive relaxation scheme [80], whereas in this work the Jacobi line scheme of Nurgat [54] is used.

In the following subsections a more detailed survey of methods used for spatial mesh adaptation is given, along with methods for dealing with the unknown cavitation position, and a brief discussion of surface roughness.

2.5.2 Adaptive EHL

Adaptivity in numerical computation is not a new idea. The desire to minimise the computational load and/or maximise numerical accuracy of a solution is common across many disciplines. EHL is no exception, although efforts have been somewhat less than in other areas of engineering. With the majority of numerical solutions historically based on finite difference discretisations, spatial adaptivity is very much the exception rather than the norm. The first adaptive finite difference solution was courtesy of [49], shortly followed by [4] and [80]. The second of these is the more comprehensive, with an alternative discretisation and automatic refinement algorithm. A lack of citation of this paper over the years is likely due to the unfashionable choice of solution method, the Newton iteration, and the incompressible nature of the formulation. All three were restricted to smooth EHL. More recently, work on adaptive grids has been conducted by Goodyer [26, 30], including adaptive time-stepping, but in the words of the author "...it has been seen that there are powerful numerical tools available, such as grid adaptation, which require further exploration and deeper understanding with regards to their application to EHL modelling."

Finite element solutions, which perhaps lend themselves to spatially adaptive solutions more naturally than their finite difference cousins, have unsurprisingly been used to get adaptive solutions far more often. Wu [90] was in fact the first spatially adaptive EHL solution, and used finite elements. Since then, Wu and Oden [91–93] in the late eighties, and more recently the work by Durany, Garcia and Vazquez [19, 20] have all done work with adaptive finite elements. More recently, Lu has successfully combined mesh adaptivity with high order discontinuous Galerkin finite elements [46]. One of the major disadvantages for unstructured meshes remains the kernel matrix for the deformation calculation. By precomputing the kernel matrix on a regular mesh, a large amount of computational expense is saved.

2.5.3 Free boundary

Toward the outlet of an EHL contact there is a sudden drop in oil pressure to ambient pressure. At this point, air and other gases dissolved in the lubricant form bubbles and the fluid cavitates. The position of this cavitation is not known *a priori*, and hence a free boundary is introduced into an already complicated problem. Formulation of this phenomenon mathematically is covered in detail in [18], although here only the Reynolds condition is considered. The Reynolds condition states that the pressure and the pressure gradient should be zero at the cavitation point, X_c. A number of approaches to finding the correct cavitation position have been taken over the years.

First, the use of an over-sized domain is explored. The Reynolds equation (2.2) includes no physical constraints on the solution produced. This simply means that a physically and numerically valid set of input parameters may solve to give values that are a valid numerical solution of the equation, but that does not give physically meaningful results. Unfortunately, this happens in the cavitation region, where negative pressures are generated. Whilst this is clearly not physically realistic, additional difficulties arise when attempting to calculate values of viscosity and density. Several ways of dealing with this problem have been identified for this sub-problem.

The simplest, though least accurate, is to essentially ignore the cavitation point, and just let the points whose pressure is negative form the cavitation region. During the solution procedure, and indeed after convergence of the Reynolds equation on a fixed grid, the negative pressure values are simply set to zero. Unfortunately, unless the domain is close to the correct size, through *a priori* knowledge, this not only gets the cavitation position wrong, it also means the pressure solution may be inaccurate, and hence so are all the other quantities calculated from it. This is the approach taken by [95].

The next approach, and the one taken in the numerical solution described in Section 2.4, is to have some kind of outer iteration. Given the boundary conditions, that both the pressure and the pressure gradient are zero at the cavitation position, X_c, then X_c will be the last grid point to give a non-positive pressure value. Once this has been found, the cavitation condition can then be imposed as a Dirichlet (fixed value) boundary, and subsequent solutions calculated on that smaller domain. However, due to the highly non-linear system of equations being solved, this boundary cannot be imposed exactly where it might seem correct, as the cavitation position may “move around” while the solution is converging. This method has been observed to be sensitive to the discretisation. A suitable choice of domain will result in the cavitation point resting on or very near a grid

point. A bad choice may lead to difficulties solving the system as the cavitation point tries to move between grid points, although adaptive refinement or a slight perturbation of the domain may well alleviate this problem.

Solutions using Finite Element methods often use the penalty method to obtain a cavitation position [90]. Rather than finding the cavitation position explicitly, a penalty function is introduced into the discretisation of the Reynolds equation. This term forces any negative pressure to be zero (arbitrarily small) by penalising any negative values through a jump in the residual, but has no effect on the solution where the pressure is positive. [56] uses an approach similar to that described for finite differences.

2.5.4 Surface roughness

It was realised fairly early on that realism would not be achieved without some attempt to account for the rough surfaces which are inevitably found on machine components. Some of the very early work on surface roughness was done by Chow and Cheng [14] in 1976, although at this stage it was simply based on the asperities causing a different pressure at the inlet. Full numerical solutions for simple bumps or sinusoidal waviness have been conducted for steady state EHL by many authors. In modelling terms, this means the addition of a further geometry term to the film thickness equation, thus modifying the shape of the undeformed surface. Works include those of Lubrecht *et al.* [51] and Kweh, Evans and Snidle [42]. A simple bump, and subsequently waviness, were applied to a simple EHL conjunction by Venner and Lubrecht [81], and the conclusion was that transient analyses are essential, and they went on to do this two years later in [82], as did Yang, Perian and Shen [94]. Again, both were for simple harmonic roughness, although the latter work did include non-Newtonian fluid behaviour. At the same time, Evans and Snidle [21] conducted a line contact simulation with real surface roughness, but only for the steady-state case.

More recently, work has been done by Fang *et al.* [23] about ascertaining information on how EHL conjunctions behave without resorting to numerical modelling of the complete problem. However, only sinusoidal roughness is considered and, although useful in getting trends in certain conditions, it is limited in its wider applicability to more general problems.

In [96], Zhu details how surface roughness is modelled, including the transition from full film to mixed lubrication. This is a challenging problem, and one which may well

need far greater mesh resolution to capture accurately. While the computational mesh spacing is comparable to that used in other papers, these are for smooth contacts, and would need many more points to capture the roughness profile accurately, as shown in [31]. Since this, Holmes *et al.* have performed transient rough surface calculations with significantly more mesh points [37]. There, asperity contact is said to have taken place where the film thickness values are negative in the solution. This seems a very sensible starting point, although even with the increased mesh resolutions, there is concern that the numerical model may still not be solved with sufficient accuracy. There is also concern over exactly how the force balance equation is utilised since arguments based upon physical realism are best used at the mathematical modelling stage, rather than the stage of the numerical calculation.

Lubrecht and Venner [52] make two interesting points regarding surface roughness. The first, that grid resolutions must be sufficient to capture the features, and hence will take the order of 10^5 points to resolve the surface properly in 1D, and then a similar number of time steps for the transient solve. In itself, this is not the challenge that it posed at the time of writing, but when consideration is taken of the large amount of different solves required when designing a lubricant, it quickly becomes clear that some way of reducing the computational load of each solve would be very beneficial. The question of the appropriate time-step size for rough surfaces was considered by [28]. They found that the temporal error estimate required that the timestep be very much smaller than would usually be assumed (a factor of 32 smaller) when the surface roughness had large amplitudes. They also considered, in [28], how parallel computing techniques could be applied to EHL cases in order to get sufficient grid resolution for point contact surface roughness cases.

The second point made by Lubrecht and Venner is “more fundamental” in that the usefulness of solving for rough surfaces is called into question. The point made is that solving for a roughness profile would not allow the prediction of a second roughness profile measured a millimetre further on. Whilst this is undoubtedly true, we consider it a useful goal to be able to parameterise roughness profiles, and hence predict how surfaces with similar parameter values might behave.

Work on discontinuous Galerkin finite element methods for transient surface roughness problems has been considered in [47], which is the transient extension of [48].

Chapter 3

Background to Adjoints

3.1 Adjoint background

The study of adjoints is a wide and varied field. They are primarily used for sensitivity analysis, but from this many different uses may be derived. Examples include duality in linear programming [13], shape optimisation [53], and error estimation [73]. In this work we shall concern ourselves exclusively with the last. A general paper discussing error analysis from a mathematical perspective is by Giles and Süli [25].

In particular, in this work concentration is focused on error estimation based upon the accuracy of specific outputs of interest. Adjoint theory can be used to provide a framework for finding such estimates. That is, finding the sensitivity of the output quantity of interest to other computable quantities. Exactly how this is achieved is explained in greater detail in the next section, but it revolves around formulating and solving an adjoint system which is related to the original "forward" problem. There are two distinct but related approaches to formulating the adjoint system: continuous and discrete. A comprehensive comparison of the two methods for a shape optimisation problem is given by Nadarajah and Jameson [53], but the basic differences between the two approaches are highlighted here. In the continuous approach, the adjoint PDE is formed analytically from the continuous PDE, and then discretised afterwards, e.g. [58]. If the analysis can

be performed to get to the adjoint PDE, the boundary conditions can be difficult to formulate [45]. In the discrete adjoint approach, however, the adjoint system is formed directly from the discretisation of the continuous forward problem. One advantage of this method is that it can be applied to complex problems, where an analytic solution of the continuous adjoint problem may be difficult or impossible to find. The method followed in this thesis is that developed by Darmofal and Venditti [72–78]. This is a discrete approach which, as stated in [77], "is a discrete analogue of the Pierce and Giles [58] technique". One of the main reasons for our choice of this method over the Pierce and Giles approach is that, for a complex engineering problem such as EHL, formulating the adjoint PDE problem (including appropriate boundary conditions) would be extremely difficult, if not impossible. However, by realising that, to benefit from a comparable increase in functional accuracy, all that is required is a discretisation of the "forward" system being solved. Through the use of the discrete approach, adjoint error estimation becomes a realistic prospect for application to EHL. The details of the discrete approach used will be discussed further in the next section.

Having discussed the detail of the adjoint error estimation, a less formal description of the process forms the following section; the idea being to provide further insight into what is actually going on in the formal description. Following this, a simple linear problem is provided to introduce the effectivity index. The chapter concludes with some justification for the choice of cubic spline interpolation between grids, and some notes on the boundary values for the adjoint systems used for the work in this thesis.

3.2 Adjoint error estimation

In this section, the theoretical background to the adjoint estimation of an error is introduced. The starting point is to define two meshes with spacing $h = \Delta x$ and $H = \Delta X = m \times \Delta x$, $\{m \in \mathbb{N} \mid m > 1\}$ (i.e. H is some multiple of the mesh space size h). The idea is that mesh size H is fine enough to capture the features of the problem being solved, and coarse enough to be solved in a reasonable time, while the fine mesh size h would give the solution to a greater accuracy but in an unacceptable time. Whilst the coarser of the two meshes need not necessarily be very coarse, nor necessarily the finer mesh particularly fine, for ease of terminology these two meshes will be referred to as the coarse mesh and the fine mesh hereafter.

Consider an arbitrary non-linear problem whose discrete form may be represented as

$A_h(u_h) = f_h$ on the fine mesh, and $A_H(u_H) = f_H$ on the coarse mesh, where in each case $A(u)$ is a non-linear operator. Let u_h^H be an approximation to u_h obtained by interpolation of the coarse mesh solution: $u_h^H = I_h^H u_H$. Throughout this work the interpolation for the adjoint solution will be through cubic splines, unless otherwise stated. The reason for this choice is justified later in this chapter. The solution u will be referred to as the forward solution. The discrete fine grid residual is given by

$$R_h(u_h) = f_h - A_h(u_h).$$

A Taylor series expansion about the interpolated coarse grid solution, u_h^H, shows that

$$\begin{aligned} R_h(u_h) &= R_h(u_h^H + (u_h - u_h^H)) \\ &= R_h(u_h^H) + \left[\frac{\partial R_h}{\partial u_h}\bigg|_{u_h^H} \right] (u_h - u_h^H) + h.o.t. \end{aligned} \tag{3.1}$$

which, ignoring the higher order terms, is the linearisation of the fine mesh system of equations, where $\left[\frac{\partial R_h}{\partial u_h}\Big|_{u_h^H} \right]$ is the Jacobian evaluated using u_h^H. Given that $R_h(u_h) = 0$,

$$-R_h(u_h^H) = \left[\frac{\partial R_h}{\partial u_h}\bigg|_{u_h^H} \right] (u_h - u_h^H),$$

and re-arranging gives

$$(u_h - u_h^H) = -\left[\frac{\partial R_h}{\partial u_h}\bigg|_{u_h^H} \right]^{-1} R_h(u_h^H), \tag{3.2}$$

an expression for the error in the interpolated coarse grid solution with respect to the fine grid solution.

Suppose that the quantity of interest for this problem is a functional which may be expressed as $F_h(u_h)$ on the fine grid. As with the fine grid residual, this can be expanded about the interpolated coarse mesh solution to give

$$F_h(u_h) = F_h(u_h^H) + \left(\frac{\partial F_h}{\partial u_h}\bigg|_{u_h^H} \right)^T (u_h - u_h^H) + h.o.t. \tag{3.3}$$

Substitution of equation (3.2) into equation (3.3) for $(u_h - u_h^H)$, and again ignoring the

higher order terms, yields

$$F_h(u_h) = F_h(u_h^H) - \left(\left. \frac{\partial F_h}{\partial u_h} \right|_{u_h^H} \right)^T \left[\left. \frac{\partial R_h}{\partial u_h} \right|_{u_h^H} \right]^{-1} R_h(u_h^H). \tag{3.4}$$

By introducing a new variable, Ψ_h,

$$\Psi_h^T = \left(\left. \frac{\partial F_h}{\partial u_h} \right|_{u_h^H} \right)^T \left[\left. \frac{\partial R_h}{\partial u_h} \right|_{u_h^H} \right]^{-1} \tag{3.5}$$

equation (3.4) may be rewritten as

$$F_h(u_h) = F_h(u_h^H) - \Psi_h^T R_h(u_h^H). \tag{3.6}$$

Post multiplying equation (3.5) by $\left[\left. \frac{\partial R_h}{\partial u_h} \right|_{u_h^H} \right]$ gives

$$\Psi_h^T \left[\left. \frac{\partial R_h}{\partial u_h} \right|_{u_h^H} \right] = \left(\left. \frac{\partial F_h}{\partial u_h} \right|_{u_h^H} \right)^T.$$

Taking the transpose of both sides, and given $(Av)^T = v^T A^T$, it follows that Ψ_h must satisfy

$$\left[\left. \frac{\partial R_h}{\partial u_h} \right|_{u_h^H} \right]^T \Psi_h = \left(\left. \frac{\partial F_h}{\partial u_h} \right|_{u_h^H} \right). \tag{3.7}$$

Hereafter, equation (3.7) will be referred to as the fine grid adjoint system, and Ψ_h the fine grid adjoint solution. Once the adjoint solution has been obtained, an approximation to $F_h(u_h)$ may be calculated using equation (3.6) without actually having solved for u_h explicitly. For highly non-linear problems, the need to only perform a linear solve on the fine mesh (i.e. equation (3.7)) to get a value of the functional to the same order of accuracy as that gained from the solution of a whole non-linear problem, possibly consisting of many linear solves, is hugely advantageous. In fact, if A is a linear operator, rather than a non-linear operator, then the "functional correction" term $\Psi_h^T R_h(u_h^H)$, obtained in equation (3.6), will be exact. However, there is a further advantage to be gained at this stage.

Whilst the forward solution u_h^H used in equation (3.6) is only solved for on the coarse mesh, the adjoint solution is still solved for on the fine mesh. Fortunately, it is possible to

solve an alternative system to equation (3.7), also on the coarse mesh, shown here as

$$\left[\frac{\partial R_H}{\partial u_H}\right]^T \Psi_H = \left(\frac{\partial F_H}{\partial u_H}\right). \tag{3.8}$$

This adjoint system, which will be referred to as the coarse grid adjoint system, with Ψ_H the coarse grid adjoint solution, is an approximation to the fine grid adjoint system given in equation (3.7). This is formed directly on the coarse grid from the coarse grid solution and coarse grid residual equations, rather than on the fine grid using the interpolated coarse grid solution. The basis for this approach is that the approximation should be satisfactory once the meshes are refined sufficiently such that the solutions have entered their asymptotic ranges. In other words, as the meshes become more refined, the higher-than-first order errors should become small in comparison to the linear approximation. This coarse grid adjoint solution is then interpolated onto the fine grid to give $\Psi_h^H = I_h^H \Psi_H$. Equation (3.6) can now be reworked in terms of the coarse grid adjoint solution, to give

$$F_h(u_h) \approx \tilde{F}_h(u_H) = F_h(u_h^H) - (\Psi_h^H)^T R_h(u_h^H). \tag{3.9}$$

An approximation to the fine grid functional has now been obtained simply by solving an additional linear problem on the coarse grid, the adjoint system given in equation (3.8). As was previously mentioned, the expression $(\Psi_h^H)^T R_h(u_h^H)$ will be referred to as the "correction" to the functional $F_h(u_h^H)$, since this is essentially what is happening.

The final point that must be made pertains to the application of the above theory to a finite difference discretisation. In [77], is it pointed out that "A typical finite difference stencil would need to be scaled by an appropriate volume term (or an area term in two dimensions) so that the residual became analogous to an integral expression". This is key in applying the procedure to non-uniform finite difference meshes. This idea is expanded on further in Chapter 5.

3.3 A less rigorous view of adjoints

Having seen the mathematical theory underpinning adjoint error estimation, a rather more informal description of the approach is attempted in this section.

The approach taken in this method is to take two things which are easily calculated, and use them to estimate a quantity which is computationally useful, but not directly

accessible. It is straightforward to compute the linear sensitivities of both the friction calculation and the residual equations to the solution variables. By formulating the adjoint problem, a solution can be obtained giving the linear sensitivity of the friction calculation to the residual equations, a far more useful quantity. This is because the residuals are easily calculated, and given a change in the residuals, a linear approximation to the change in the friction can be predicted.

First, a similar example is presented, the Newton Iteration. In this,

$$\frac{\partial R}{\partial u}\delta u = -R$$

is solved for δu, where the δ is used to signify a (hopefully) small change in u. We can also calculate the (linear) sensitivity of any residual equation to the unknown u at any point. Let $\left[\frac{\partial R}{\partial u}\right]$ denote the Jacobian matrix whose entry in the ith row and jth column gives the rate of change of the ith residual equation w.r.t. the jth solution value. A particular row of the Jacobian gives the sensitivity of a particular residual equation to all the different solution values, whereas a particular column of the Jacobian gives the sensitivity of all the residual equations to one of the solution values.

So now, for our adjoint problem, we have

$$\left[\left.\frac{\partial R_h}{\partial u_h}\right|_{u_h^H}\right]^T \left(\Psi_h|_{u_h^H}\right) = \left(\left.\frac{\partial f_h}{\partial u_h}\right|_{u_h^H}\right)^T.$$

A row of the transposed Jacobian is just a column of the original Jacobian, i.e.

$$\left(\frac{\partial R_1}{\partial u_j}, \frac{\partial R_2}{\partial u_j}, \cdots, \frac{\partial R_i}{\partial u_j}, \cdots\right)$$

and multiplied out with the adjoint variable vector Ψ,

$$\frac{\partial R_1}{\partial u_j}\Psi_1 + \frac{\partial R_2}{\partial u_j}\Psi_2 + \cdots + \frac{\partial R_i}{\partial u_j}\Psi_i + \cdots = \frac{\partial f}{\partial u_j}.$$

It follows, using the chain rule, that the adjoint variables are the sensitivities of the functional to the residuals. That is,

$$\frac{\partial R_1}{\partial u_j}\frac{\partial f}{\partial R_1} + \frac{\partial R_2}{\partial u_j}\frac{\partial f}{\partial R_2} + \cdots + \frac{\partial R_i}{\partial u_j}\frac{\partial f}{\partial R_i} + \cdots = \frac{\partial f}{\partial u_j},$$

and so

$$\Psi_i = \frac{\partial f}{\partial R_i}.$$

3.4 Example problem

In this section a very simple linear problem is used to illustrate the adjoint error estimation procedure. This will serve purely as an introduction to one of the main analysis tools used with this work, the effectivity index. As such, the forward problem and adjoint correction procedure are briefly described.

3.4.1 The forward problem

A simple linear PDE is defined by the following equations:

$$\frac{d}{dX}\left(H(X)\frac{dP}{dX}\right) = \lambda X,$$

where

$$H(X) = H_0 + \frac{X^2}{2}$$

on a finite computational domain $X_l < X < X_r$. The boundary conditions are given as $P(X_r) = P(X_l) = 0$, and the operating parameters for this example are $H_0 = 5.0$, $X_r = 1.502$ and $X_l = 1.502 - 50$. Using the finite difference approximations derived in Chapter 2, these equations may be discretised on a coarse regular grid of n points, yielding the discrete equations

$$\frac{(P_{i+1} - P_i)H_{i+1/2} - (P_i - P_{i-1})H_{i-1/2}}{(\Delta X)^2} = \lambda X_i$$

and

$$H_i = H_0 + \frac{X_i^2}{2},$$

for $i = 1 \ldots n-2$, with $P_0 = P_{n-1} = 0$. The next step is to form the system $AP = f$, with A the linear tri-diagonal matrix of coefficients, P the solution vector, and f the right-hand side with the values λX_i. This is easily solved for P and the functional of interest, defined to be

$$F = \sum_{i=0}^{n-2} 0.5(P_i + P_{i+1})\Delta X \approx \int_{X_l}^{X_r} P dX,$$

is easily calculated from it. The residual equations can then be defined as

$$R_i = \lambda X_i - \frac{(P_{i+1} - P_i)H_{i+1/2} - (P_i - P_{i-1})H_{i-1/2}}{(\Delta X)^2},$$

for $i = 1, \ldots, n-2$. Having differentiated each of these with respect to the all of the solution variables, P_j, the Jacobian can be formed. In this case, the Jacobian is just the $(n-2) \times (n-2)$ matrix A, which also happens to be symmetric in this case. The right-hand side of the adjoint system is then the vector of ΔX values, and the adjoint system can be formed and solved for Ψ_H. Once these two solutions have been calculated, they are then interpolated onto the fine grid (i.e. a uniform refinement of the current coarse grid), using quadratic interpolation in this case. Having obtained the interpolated solutions on the fine grid, the functional can be computed. Once the interpolated solution has been used to generate the residuals for that level, the correction can be calculated. Results are shown in the following subsection.

3.4.2 Results

In Table 3.1, results are shown for the example problem above. The main purpose of this table, and those like it in the following chapters, is to show whether or not the calculated correction to the functional (i.e. the estimate of the inter-grid functional error) is close to the actual error when measured. This is achieved by solving the system and calculating the quantity of interest on the fine grid, giving the true value for that mesh. Thus, when the solutions are solved on the coarse grid and interpolated to the fine grid, followed by the calculation of the estimate of the quantity of interest and subsequent correction, it is possible to see how close the two are.

The columns of Table 3.1 are as follows: Column 1 shows the coarse grid on which the solutions of the forward and adjoint problem are solved, with column 2 the number of mesh points on that grid. Column 3 shows the interpolated functional. That means the functional calculated on grid $g+1$ using the solutions calculated on grid g. The correction to the value in column 3 as calculated by the adjoint error estimation procedure is then shown in column 4. It is this quantity in whose accuracy we are interested. Column 5 contains the resulting computed corrected functional value, which can then be easily compared to the actual functional value for grid $g+1$ which is shown in column 6. The measured error, as shown in column 7, is the difference between columns 6 and 3, i.e. the actual error in the functional computed from a solution interpolated to the fine

Grid (g)	No. Points	Interpolated Func. (g)	Calculated Correction	Corrected Func. (g)	Functional ($g+1$)	Measured Error	Effectiv. Index
3	17	1.10973	0.19470	0.94278	1.36493	0.25520	1.311
4	33	1.36194	0.09868	1.26625	1.47011	0.10817	1.096
5	65	1.47049	0.02760	1.44251	1.49940	0.02890	1.047
6	129	1.49941	0.00750	1.49190	1.50698	0.00757	1.009
7	257	1.50698	0.00191	1.50507	1.50889	0.00191	1.002
8	423	1.50889	0.00048	1.50841	1.50937	0.00048	1.000
9	692	1.50937	0.00012	1.50925	1.50949	0.00012	1.000
10	964	1.50949	0.00003	1.50946	1.50952	0.00003	1.000
11	1152	1.50952	0.00001	1.50951	1.50952	0.00001	1.000

Table 3.1: Adjoint based inter-grid functional error on uniform meshes for a linear model problem

grid, compared to the functional value as solved on the fine grid. This is the value that the adjoint error estimate from column 4 should closely approximate. Finally, the last column in the table gives the effectivity index of the adjoint error estimate. This is defined to be the ratio of the actual error (that in column 7) to the predicted error (i.e. the adjoint error estimation in column 4). For this linear problem, it is clear that the effectivity index tends towards a value of unity with increased grid refinement, showing the accuracy of the predicted correction to the functional. Furthermore, even for very coarse grids the error estimate is demonstrated to be remarkably accurate.

3.5 Cubic spline interpolation

Cubic spline interpolation is a third order accurate method of interpolation (i.e. when data points from a sufficiently smooth function are interpolated using cubic splines the error is third order [12]). It is piecewise cubic interpolation, with the cubic on each interval constrained to be such that:

- The cubic segment interpolates the values at either end of the segment;
- The first derivative of the segment matches the first derivative at the interface with the adjoining segments (i.e. it is continuous);
- The second derivative is continuous.

Along with the information from the end point conditions (not-a-knot is used for this work), this gives sufficient information to be able to solve a system of equations to get the interpolating cubics. Further details of this can be found in [59].

As mentioned near the beginning of this chapter, cubic spline interpolation is used throughout this work. In Chapter 5, the discretisation of the model problem is second order. According to [73], the order of the interpolation used to move coarse grid solutions onto the fine grid should be at least as high as the discretisation of the system being used. Therefore, second order interpolation would be sufficient in that case, and so using quadratics would be an option. However, fitting a quadratic through the last three points of the domain would always exactly satisfy the cavitation condition, equation (5.8), on the fine mesh. This would lead to a loss of information about the how the functional should be corrected due to the boundary being incorrectly placed. For this reason, and since higher accuracy is generally regarded as a good thing, cubic splines are used.

3.6 Sparsity patterns

In this section, the reason that the boundary points are not solved for in the adjoint system is described. There are two reasons why the boundary points could potentially be necessary in the formulation of the adjoint equation system. The first is because there may be a contribution to the correction term from that point, and the second is because the equations there may affect the adjoint system, leading to a different adjoint solution. Here, the reasons why the adjoint values at the boundaries are not needed for this work are outlined.

Throughout this work, the boundary conditions are all defined to be Dirichlet, or fixed value, points. This means that the residual on any grid at the boundary points must always be zero, and so in the context of the adjoint error estimation, these points will make no contribution.

The adjoint solution variables specify the linear combination of the Jacobian matrix columns which, when multiplied, yield the corresponding sensitivity of the functional to the solution variables. Since the residual equations at the boundaries for all of the problems considered in this thesis are essentially

$$R_0 = -P_0 \text{ and } R_{n-1} = -P_{n-1},$$

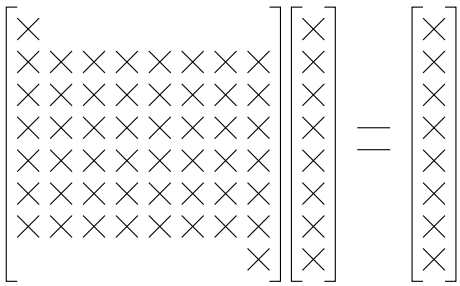

Figure 3.1: The sparsity pattern for an example Jacobian system, with zero Dirichlet boundary conditions

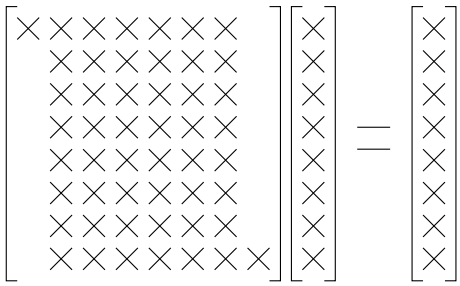

Figure 3.2: The transposed sparsity pattern for an example Jacobian system, with zero Dirichlet boundary conditions

there is no sensitivity to any solution variable other than the one at that point, and as such the row in the Jacobian is empty apart from the one on the diagonal. Once the Jacobian matrix has been transposed, this becomes a column. Now, since all of the entries are zero apart from those pertaining to the boundaries, whatever the adjoint boundary values are after the adjoint system has been solved makes no difference to the other adjoint variables. In other words, the boundaries have been de-coupled from the rest of the adjoint solution. This means that there is no need to consider the boundary points when formulating the adjoint system because the variables there are a) not important in their own right as the residual there will always be zero, and b) do not influence the rest of the adjoint solution since they are decoupled from it. The situation for an adjoint system that would arise from a system similar to that considered in Chapter 7 is shown in Figure 3.1, along with the transpose of the system in Figure 3.2. This shows pictorially how, after being transposed, the first and last columns contain entirely zeros apart from on the diagonal. This fits with the theory for continuous adjoints since homogeneous boundary conditions for the forward problem often lead to in-homogeneous boundary conditions for the adjoint problem [45].

Finally, a technical consideration is highlighted. When considering interpolation between grids, special treatment must now be used for the endpoints since there will be

points on the finer mesh outside the end points on the coarse mesh. This is easily remedied by extrapolating the cubic spline segments at the edges.

Chapter 4

Friction as a Quantity of Interest

Historically, research into error estimation and control has tended to assume that, in a numerical simulation, it is the accuracy of the computed solution which is of interest. In many practical situations however, the solution field is used to calculate some derived quantity, such as friction, drag, lift, etc. In this work, we are interested in such cases, where a quantity of interest depends on the solution. It is this quantity in which the accuracy is really required, rather than for the whole of the solution. In this chapter an output of interest in EHL problems, the friction within the contact, is introduced. In subsequent chapters it will be seen how these ideas can be married to those of the previous chapter, where the accuracy of an output functional can be estimated. The results in this chapter are for EHL on a uniform grid using the numerical code developed as part of the Carmehl [71] software.

4.1 Motivation

Solution times for numerical models for solving elastohydrodynamic lubrication (EHL) problems continue to decrease as the algorithms used improve and the computers on which they are solved become more powerful. Conversely, as the lubricant models used by industry become more complex, the demands for robustness, accuracy and speed of

the software increase. In addition as the breadth of cases increases the generality of the software must also increase, so a single code should be able to tackle a wide range of problems with the minimum of user input.

The main requirement of a user of such a code is to obtain the "correct" solution as quickly as possible. This leads to the consideration of the question of what is meant by "correct". In order to consider a solution "correct" it must satisfy some objective criteria and it could be that the spatial mesh resolution required to meet these criteria for one solution component is inadequate for another. Typically, a finer resolution computational mesh leads to more accuracy but at the expense of increased solution times. Therefore if the user is only concerned with solution components that already meet the objective "correctness" criteria at a certain level of grid resolution, it may be unnecessary to increase the grid resolution further. However care must be taken as not only can solution components which are not accurately resolved affect other components, but in transient problems the growth of errors in these other components can result in completely inaccurate solutions at later times. In this chapter it is shown how account may be taken of some of these requirements when considering accuracy in terms of the ability to reliably estimate solution-dependent quantities such as friction.

In order to measure the error in a computational experiment it is necessary to measure how far the computational result is from the true solution. Since EHL problems only have an analytic solution in very special cases, the "true" solution will be taken to be that obtained as the number of points increases, and hence the mesh spacing decreases. In particular, the "true" solution will be defined here by that computed on a very fine mesh, often termed a "truth mesh" in the computational science community. Providing the truth mesh is sufficiently fine, it is possible to model the discretisation error numerically on much coarser meshes.

In this chapter only the key quantity of friction will be considered. The motivation for this is that in many real simulations being performed, this will be the only quantity considered by, and of interest to, the user [29].

Investigations into friction have been mainly confined to experimental work such as Blencoe *et al.* [6] and Workel *et al.* [88]. As will be shown later in this chapter, e.g. Figures 4.1 to 4.4, the friction appears to be closely related to accurately capturing the profile of the pressure spike. Work by Bisset and Glander [4] showed that when more fine mesh points are used in the region of the spike then it is no longer seen as a singularity in the solution, but a smooth profile. This work only resolved the spike using up to 1000 points,

however it did still highlight the importance of this area of the solution. Results later in this chapter show this resolution extended to over a million mesh points. Further consideration of this area in respect to the elastic properties is given by Hall [33] and the benefits of this approach for better accuracy is shown by Lee and Hsu [43].

The consideration of friction will be seen to have great dependence on the resolution of the pressure profile, as will be explained with reference to the governing equations. The consideration of the resolution of the single pressure spike in a line contact case will be used as an example which must be applied to the much more general cases of surface roughness, where sharp pressure spikes will occur through the length of the contact region. Accurate resolution of these features will lead to more reliable computational results for the key quantities of interest.

Whilst not considered in this work, subsurface stress components [38, 44] calculated from the pressure play a significant role in determining the life of a bearing. Accurate resolution of the pressure solution will be equally important in computing this and other quantities of interest.

4.2 Friction

As mentioned in Chapter 1, friction is a force which opposes motion. The friction generated in an EHL contact is given by the shear stress generated within the lubricant. This comes about through two mechanisms, rolling friction and kinetic (sliding) friction.

Within the contact, a pressure gradient is generated. This is because the deformation of the contact is largest in the centre, requiring the greatest pressure to maintain it. As the two surfaces move into the contact, lubricant is pulled with them (entrained). However, it is also squeezed out by the pressure generated in the contact region, and so the lubricant in the middle is moving at a different speed to the surfaces, causing it to shear. The resistance to this motion is called the rolling friction and forms the first term of (4.1) and (4.2) below.

The second mechanism for the generation of shear stress, only happens when the surfaces are in relative motion, hence sliding friction. Now, the lubricant is sheared at the rate of the difference in speed of the two surfaces per unit thickness. Given the viscosity, η, i.e. the resistance to shear, the force at any position in the contact can be determined.

It is possible to derive the shear stress on each surface [65]:

$$\tau_{xz;a}(x) = -\frac{h}{2}\frac{\partial p}{\partial x} + \frac{\eta}{h}(u_b - u_a), \tag{4.1}$$

$$\tau_{xz;b}(x) = \frac{h}{2}\frac{\partial p}{\partial x} + \frac{\eta}{h}(u_b - u_a), \tag{4.2}$$

for the lower and upper surfaces moving at speeds u_a and u_b respectively. From these expressions it is possible to work out the total (dimensional) friction through a line contact, F as either

$$F = \int_{-\infty}^{\infty} \tau_{xz;a}(x)\mathrm{d}x \tag{4.3}$$

or

$$F = \int_{-\infty}^{\infty} -\tau_{xz;b}(x)\mathrm{d}x \tag{4.4}$$

depending on which surface is required. In this work, the friction on the lower surface will be used, i.e. equation (4.3), although this choice is arbitrary. This is a key quantity of interest as it gives a measure of the force opposing the shear in the lubricant, e.g. [5, Chapter 6]. Experimentally, the rolling friction and the sliding friction cannot be measured independently, and hence in this work only the total friction will be considered, although in some cases this will be made up of only rolling friction.

4.3 Pressure spike resolution and friction

The speed of modern EHL codes and the computers they are run on makes it possible to obtain solutions to line contact problems with up to 10^6 mesh points, as will be shown below. The quality of the results obtained varies between grid levels. This variation may give a larger error in key quantities of interest, such as the total friction defined by equation (4.3), than just the discretisation error in the pressure. For example, the total error in the friction depends on errors in the pressure derivative $\frac{\partial P}{\partial X}$, the film thickness, the reciprocal of film thickness and also on the viscosity. As film thickness depends on all the pressures, the error in the film thickness at any point depends on all the errors in the pressure values.

An example of the differing quality of solution is shown in [31]. They considered

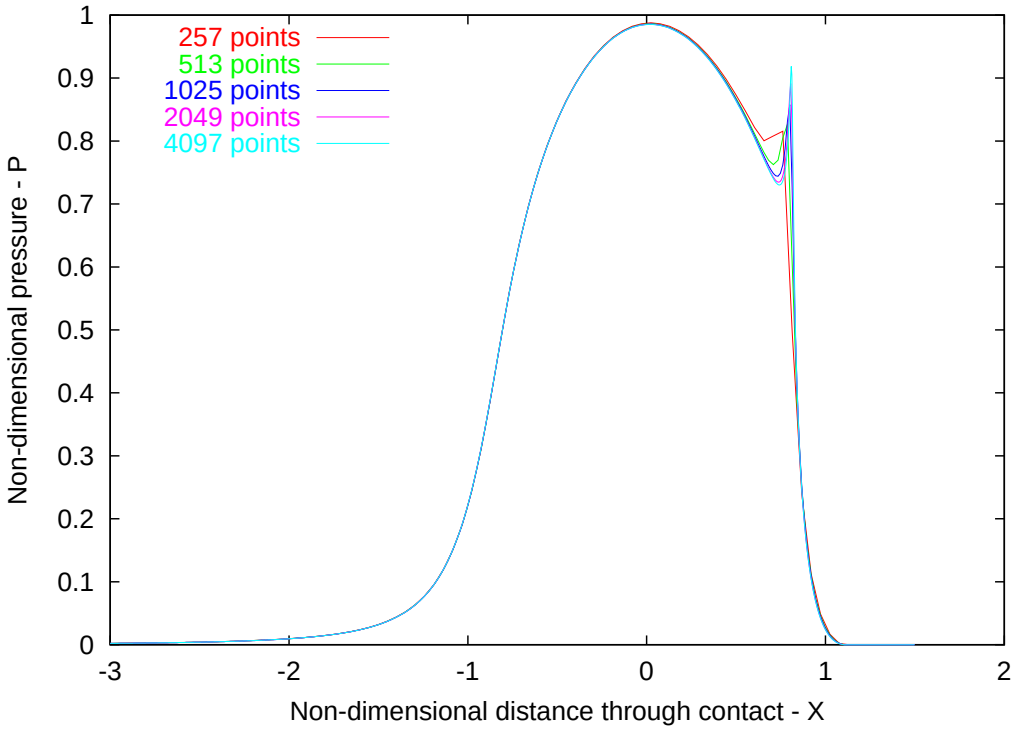

Figure 4.1: Non-dimensional pressure plot of a line contact problem with increasing mesh resolution

increasing the mesh resolution and observed the change in both the primary solutions and the derived friction. In Figure 4.1, the pressure distribution across the whole domain is shown. It can be seen that the curves are almost coincidental apart from around the pressure spike. This area is shown in detail in Figure 4.2, where the addition of several orders of magnitude more points has now captured the pressure spike completely and appears to have achieved a converged continuous solution. More work has been done recently to achieve convergence of the pressure spike with only a fraction of the mesh points used here, using high order Discontinuous Galerkin finite element solutions [48].

The effect of extra grid resolution can be seen to only affect a small portion of the pressure plot, namely the spike area, and only to a very small degree once the grids greater than 4097 points have been reached. However, as Figure 4.3 illustrates, an increasingly refined spike, achieved through finer meshes, has a more global effect on the film thickness. Similarly, considering the total friction through the contact, as shown in Figure 4.4, the resolution of the pressure profile, and hence pressure spike, is important if the total friction through the contact is to be calculated accurately.

It is the derivatives of pressure in equation (4.2) that are especially important in purely

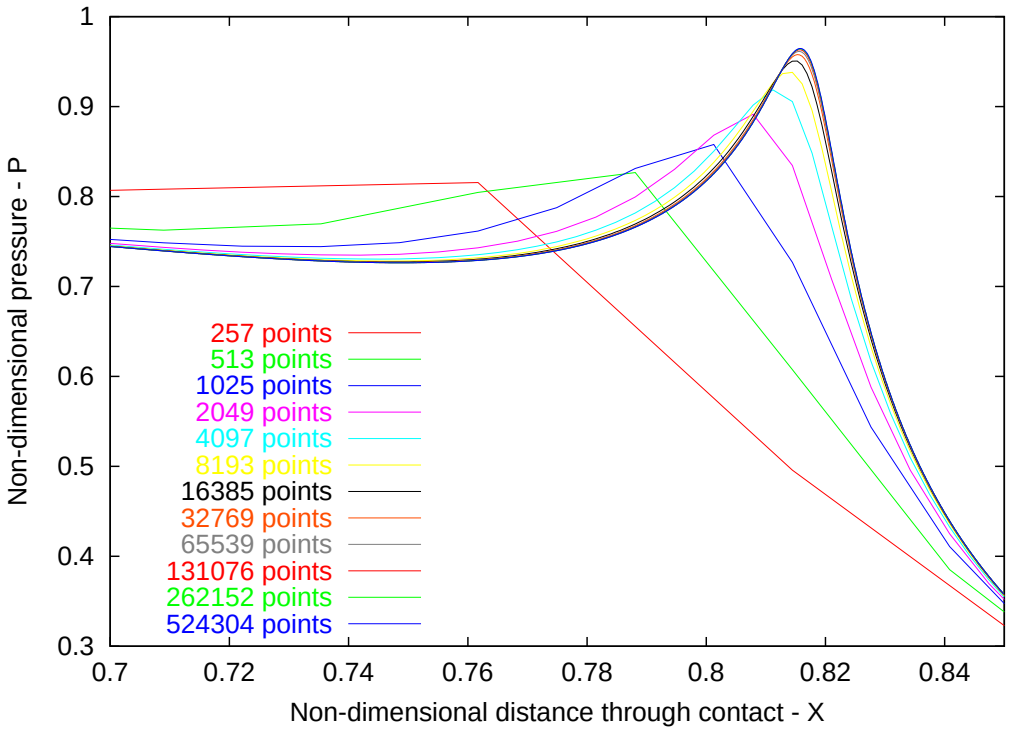

Figure 4.2: Non-dimensional pressure plot around spike with increasing mesh resolution

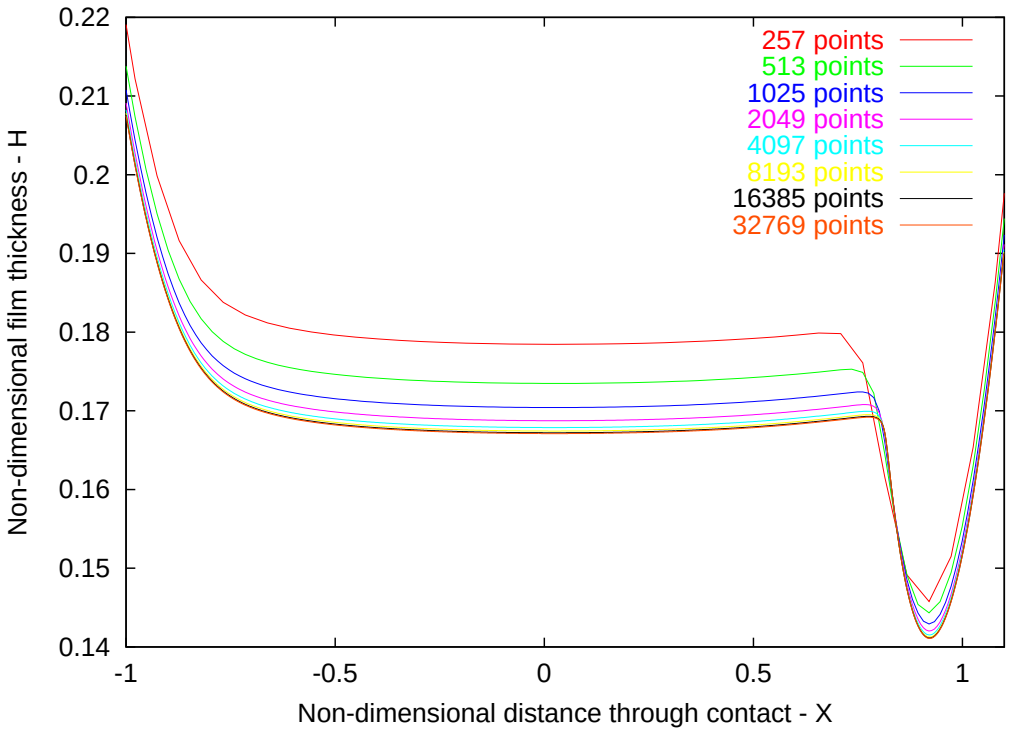

Figure 4.3: Non-dimensional film thickness plot of a line contact problem with increasing mesh resolution

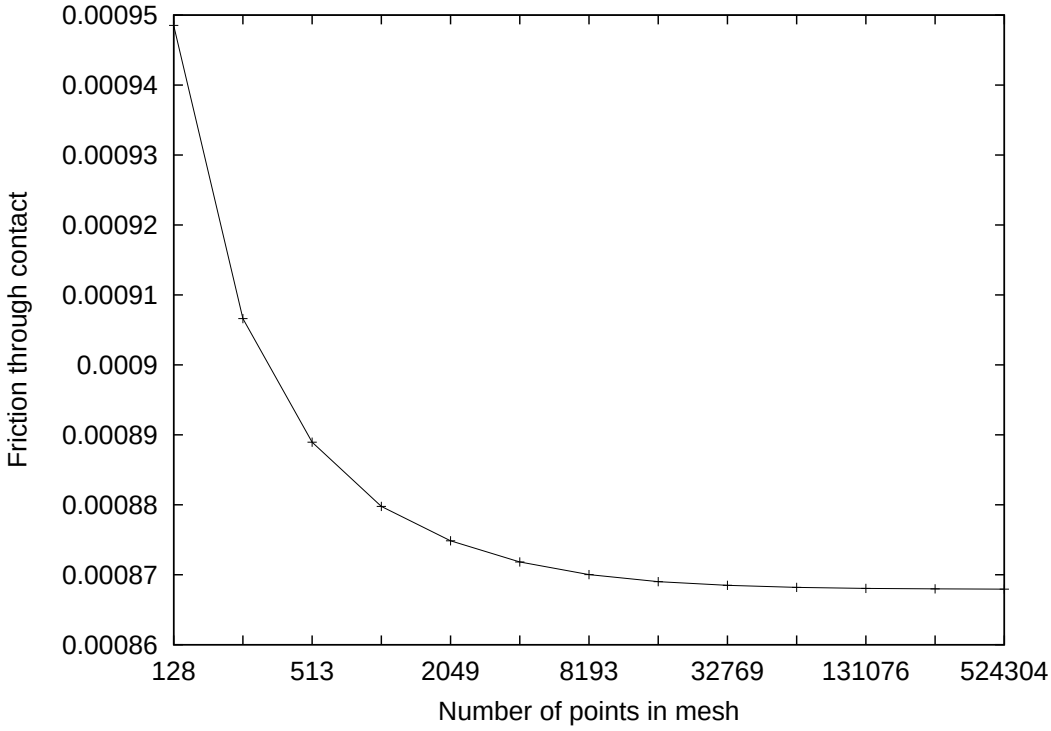

Figure 4.4: Total friction through the contact calculated with increasing mesh resolution

rolling friction calculations. If the pressure spike is not captured well enough then these derivatives will not represent the true friction through the contact. These derivatives are also present through the calculation of the shear stress, as given in equations (4.1, 4.2). These shear stresses have an even more extreme profile on finer meshes as shown in Figure 4.5. It can be seen how the results on grid levels where the calculated key quantities have converged are still not capturing the maximum shear stress quite so accurately.

4.4 Domain size

The size of the domain used for the calculation of purely rolling friction is also very important. In Figure 4.6, again taken from [31], the calculated friction against the length of the negative X domain is shown, i.e. $-X_l$, for fixed grid levels. It is seen that with very large negative domains, i.e. large inlet regions, the sensitivity of the friction to further changes in the domain size will be negligible. Obviously, for each grid level the mesh spacing will increase as the value of X_l gets larger, however it can be seen from the coincident curves for the finest meshes that this is not enough to account for the convergence behaviour of the friction. The conclusion to be drawn is that the inlet region has a very important

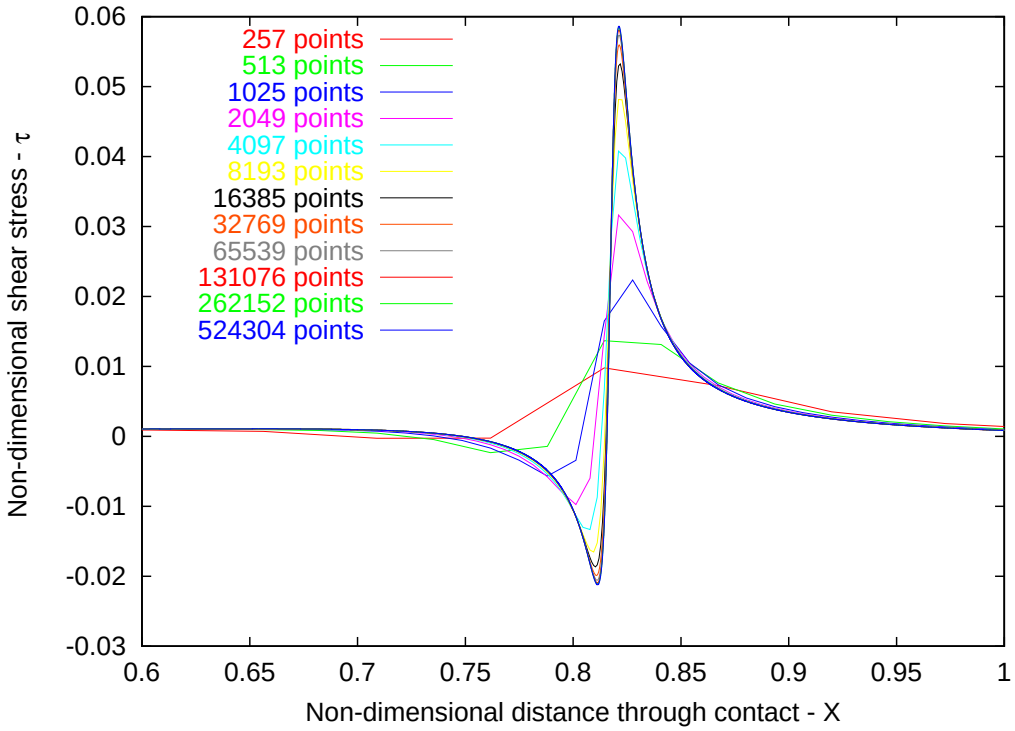

Figure 4.5: Shear stress profiles with increasing grid resolution for a line contact case

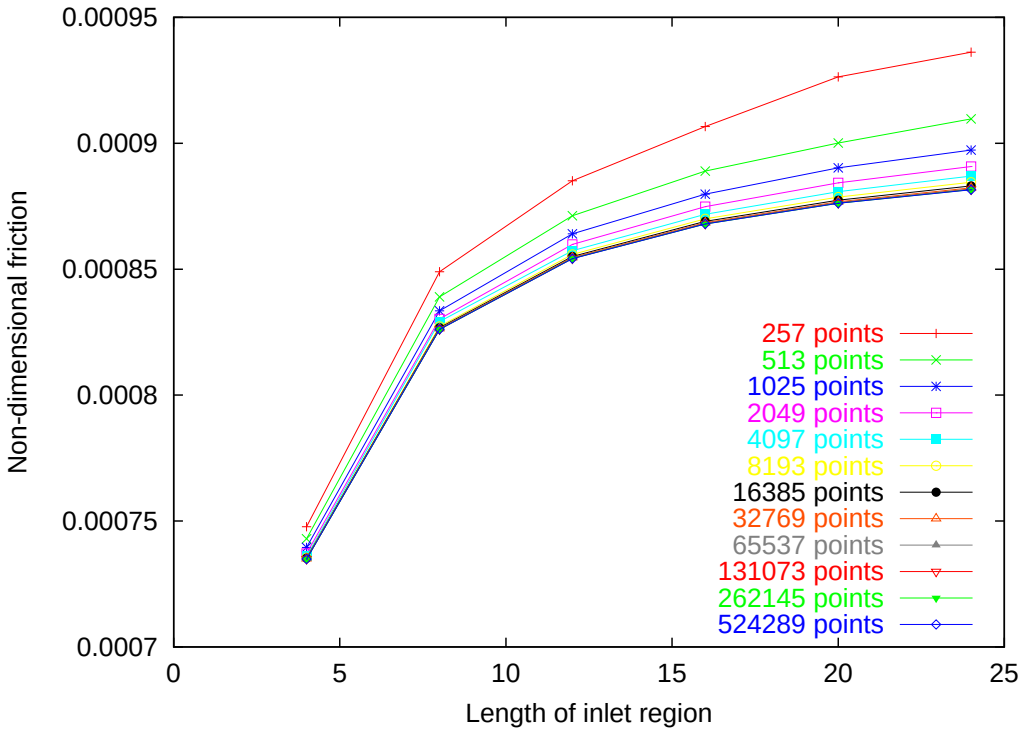

Figure 4.6: Calculated friction against length of inlet domain for increasing grid resolution in a line contact case

effect on the friction results calculated, in many cases over 10% of the calculated friction. This result will be significant in the next three chapters since, in all of those chapters, the left-hand boundary will not be identically placed between cases, so it is important that the domain is sufficiently large so as to have negligible effect when this happens. Fortunately this result is mitigated to some extent by two factors. The first is that the introduction of some sliding to the contact reduces the increase of friction with domain size. The second, and more important point, is that due to the solution process used, the left hand boundary will only move at most by one mesh point when a finer grid is used to gain a more accurate solution. This means that the domain only needs to be large enough that a small change in the size results in a negligible change in the friction.

4.5 Discussion

In this chapter it has been shown how accurate resolution of the pressure profile leads to accurate values of computed friction. In the next chapter a model free boundary problem is introduced, and this is used to show how adjoint error estimation techniques can be used for accurate prediction of the friction on a uniformly refined mesh and also how it can be applied to driving adaptive refinement.

Chapter 5

A Model Free Boundary Problem

For such a complex and highly non-linear problem as that described in Chapter 2, it is useful to take several simplifying steps. These facilitate better understanding of how adjoint error estimation needs to be applied to each of the various problem-specific mechanisms at work. To this end, a sequence of model problems are proposed which retain sufficient similarities to the full EHL problem to be useful, whilst providing a relatively straightforward set of increments. In this chapter, a linear PDE with a free boundary is considered, and in the next chapter this is generalised to a non-linear PDE. Although the PDE considered here is linear, because the position of the free boundary depends upon the solution of the PDE in a non-linear way, the overall free-boundary problem is still non-linear. Force balance is also present in this model through the separation parameter H_0.

5.1 Forward problem

This section defines the forward problem to which adjoint error estimation will then be applied. First, the mathematical model is described. This is followed by its discretisation, and finally its solution method. An expression for "friction" is also defined and discretised.

5.1.1 Mathematical model

Although the model proposed here may be thought of as an incompressible, isoviscous hydrodynamic problem, this is just a model problem. The equations have been chosen to look similar to the EHL equations, but the quantities, whilst referred to as such, have no physical meaning. By using this model, the non-linearities arising from the density, viscosity, and elastic deformation are removed: $\overline{\eta}$ and $\overline{\rho}$ having been assigned nominal values of unity. The PDE, similar to the non-dimensional Reynolds equation, after taking account of $\overline{\eta}$ and $\overline{\rho}$, is given by:

$$\frac{\mathrm{d}}{\mathrm{d}X}\left(H^3\frac{\mathrm{d}P}{\mathrm{d}X}\right) - \lambda\frac{\mathrm{d}H}{\mathrm{d}X} = 0. \tag{5.1}$$

With no deformation of the solid bodies, the film thickness is simply given by the separation H_0, and the parabolic geometry of the surfaces, thus

$$H(X) = H_0 + \frac{X^2}{2}. \tag{5.2}$$

As usual, the force balance equation is applied, so that the applied load is balanced by the sum of the pressures generated within the lubricant film,

$$\int_{X_{in}}^{X_c} P(X)\,\mathrm{d}X = L. \tag{5.3}$$

The presence of a load, L, on the right-hand side of equation (5.3) enables a range of cases to be tackled. This is akin to non-dimensionalisation against a reference loading, as is done for transient cases with variable loads, such as in [26, 27, 87]. The boundary and cavitation conditions are specified as in the full EHL case, such that

$$P(X_{in}) = P(X_c) = P'(X_c) = 0. \tag{5.4}$$

Although $P(X_{in}) = P(X_c) = 0$ is enforced at the boundaries, $P'(X_c) = 0$ becomes one of the conditions to be satisfied by the solution. This is achieved by finding the value of X_c such that the above cavitation condition is satisfied. This is unknown *a priori*, and as such forms part of the set of solution variables which must be found. In equations (5.3) and (5.4) X_{in} is defined to be equal to X_c minus a given, constant, domain size, D. As discussed in Chapter 4, this is chosen to be sufficiently large as to not influence the solution in the contact region, and hence the friction. Precise details of X_c and the role it plays in the solution are detailed in the next section.

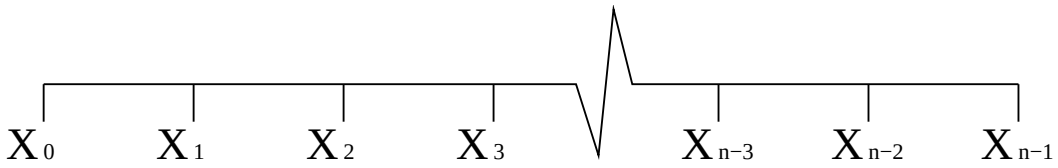

Figure 5.1: A uniform computational mesh

5.1.2 Numerical model

Having specified the mathematical model, it is simple to formulate the numerical problem using finite difference approximations on a uniform grid using n nodes, numbered $i = 0,\ldots,n-1$, as in Figure 5.1. On this mesh, the values of X_i can be calculated by $X_i = X_c - D + i\Delta X$, where ΔX is the spacing between the grid points. First, given equation (5.2), clearly $\frac{\mathrm{d}H}{\mathrm{d}X} = X$. Hence the discretisation of the Reynolds equation, (5.1), gives

$$\frac{\frac{(P_{i+1}-P_i)H^3_{i+\frac{1}{2}}}{\Delta X} - \frac{(P_i-P_{i-1})H^3_{i-\frac{1}{2}}}{\Delta X}}{\Delta X} - \lambda X_i = 0.$$

This approximation is derived using a central difference at each of $i+1/2$ and $i-1/2$, both of which are second order accurate. The central difference is then taken between these two to form the above equation. The second order derivative is approximated by the difference of two first order differences. This uses the film thickness at the midpoint in the cell, defined as $H^3_{i\pm\frac{1}{2}} = \frac{H_i^3+H_{i\pm1}^3}{2}$. Alternatives to this approximation exist, e.g. $H^3_{i\pm\frac{1}{2}} = (\frac{H_i+H_{i\pm1}}{2})^3$. Simplifying and rearranging gives

$$\frac{H^3_{i+\frac{1}{2}}P_{i+1} - (H^3_{i+\frac{1}{2}} + H^3_{i-\frac{1}{2}})P_i + H^3_{i-\frac{1}{2}}P_{i-1}}{(\Delta X)^2} - \lambda X_i = 0, \tag{5.5}$$

for $i = 1,\ldots,n-2$. The film thickness equation becomes

$$H_i = H_0 + \frac{X_i^2}{2}, \tag{5.6}$$

with the force balance

$$\sum_{i=0}^{n-2} \frac{P_i + P_{i+1}}{2}\Delta X = L. \tag{5.7}$$

The cavitation boundary condition in equation (5.4) can be given, as shown in Section 2.3, using a second order backwards difference stencil,

$$\frac{3P_{n-1} - 4P_{n-2} + P_{n-3}}{2\Delta X} = 0, \tag{5.8}$$

and Dirichlet boundary values $P_0 = P_{n-1} = 0$ are imposed. The cavitation condition above then reduces to

$$\frac{-4P_{n-2} + P_{n-3}}{2\Delta X} = 0. \tag{5.9}$$

As previously mentioned, the cavitation position is an extra unknown to be solved for. X_c is the value of X that satisfies the cavitation condition (5.9). Using a sliding grid (moving domain), as detailed in Section 5.1.4, the right-hand boundary can be moved such that X_c is at the cavitation point. In other words, the domain $[X_{in}, X_c]$ is repeatedly moved until X_c satisfies (5.9) to within some tolerance.

5.1.3 Friction

The friction calculation for the model problem proposed in this chapter is given by

$$F(P) = \int_{X_{in}}^{X_c} \left(-\frac{\partial P}{\partial X}\frac{H}{2} + \frac{\chi}{H} \right) \mathrm{d}X. \tag{5.10}$$

In this, χ is used to emulate the sliding term in equation (4.3). This is necessary for this problem because the viscosity is simply $\eta = 1$, and the individual roller speeds, u_a and u_b, are not defined for this model problem. As such χ is taken to be a combination of the two factors, i.e. $\chi \equiv \eta(u_b - u_a)$. By varying χ it is possible to introduce a sliding component to the friction, and results are presented that show this to be sufficient to illustrate how the adaptive mesh should change for different sliding values. Discretising (5.10) over the cell mid-points, yields

$$F(P) = -\sum_{i=0}^{n-2} \frac{(P_{i+1} - P_i)}{2} H_{i+\frac{1}{2}} + \sum_{i=0}^{n-2} \frac{\chi}{H_{i+\frac{1}{2}}} \Delta X. \tag{5.11}$$

5.1.4 Sliding grid solution method

Having defined a system of equations to solve, attention is turned to the solution method. It should be noted that this solution method has not been designed with speed or efficiency

in mind, rather as a simple, robust way to solve the model problem. The sliding grid approach outlined below is used because it allows X_c to vary continuously, thus easing the derivation of the adjoint system, and also allowing arbitrary accuracy of solving the cavitation boundary condition.

There are three steps (which must be repeated) to solving the numerical system as defined by equations (5.5)-(5.8). They are:

1. Solve the linear system (5.5) for P
2. Find the correct X_c for the current H_0 (using (5.9))
3. Find the correct H_0 for the input parameters L and λ (using (5.7))

Each of these is discussed in turn, with the overall description of the algorithm following in Figure 5.3.

5.1.4.1 1: Solve for P

The discretisation shown in equation (5.5) leads to a tri-diagonal matrix, which for given values of H (and hence H_0), λ, ΔX, and X_i (and hence X_c), a solution for P is easily obtained using (banded) LU decomposition. Having found the solution for P, the algorithm moves on to step 5.1.4.2.

5.1.4.2 2: Find X_c

Given a solution for P (solved for in the previous step), the cavitation boundary condition (5.9) can be evaluated. If the gradient is sufficiently close to zero ($\left|\frac{-4P_{n-2}+P_{n-3}}{2\Delta X}\right| < 10^{-8}$ in this case), the cavitation point X_c has already been found and the algorithm proceeds to step 5.1.4.3. If not, X_c moves according to Figure 5.2. Clearly, in Figure 5.2 (a), the gradient is positive at X_c, and the boundary is too far to the right. Therefore, X_c (and hence the grid) should be moved left. Conversely, in Figure 5.2 (b), the gradient is negative because the boundary is too far left, and so X_c should be moved to the right.

The new position of X_c is determined by the repeated use of a bisection algorithm. Given that the cavitation position must be to the right of the centre of the contact $(X = 0)$, and starting with a large value of X_c (such as that pictured in Figure 5.2 (a)), it is simple to form the initial solution bracket. At this point, X_c is set to be the mid-point of the interval.

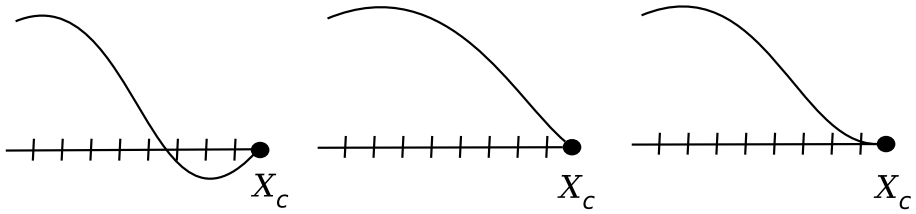

(a) $P'(X_c) > 0$ (b) $P'(X_c) < 0$ (c) $P'(X_c) = 0$

Figure 5.2: The three cases for the right-hand boundary. When deciding how to move this boundary position, cases (a) and (b) result in the mesh moving either left or right respectively.

Consequently, X_{in} is recalculated as $X_c - D$ and the values of X_i and H_i are calculated for all of the n grid points, and the algorithm returns to step 5.1.4.1. Once step 5.1.4.1 has been completed again (assuming that P' is not yet close enough to zero), one of the right or left-hand brackets will be set to the value of X_c, depending on the sign of $P'(X_c)$. X_c can then be set to the midpoint of this new bracket and the procedure repeated.

In Chapter 7, where one solve for a given value of X_c takes longer ($O(n^2)$ compared to $O(n)$ here), a faster way of finding X_c is introduced.

5.1.4.3 3: Find H_0

Having found a solution for P and X_c, the force balance equation (5.7) must be evaluated. If the force balance residual, equation (5.13) defined in Section 5.2, is sufficiently small (again, 10^{-8} for the work in this chapter), the whole system of equations has been satisfied and the solution has been obtained. If it is not, then H_0 must be adjusted according to the following procedure. The reason for this approach has been explained in Section 2.4.2, but is recapped here for convenience. If the sum of the pressures is currently greater than the applied load, the pressure generated in forcing the liquid through the gap is too large, and H_0 must be increased. If the sum of the pressures is less than the applied load, the pressures generated are insufficient to balance the applied load, and so the surfaces must move together, i.e. H_0 must be decreased. This happens according to

$$H_0 \leftarrow H_0 - \omega \left(L - \sum_{i=0}^{n-2} \frac{P_i + P_{i+1}}{2} \Delta X \right),$$

where ω is a relaxation parameter (typically 0.2 here). Once H_0 has been adjusted, the H_i values can be recalculated and the algorithm goes back to step 5.1.4.1.

```
1 Solve for P
2 If P'( X_c ) > TOL
3 Then
4    Adjust  X_c
5    Goto 1
6 Else If FBres > TOL
7 Then
8    Adjust H_0
9    Goto 1
10 END
```

Figure 5.3: Model problem solution algorithm

5.1.4.4 Overall algorithm

The overall process is illustrated in Figure 5.3.

Before moving on to the formulation of the adjoint problem, an alternative approach to the sliding grid method is discussed. One idea which would keep X_c as a continuous variable, would be to fix the left hand boundary of the grid, and "concertina" the grid to find the correct cavitation position. So a solution procedure could be followed, similar to that above, only instead of shifting all of the grid points by the same amount as X_c is moved, the mesh points become closer together as X_c moves left, and further apart as X_c moves right. One disadvantage to this approach would be that ΔX would then be dependent on X_c, and so extra terms would be introduced into the Jacobian through the force balance and the cavitation condition. Whilst not a consideration for the model problem introduced in this chapter, a further disadvantage in the full EHL line contact case would be the need to recalculate the discrete kernel used in the deformation calculation.

5.2 Adjoint problem

The residual equations implicitly solved for in achieving the solution detailed in the previous section, are listed here for $i = 1, \ldots, n-2$,

$$R_i = \Delta X \left(\lambda X_i - \frac{H^3_{i+\frac{1}{2}} P_{i+1} - (H^3_{i+\frac{1}{2}} + H^3_{i-\frac{1}{2}}) P_i + H^3_{i-\frac{1}{2}} P_{i-1}}{(\Delta X)^2} \right) = 0, \tag{5.12}$$

along with,

$$R_{H_0} = L - \sum_{i=0}^{n-2} \frac{P_i + P_{i+1}}{2} \Delta X = 0, \tag{5.13}$$

and

$$R_{X_c} = -\frac{3P_{n-1} - 4P_{n-2} + P_{n-3}}{2\Delta X} = 0. \tag{5.14}$$

Unlike standard pointwise finite difference residuals associated with the discretisation of the Reynolds equation, the residual equations here have been multiplied through by ΔX. In order to understand why this scaling is necessary, it is important to remember what is happening. The solution of the adjoint system should give the sensitivity of the friction calculation to the residuals [77]. Since the friction is an integral quantity, each pointwise shear stress value is effectively multiplied by the area over which it is acting, ΔX. Equally, in order to find the total effect of each residual, it must be multiplied by the area over which it acts. This makes the finite difference residuals roughly analogous to finite element residuals. So now, each element of friction calculated is related to an equivalent element of residual. The other two residuals, equations (5.13) and (5.14), have no need for such scaling. This is because the whole integral computed when calculating the friction is sensitive to both H_0 and X_c. This means there is no mesh dependence of the right-hand side of the adjoint, and so no scaling is necessary.

For uniform meshes it is equally valid to remove the mesh dependency from the right-hand side of the adjoint system and use standard finite difference residuals to get the adjoint system, i.e. relate pointwise residuals to pointwise friction values. This is because all of the grid points contribute equally to the overall quantity calculated. However, this approach is not valid for non-uniform meshes, because no account is then taken of the amount by which a particular element contributes to the overall quantity calculated, and so the effect on the friction from coarse regions of the mesh would be underestimated.

5.2.1 Jacobian

Here, the non-zero entries in the Jacobian, made up of the derivatives of the residuals (5.12)-(5.14) with respect to the $n-2$ pressures, H_0 and X_c, are presented.

Once transposed, these form the system of equations to be solved for the adjoint problem (3.8). The first terms to consider are those associated with the Reynolds residuals. Clearly, each residual equation depends on three pressures, the pressure at the same place,

and the ones on either side:

$$\frac{\partial R_i}{\partial P_{i-1}} = -\left(\frac{H^3_{i-\frac{1}{2}}}{\Delta X}\right), \qquad \frac{\partial R_i}{\partial P_i} = \left(\frac{H^3_{i+\frac{1}{2}} + H^3_{i-\frac{1}{2}}}{\Delta X}\right), \qquad \frac{\partial R_i}{\partial P_{i+1}} = -\left(\frac{H^3_{i+\frac{1}{2}}}{\Delta X}\right),$$

giving the Jacobian its main tri-diagonal structure. The other two terms on each row of the Jacobian are

$$\frac{\partial R_i}{\partial H_0} = -3\left(\frac{H^2_{i+\frac{1}{2}}P_{i+1} - (H^2_{i+\frac{1}{2}} + H^2_{i-\frac{1}{2}})P_i + H^2_{i-\frac{1}{2}}P_{i-1}}{\Delta X}\right)$$

where $H^2_{i\pm\frac{1}{2}} = \frac{H^2_i + H^2_{i\pm1}}{2}$, and

$$\frac{\partial R_i}{\partial X_c} = \lambda - 3\left(\frac{\varepsilon^2_{i+\frac{1}{2}}P_{i+1} - (\varepsilon^2_{i+\frac{1}{2}} + \varepsilon^2_{i-\frac{1}{2}})P_i + \varepsilon^2_{i-\frac{1}{2}}P_{i-1}}{\Delta X}\right)$$

where $\varepsilon^2_{i\pm\frac{1}{2}} = \frac{H^2_i X_i + H^2_{i\pm1}X_{i\pm1}}{2}$. The remaining terms to consider come from equations (5.13) and (5.14),

$$\frac{\partial R_{H_0}}{\partial P_j} = -\Delta X, \qquad \frac{\partial R_{H_0}}{\partial H_0} = 0, \qquad \frac{\partial R_{H_0}}{\partial X_c} = 0,$$

$$\frac{\partial R_{X_c}}{\partial P_{n-3}} = -\frac{1}{2\Delta X}, \qquad \frac{\partial R_{X_c}}{\partial P_{n-2}} = \frac{2}{\Delta X}, \qquad \frac{\partial R_{X_c}}{\partial H_0} = 0, \qquad \frac{\partial R_{X_c}}{\partial X_c} = 0.$$

The structure of the Jacobian therefore is an arrow, as shown in Figure 5.4.

5.2.2 Adjoint right-hand side

Here, the values for the right-hand side of the adjoint system are derived. These represent the sensitivity of the friction to each of the variables.

First, the discrete friction calculation, (5.11), is restated as

$$F(P) = -\sum_{i=0}^{n-2}\frac{(P_{i+1} - P_i)}{2}H_{i+\frac{1}{2}} + \sum_{i=0}^{n-2}\frac{\chi}{H_{i+\frac{1}{2}}}\Delta X.$$

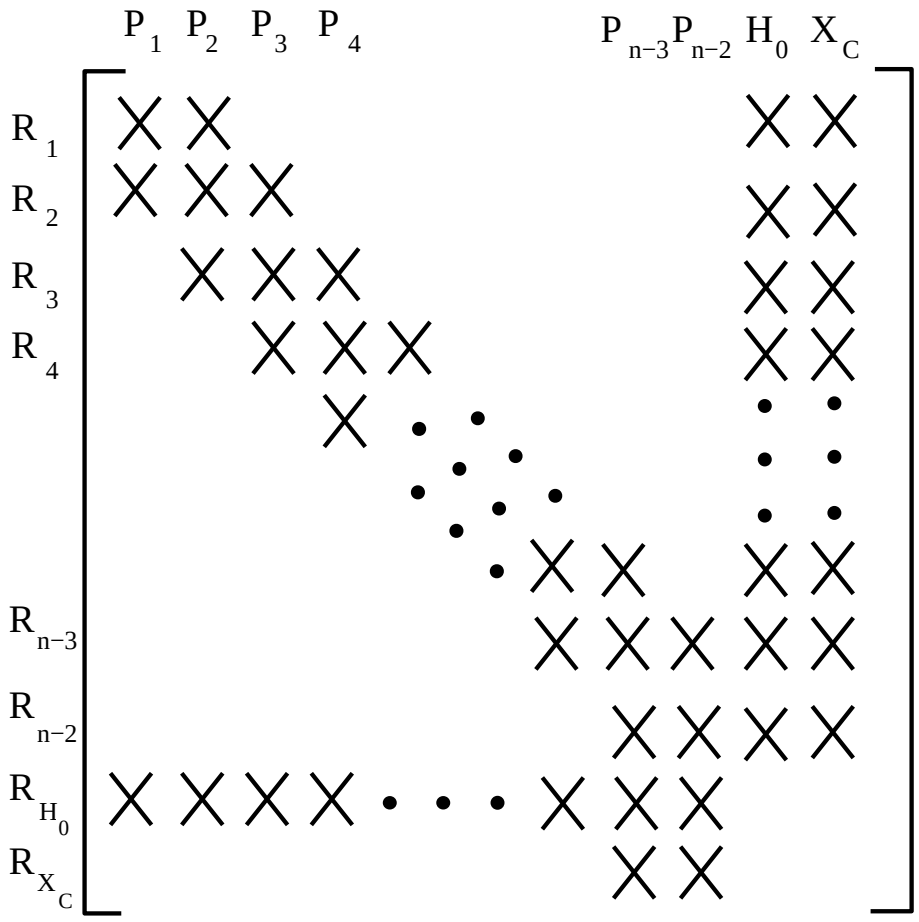

Figure 5.4: Model problem Jacobian sparsity pattern

The sensitivities of this sum to the pressure variables P_j, $j = 1 \ldots n-2$, are given by

$$\frac{\partial F}{\partial P_j} = -\frac{H_{j-\frac{1}{2}} - H_{j+\frac{1}{2}}}{2}.$$

Next, the sensitivity to H_0 is considered. Noting that $\frac{\partial H}{\partial H_0} = 1$,

$$\frac{\partial F}{\partial H_0} = -\sum_{i=0}^{n-2} \frac{P_{i+1} - P_i}{2} + \sum_{i=0}^{n-2} \frac{-\chi}{H_{i+\frac{1}{2}}^2} \Delta X \tag{5.15}$$

$$= -\frac{P_{n-1} - P_0}{2} - \sum_{i=0}^{n-2} \frac{\chi}{H_{i+\frac{1}{2}}^2} \Delta X. \tag{5.16}$$

Given that since

$$P(X_{in}) = P(X_c) = 0, \tag{5.17}$$

$P_0 = P_{n-1} = 0$, it is immediately clear the first term is identically equal to zero, and so the expression becomes

$$\frac{\partial F}{\partial H_0} = -\sum_{i=0}^{n-2} \frac{\chi}{H_{i+\frac{1}{2}}^2} \Delta X.$$

Last, the sensitivity to the cavitation boundary position, X_c, is found. By taking only the first term of the integrand in equation (5.10), and noting that $\frac{\partial H}{\partial X_c} = X$, the expression becomes

$$\frac{\partial F^1}{\partial X_c} = -\sum_{i=0}^{n-2} \frac{P_{i+1} - P_i}{2} X_{i+\frac{1}{2}}.$$

Finally, considering the second part of (5.11),

$$\frac{\partial F^2}{\partial X_c} = +\sum_{i=0}^{n-2} \frac{-\chi X_{i+\frac{1}{2}}}{H_{i+\frac{1}{2}}^2} \Delta X,$$

which put altogether, gives

$$\frac{\partial F}{\partial X_c} = -\sum_{i=0}^{n-2} \frac{P_{i+1} - P_i}{2} X_{i+\frac{1}{2}} - \sum_{i=0}^{n-2} \frac{\chi X_{i+\frac{1}{2}}}{H_{i+\frac{1}{2}}^2} \Delta X.$$

5.2.3 Sparse matrix solution method

The numerical package used to solve the adjoint system defined in the previous two sections is SPARSKIT [64]. The sparse matrix format used is the compressed row format,

and the specific method is ILUT preconditioned GMRES (Generalised Minimal Residual).

5.3 Results

In this section, a series of results are presented starting with uniform meshes and global refinement. This is followed by non-uniform adaptivity, driven by the adjoint solution. The method provides similar tables of results for all loadings and so a single representative case is presented in detail here.

5.3.1 Uniform mesh results

Before considering a sequence of locally refined meshes, results on uniform meshes are presented. This case has been solved for a nominal load of $L = 5.0$, and sliding parameter $\chi = 20.0$. Table 5.1 shows the performance of the predicted error in the friction, as calculated using the adjoint approach, by comparing it with the true error when solving on the next mesh. Note that in this context the term error is used to mean $F(u_h^H) - F(u_h)$ (as opposed to $F(u_h^H) - F(u)$ where u is the unknown exact solution of the continuous problem).

The first column of the table shows the grid level for the coarser of the two grids, and has a number of points equal to $2^{g+1} + 1$. Using the solution from this grid, interpolated onto grid $g+1$, a friction value is calculated which is shown in the second column. Column 3 shows the correction to this friction, as calculated using the adjoint system solved on the coarse grid g. The corrected friction is shown in column 4, with the "true" friction value for grid $g+1$ shown in column 5. The measured error between columns 2 and 5 is shown in column 6. The final column shows the ratio of the measured error to the estimated error (known as the effectivity index). One of the central beliefs of this work is that with increasing mesh resolution the estimated error should become increasingly close to the measured error. This is because the higher order terms not accounted for in the Taylor expansions in (3.3) and (3.1) will become less significant with increasing mesh resolution, so the system solved will be a better approximation. Since the effectivity index can be seen to approach unity as the number of mesh points used increases, this gives a strong indication that for uniform grids the friction error estimate is remarkably accurate. The "correction" procedure can therefore be used with a high degree of confidence. If

Grid (g)	Interpolated Fric. (g)	Calculated correction	Corrected Fric. (g)	Friction ($g+1$)	Measured Error	Effectiv. Index
5	87.95668	15.27956	72.67711	68.02241	19.93427	1.304
6	68.67781	2.64095	66.03686	66.37680	2.30101	0.871
7	66.52919	0.31057	66.21862	66.31442	0.21477	0.691
8	66.35216	0.01504	66.33712	66.34818	0.00398	0.264
9	66.35761	-0.00255	66.36015	66.36125	-0.00365	1.432
10	66.36361	-0.00124	66.36484	66.36496	-0.00135	1.094
11	66.36555	-0.00037	66.36592	66.36593	-0.00038	1.035
12	66.36608	-0.00010	66.36618	66.36618	-0.00010	1.016

Table 5.1: Adjoint based inter-grid friction error on uniform meshes for a model free boundary problem; $L = 5$, $\chi = 20.0$

the adjoint solution were not available, it would be necessary to keep computing on finer and finer grids until the friction changed by less than ε, at which point the last (and most expensive) solution does not yield a friction value that is significantly more accurate than the previous. By using the adjoint estimate, the same accuracy will be achieved without the cost of computing a solution on the finest mesh in this sequence. This is a significant computational advantage.

Having considered in detail the case in Table 5.1, more results are presented for three different values of χ; 0.0, 1.0 and 2.0. These are given in Tables 5.2 to 5.4. In addition, Table 5.5 shows the predicted correction when the correction components from the H_0 and X_c adjoints are neglected, and only the corrections from the P adjoints are used. In this case the effectivity index not only does not converge to a value of 1.0, but is approximately a factor of three out. This shows the importance of the model used and the subsequent adjoint formulation.

5.3.2 Non-uniform and adaptive mesh results

Table 5.6 shows that with non-uniform meshes the adjoint error estimation approach is still reliable, in the sense that the ratio of the predicted correction to the actual difference in friction on consecutive meshes still tends to one as the meshes are refined. Note that in order to obtain these results global mesh refinement, based upon element bisection, has still been used, but now the initial mesh (and hence all subsequent meshes) is non-uniform. Clearly the residual equation (5.12) at an interface between different levels of refinement must take account of the non-uniformity in ΔX. One approach would be to define a different finite difference stencil based on the different ΔX either side of the

g	grid g func. value	error between grids g, $g+1$	computed correction	effectivity index
5	5.503589	-7.354570e-01	-6.906117e-01	9.390238e-01
6	4.768132	-3.514585e-01	-3.694314e-01	1.051138
7	4.416673	-1.833214e-01	-1.876365e-01	1.023538
8	4.233352	-9.324546e-02	-9.410017e-02	1.009166
9	4.140107	-4.689058e-02	-4.708537e-02	1.004154
10	4.093216	-2.350241e-02	-2.354944e-02	1.002001
11	4.069714	-1.176439e-02	-1.177598e-02	1.000984
12	4.057949	-5.885350e-03	-5.888227e-03	1.000489
13	4.052064	-2.943447e-03	-2.944163e-03	1.000243
14	4.049120	-1.471914e-03	-1.472092e-03	1.000121
15	4.047649	-7.360050e-04	-7.360488e-04	1.000059
16	4.046913	-3.680116e-04	-3.680250e-04	1.000036

Table 5.2: Adjoint based inter-grid friction error on uniform meshes for a model free boundary problem; $L = 5$, $\chi = 0.0$

g	grid g func. value	error between grids g, $g+1$	computed correction	effectivity index
5	8.550387e+00	-8.297460e-01	-3.698735e-01	4.457671e-01
6	7.720641e+00	-3.065513e-01	-2.688710e-01	8.770834e-01
7	7.414090e+00	-1.262497e-01	-1.310124e-01	1.037724e+00
8	7.287840e+00	-6.138486e-02	-6.465935e-02	1.053344e+00
9	7.226455e+00	-3.162180e-02	-3.269289e-02	1.033872e+00
10	7.194833e+00	-1.618346e-02	-1.648038e-02	1.018347e+00
11	7.178650e+00	-8.197283e-03	-8.274910e-03	1.009470e+00
12	7.170452e+00	-4.126227e-03	-4.146044e-03	1.004803e+00
13	7.166326e+00	-2.070142e-03	-2.075144e-03	1.002416e+00
14	7.164256e+00	-1.036843e-03	-1.038098e-03	1.001211e+00
15	7.163219e+00	-5.188670e-04	-5.191804e-04	1.000604e+00
16	7.162700e+00	-2.595404e-04	-2.596229e-04	1.000318e+00

Table 5.3: Adjoint based inter-grid friction error on uniform meshes for a model free boundary problem; $L = 5$, $\chi = 1.0$

g	grid g func. value	error between grids g, $g+1$	computed correction	effectivity index
5	1.159718e+01	-9.240350e-01	-4.913524e-02	5.317465e-02
6	1.067315e+01	-2.616441e-01	-1.683107e-01	6.432811e-01
7	1.041151e+01	-6.917809e-02	-7.438827e-02	1.075316e+00
8	1.034233e+01	-2.952425e-02	-3.521853e-02	1.192868e+00
9	1.031280e+01	-1.635302e-02	-1.830042e-02	1.119085e+00
10	1.029645e+01	-8.864516e-03	-9.411308e-03	1.061683e+00
11	1.028759e+01	-4.630173e-03	-4.773844e-03	1.031029e+00
12	1.028296e+01	-2.367103e-03	-2.403861e-03	1.015528e+00
13	1.028059e+01	-1.196836e-03	-1.206125e-03	1.007761e+00
14	1.027939e+01	-6.017713e-04	-6.041047e-04	1.003877e+00
15	1.027879e+01	-3.017290e-04	-3.023121e-04	1.001932e+00
16	1.027849e+01	-1.510691e-04	-1.512208e-04	1.001004e+00

Table 5.4: Adjoint based inter-grid friction error on uniform meshes for a model free boundary problem; $L = 5$, $\chi = 2.0$

g	grid g func. value	error between grids g, $g+1$	computed correction	effectivity index
5	1.159718e+01	-9.240350e-01	-1.209958e+00	1.309429e+00
6	1.067315e+01	-2.616441e-01	-4.992491e-01	1.908123e+00
7	1.041151e+01	-6.917809e-02	-2.360559e-01	3.412293e+00
8	1.034233e+01	-2.952425e-02	-1.150627e-01	3.897226e+00
9	1.031280e+01	-1.635302e-02	-5.685207e-02	3.476549e+00
10	1.029645e+01	-8.864516e-03	-2.826390e-02	3.188431e+00
11	1.028759e+01	-4.630173e-03	-1.409213e-02	3.043542e+00
12	1.028296e+01	-2.367103e-03	-7.036178e-03	2.972484e+00
13	1.028059e+01	-1.196836e-03	-3.515625e-03	2.937431e+00
14	1.027939e+01	-6.017713e-04	-1.757197e-03	2.920041e+00
15	1.027879e+01	-3.017290e-04	-8.784450e-04	2.911371e+00
16	1.027849e+01	-1.510691e-04	-4.391841e-04	2.907173e+00

Table 5.5: Adjoint based inter-grid friction error on uniform meshes for a model free boundary problem; $L = 5$, $\chi = 1.0$. Only the P_i components of the estimate were used in calculating the estimate, not the H_0 or X_c contributions for this case

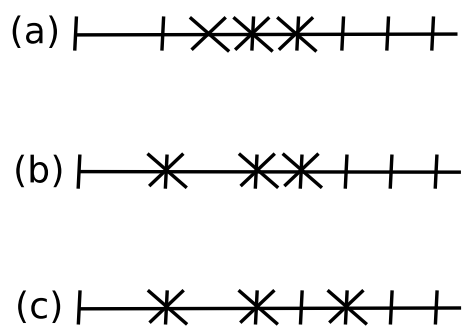

Figure 5.5: Three possible finite difference stencils for the interface between refinement levels. Case (a) shows the stencil for a fine mesh point. The left hand value would need recovering from the neighbouring points; Case (b) shows the case for a non-symmetric stencil. Care would need to be taken over the weightings of the node values to preserve second order accuracy; Case (c) shows the coarse grid stencil which is used in this work

interface. A further approach would be to treat the interface point as a fine grid point, using interpolation to get values for the missing mesh point on the coarse side of the interface. The approach taken here, however, is simply to treat the equation at the interface as a coarse grid point. This is the simplest approach, since the coarse stencil can now be applied to the interface point by ignoring the first mesh point on the refined side of the interface. The three different approaches are illustrated in Figure 5.5.

Having demonstrated that the predicted error is still reliable on non-uniform meshes it is now possible to use these values as the basis for local, rather than global, mesh refinement. It should be noted, however, that the correction value given by the last term in equation (3.9) is just a single number indicating the current error in the friction and so further information is required in order to determine where the contribution to this error is the greatest. In the following example we base the local refinement on the magnitude of $(\Psi_h^H)_i \times (R_h(u_h^H))_i$ locally, and refer to this as the correction component of mesh point i [77]. Figure 5.6 shows the computed correction components across the domain after a number of local refinements have been undertaken. In this case, the sliding-like friction χ has been set to a value of 20, with the load L set to 5.0. Starting from the left it may be seen that the contribution to the estimated friction error gradually increases until the first region of local refinement is reached, whereupon it drops suddenly. The contribution to the error then grows again until the next region of local refinement is reached, and so on. The contribution to the error is always kept below an imposed tolerance of 10^{-7} in this particular example. The dark regions of the graph are due to the oscillating nature of the residual. Figure 5.7 shows the overall effectiveness of this strategy compared to the use of uniform mesh refinement. In this case the plot is of the error in the friction

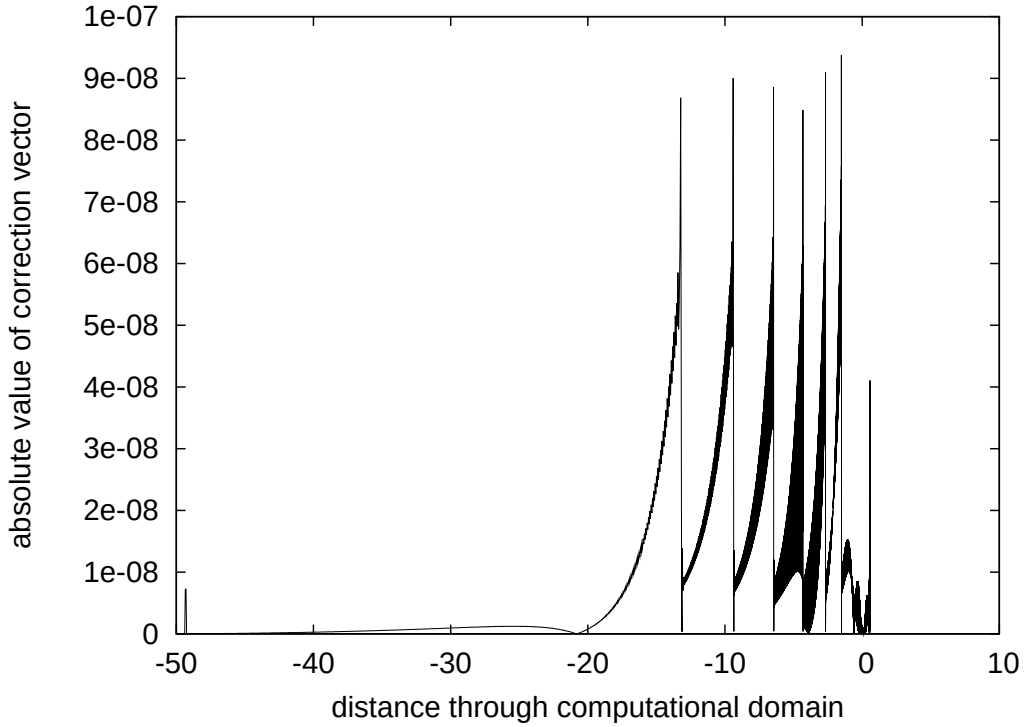

Figure 5.6: Plot showing the absolute value of the correction vector, and how it is distributed through local mesh refinement, for a model free boundary problem; $L = 5$, $\chi = 20.0$

(as compared against a friction value calculated on a so-called "truth mesh" containing approximately 250 000 equally spaced points) versus the total number of nodes present in the mesh. Unsurprisingly the uniform refinement strategy converges most slowly, the next curve shows the error in the friction on the locally refined (adapted) mesh, whilst the final curve shows the error in the corrected friction value on the adapted mesh. Figure 5.8 again shows the computed correction components across the domain, but this time for pure rolling friction ($\chi = 0.0$). A similar refinement pattern is shown, but the refinement levels are more spread out through the domain, indicating that, as expected, a different refinement is required for a different functional.

5.4 Summary

Results have been presented which show that the adjoint error estimation approach may be used effectively for a non-linear incompressible isoviscous hydrodynamic lubrication model problem containing a free boundary due to the cavitation condition. The effectivity

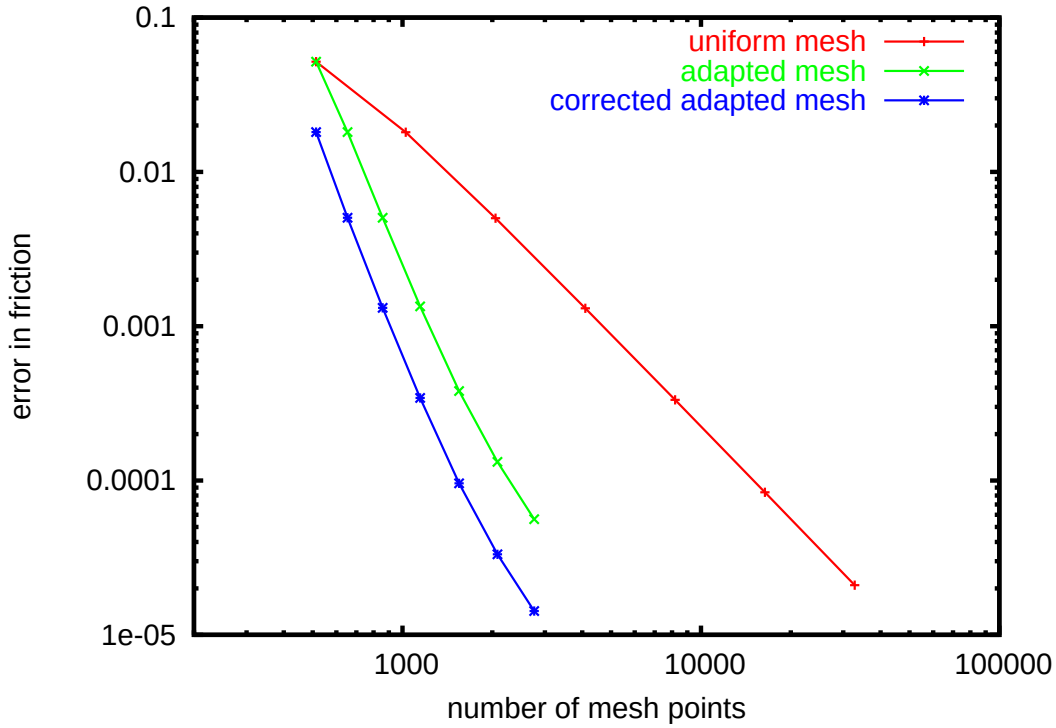

Figure 5.7: Plot showing error reduction for uniform and adaptive grids for a model free boundary problem; $L = 5$, $\chi = 20.0$

Grid (g)	Interpolated Fric. (g)	Calculated correction	Corrected Fric. (g)	Friction ($g+1$)	Measured Error	Effectiv. Index
5	87.66173	-4.56301	92.22474	67.98769	19.67404	-4.311
6	68.65988	2.62800	66.03187	66.36806	2.29181	0.872
7	66.52502	0.30892	66.21611	66.31220	0.21282	0.688
8	66.35111	0.01462	66.33649	66.34762	0.00348	0.238
9	66.35734	-0.00266	66.36000	66.36111	-0.00377	1.417
10	66.36354	-0.00127	66.36481	66.36492	-0.00138	1.093
11	66.36553	-0.00038	66.36591	66.36592	-0.00039	1.035
12	66.36608	-0.00010	66.36618	66.36618	-0.00010	1.016

Table 5.6: Adjoint based inter-grid friction error on non-uniform meshes, each with the same refinement pattern, for a model free boundary problem; $L = 5$, $\chi = 20.0$

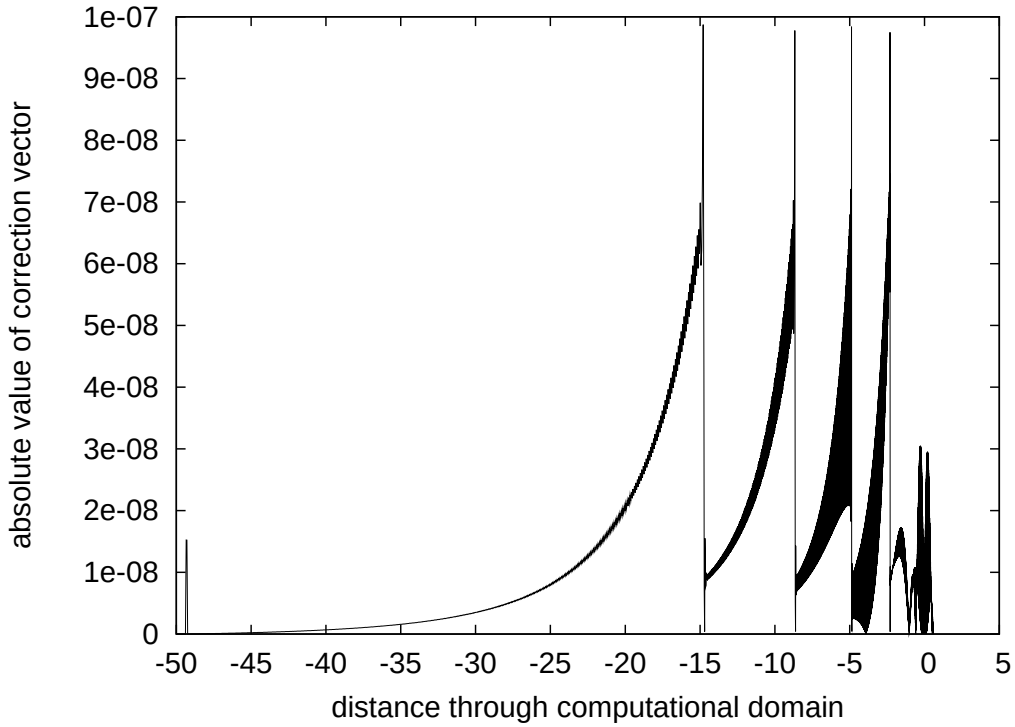

Figure 5.8: Plot showing the absolute value of the correction vector, and how it is distributed through local mesh refinement, for a model free boundary problem; $L = 5$, $\chi = 0.0$

of this estimate on uniformly refined meshes may be used to provide a reliable stopping criterion without the need to solve on the finest mesh. Moreover, it is demonstrated that adjoint variables corresponding to X_c and H_0 are required to ensure quantitative accuracy of the error estimate. Furthermore, the components of the correction term are shown to provide an appropriate basis for determining where to refine locally. The resulting meshes can yield solutions of a considerably greater accuracy (in terms of friction, for example) than obtained on correspondingly sized uniform grids. To our knowledge this is the first time that a free boundary problem has been solved adaptively in this manner, and the results have been published in [34] and [35]. Although these results are promising, it is also clear that more sophisticated refinement procedures such as those presented in [79] and [3], may pay dividends. However, the main focus of this research is on applying adjoint techniques to full EHL cases. Thus, although automatic refinement is introduced to the full EHL problem in Chapter 7, the attention in the chapters that follow is largely on extending the model. In the next chapter, the application of the adjoint error estimation will be extended to a full hydrodynamic lubrication test case.

Chapter 6

Hydrodynamic Lubrication

In this chapter, a compressible piezo-viscous hydrodynamic lubrication problem is introduced. This is an industrially relevant problem that will serve as an intermediate step between the model problem of the previous chapter and the full EHL problem described in the following chapter. An analysis of the formulation of the residual equations, and hence the Jacobian, will facilitate an understanding of the adjoint error estimation procedure when applied to complex systems of equations, and hence that used for EHL. Two different approaches will be explored: one based upon a 'compact' Jacobian; the other an 'expanded' Jacobian. This is because the variables for viscosity and density can be considered either as functions of P or as independent variables in their own right.

Hydrodynamic lubrication is a physical phenomenon found where the contact area is sufficiently large, or the load is light enough, such that deformation of the contacting components does not occur or is negligible. Pressure is generated to separate the surfaces through motion of the lubricant (hence the name dynamic). This study of hydrodynamic lubrication, whilst not the main goal of this work, will prove useful in that it augments the previous model problem with both non-linear viscosity and density, thus taking it a step towards the full EHL regime. However, since the surface geometry is considered to be fixed, there is no global deformation calculation which means that the Jacobian of the discretised system of equations is still sparse.

6.1 Forward problem

To begin this section, the mathematical model underlying hydrodynamic lubrication is defined, followed by the discretised equations. Following this, a brief description of the solution method is given, indicating the main differences from that given for the earlier models. Sample forward solutions are also given.

6.1.1 Mathematical model

The non-dimensionalised mathematical problem is defined by the following equations: The Reynolds equation

$$\frac{\partial}{\partial X}\left(\frac{\overline{\rho}H^3}{\lambda\overline{\eta}}\frac{\partial P}{\partial X}\right)-\frac{\partial(\overline{\rho}H)}{\partial X}=0 \tag{6.1}$$

and the film thickness

$$H=H_0+\frac{X^2}{2}. \tag{6.2}$$

The viscosity is defined using the Barus equation [2],

$$\overline{\eta}=e^{\overline{\alpha}P}, \tag{6.3}$$

whilst the density is given by [17],

$$\overline{\rho}=\frac{0.59\times10^9+1.34Pp_h}{0.59\times10^9+Pp_h}. \tag{6.4}$$

As before, force balance is specified according to

$$\int_{-\infty}^{\infty}P\,\mathrm{d}X=\frac{\pi}{2}. \tag{6.5}$$

As stated, the Barus viscosity model is used for viscosity in this chapter. The Roelands model [62] has been shown to fit the empirical data better at high loads, but this adds little extra to the analysis at this stage, other than unnecessary complication.

6.1.2 Numerical model

By discretising the above equations on a regular mesh using the finite difference stencils defined earlier, the following set of discrete equations can be found. The Reynolds

equation becomes:

$$\left(\frac{(P_{i+1}-P_i)\varepsilon_{i+\frac{1}{2}}-(P_i-P_{i-1})\varepsilon_{i-\frac{1}{2}}}{(\Delta X)^2}\right)-\left(\frac{\overline{\rho}_i H_i-\overline{\rho}_{i-1}H_{i-1}}{\Delta X}\right)=0, \tag{6.6}$$

where $\varepsilon_i=\frac{H_i^3\overline{\rho}_i}{\lambda\overline{\eta}_i}$, $\varepsilon_{i\pm\frac{1}{2}}=(\varepsilon_i+\varepsilon_{i\pm1})/2$ and H_i is given by $H_i=H_0+\frac{X_i^2}{2}$. The viscosity equation is simply

$$\overline{\eta}_i=e^{\overline{\alpha}P_i}, \tag{6.7}$$

and the density equation becomes:

$$\overline{\rho}_i=\frac{0.59\times10^9+1.34P_ip_h}{0.59\times10^9+P_ip_h}. \tag{6.8}$$

Finally, a discrete force balance equation is required

$$\sum_{i=0}^{n-2}\frac{P_i+P_{i+1}}{2}\Delta X=\frac{\pi}{2}, \tag{6.9}$$

along with the boundary conditions:

$$P_0=P_{n-1}=0, \qquad R_{X_c}=-\frac{3P_{n-1}-4P_{n-2}+P_{n-3}}{2\Delta X}. \tag{6.10}$$

Before going on to talk about the residual equations in more detail, and the corresponding adjoint problem, the solution process is briefly outlined.

6.1.3 Solution process

The solution to the forward problem is obtained in a similar manner to that proposed in Chapter 5, with a small number of minor differences. The main hydrodynamic solver solves the equations (6.6)-(6.9) so that, as well as obtaining solutions for the main variables P, $\overline{\eta}$ and $\overline{\rho}$, the force balance equation is satisfied. This uses multigrid for efficiency and solves by setting the pressure after the cavitation point to be zero.

There is no deformation term in the film thickness equation, so the film thickness values are only updated when H_0 changes. This leaves only the free boundary equation, (6.10) to be satisfied. The procedure used in the previous chapter is repeated here, i.e. moving the computational mesh according to a bisection scheme until a value of X_c is

found which satisfies equation (6.14) to within some tolerance. One slight complication with this occurs after the first solve, when the cavitation point is not at the right-hand boundary. This means the cavitation pressure gradient computed from the last non-zero pressure points can not be relied upon to move the computational domain in the correct direction. This is easily remedied though, since whenever the cavitation point is found at a mesh point to the left of the right-hand boundary, the right-hand boundary is moved to the location of the cavitation position for the next solve (although in the next chapter a more reliable method is introduced to find the cavitation position). By using a continuation strategy to provide initial guesses into the black-box solver, the solution can be found increasingly quickly with subsequent solves [29]. This has also been found to counteract the occasional stalling of the numerical convergence, which appears to result from incorrect boundary positions, which can sometimes impair the solution procedure.

6.2 Adjoint problem

As in the earlier chapters, the steps used to calculate the correction in a computed quantity of interest are as follows:

- Solve for the forward solution;
- Solve for the adjoint solution;
- Interpolate both solutions from the coarse grid to the fine grid;
- Calculate the fine grid residuals using the interpolated coarse grid solution;
- Multiply the adjoint by the residuals to obtain an estimate for the correction term.

This hydrodynamic problem provides a useful test as to how the residual equations should be defined and used. Firstly, two different ways that the residual equations can be formulated are introduced. Following this, the derivation of both corresponding Jacobians is included. In order to aid comparison of the two methods, Figures 6.1 and 6.2 show the sparsity patterns of the Jacobians in each case.

6.2.1 Residual equations

The residual equations can be formulated in at least two ways. This is because we can treat the variables representing viscosity and density as either "primary" or "secondary" dependent variables. For this problem, clearly the independent variable is X. Similarly, it is clear that P is a dependent variable. However, it is not immediately clear whether $\overline{\rho}$ and $\overline{\eta}$ should be considered as in the same class as P. It is definitely the case that as part of the solution procedure, $\overline{\rho}$ and $\overline{\eta}$ are calculated, and at the end, values are known for these important quantities. One approach therefore is that they should have residual equations and hence corresponding adjoint variables to indicate the sensitivity of the quantity of interest to them. Alternatively, one could use equations (6.3) and (6.4) to eliminate $\overline{\rho}$ and $\overline{\eta}$ by writing them explicitly as functions of P. In this case, there are no residual equations and hence no corresponding variables in the adjoint system.

In the following subsections, these two different approaches are explained.

6.2.1.1 Expanded equations

This approach treats (6.3) and (6.4) as equations to be solved with all of the other residual equations. As always, the Reynolds residual is given by

$$\begin{aligned} R_i &= \Delta X \left(\left(\frac{\overline{\rho}_i H_i - \overline{\rho}_{i-1} H_{i-1}}{\Delta X} \right) - \left(\frac{(P_{i+1} - P_i)\varepsilon_{i+\frac{1}{2}} - (P_i - P_{i-1})\varepsilon_{i-\frac{1}{2}}}{(\Delta X)^2} \right) \right) \\ &= \left(\overline{\rho}_i H_i - \overline{\rho}_{i-1} H_{i-1}\right) - \left(\frac{(P_{i+1} - P_i)\varepsilon_{i+\frac{1}{2}} - (P_i - P_{i-1})\varepsilon_{i-\frac{1}{2}}}{\Delta X} \right) \qquad (6.11) \\ &= \left(\overline{\rho}_i H_i - \overline{\rho}_{i-1} H_{i-1}\right) - \left(\frac{\varepsilon_{i+\frac{1}{2}} P_{i+1} - (\varepsilon_{i+\frac{1}{2}} + \varepsilon_{i-\frac{1}{2}}) P_i + \varepsilon_{i-\frac{1}{2}} P_{i-1}}{\Delta X} \right) \qquad (6.12) \end{aligned}$$

where $\varepsilon_i = \frac{H_i^3 \overline{\rho}_i}{\lambda \overline{\eta}_i}$, $\varepsilon_{i\pm\frac{1}{2}} = (\varepsilon_i + \varepsilon_{i\pm1})/2$ and H_i is given by $H_i = H_0 + \frac{X_i^2}{2}$. Equations (6.11) and (6.12) are simply two equivalent ways of grouping the terms, which will both be useful for the derivation of the Jacobian later on. Again the force balance residual is given by

$$R_{H_0} = \frac{\pi}{2} - \sum_{i=0}^{n-2} \frac{P_i + P_{i+1}}{2} \Delta X, \qquad (6.13)$$

and the cavitation pressure derivative corresponding to the free boundary condition is given as

$$R_{X_c} = -\frac{3P_{n-1} - 4P_{n-2} + P_{n-3}}{2\Delta X}. \tag{6.14}$$

In this expanded equation model the equations for the viscosity and density residuals are also included. The viscosity residuals are

$$R_{\overline{\eta}_i} = \Delta X \left(e^{\overline{\alpha} P_i} - \overline{\eta}_i \right), \tag{6.15}$$

and the density residuals are

$$R_{\overline{\rho}_i} = \Delta X \left(\frac{0.59 \times 10^9 + 1.34 P_i p_h}{0.59 \times 10^9 + P_i p_h} - \overline{\rho}_i \right). \tag{6.16}$$

6.2.1.2 Compact equations

The alternative approach considered here is to treat $\overline{\rho}$ and $\overline{\eta}$ as given functions of P. In this sense, the viscosity and density are not really solved for, but rather eliminated, to be replaced by expressions for P. For this reason we make a distinction between "primary" and "secondary" dependent variables: primary dependent variables (P, H_0, X_c) are those which are solved for, and so are independent of each other, whereas secondary dependent variables ($\overline{\eta}$, $\overline{\rho}$) are merely used to aid the solution process, and are dependent on some other variable (in this case P). There are two consequences of this. The first is that only equations (6.12) to (6.14) need be considered when formulating the discrete system. The second is that the resulting Jacobian becomes more complicated to derive, as $\overline{\eta}$ and $\overline{\rho}$ are quite complex expressions (in terms of P).

In terms of efficiency of solution, clearly the compact solution is likely to win out, as the expanded version is almost three times as big (for a grid of n mesh points, the compact Jacobian will be $(n+2) \times (n+2)$, while the expanded will have $(3n+2) \times (3n+2)$ entries). This larger system is likely to take significantly longer to solve, and while in this work efficiency is not the main concern, a factor this large is an important consideration.

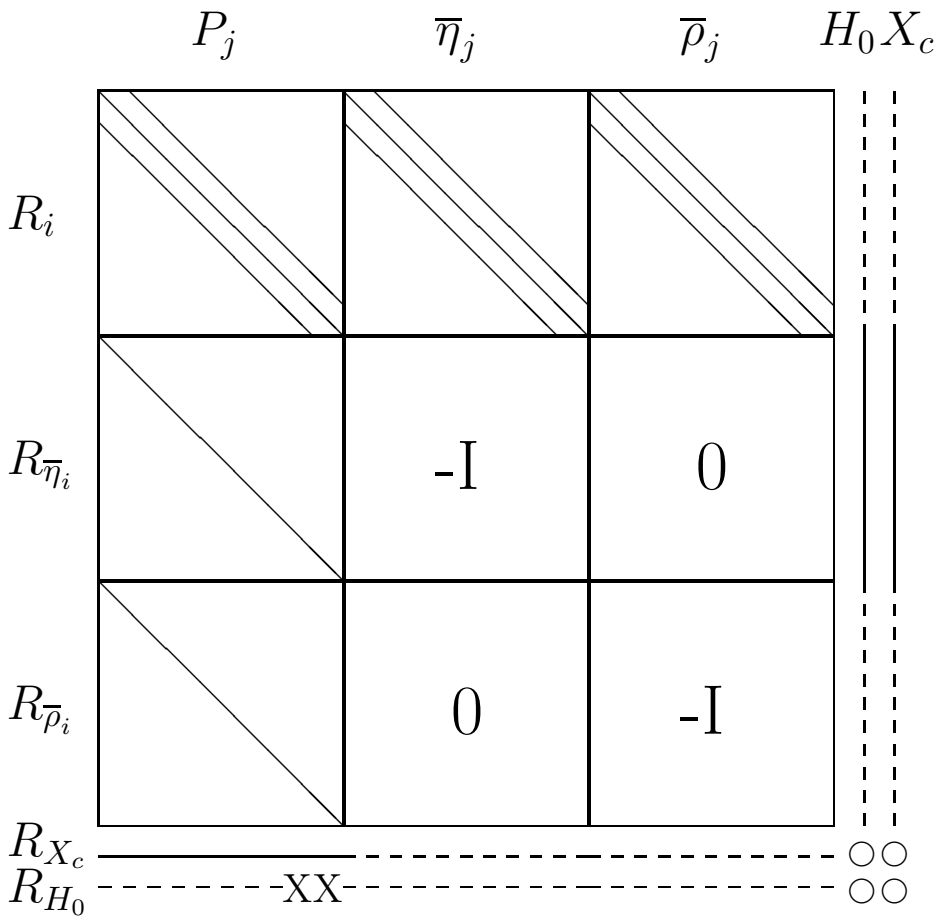

Figure 6.1: Expanded Jacobian sparsity pattern for the hydrodynamic line contact problem

6.3 Jacobian sparsity for the expanded system

In Figure 6.1, the sparsity pattern of the Jacobian is shown. This is block tri-diagonal with two additional lines on the outer rows (for the free boundary and force balance equation) and outer columns (for the cavitation boundary position, X_c, and separation parameter H_0).

6.3.1 Expanded Jacobian derivation

In order to derive the values of the non-zero entries shown in Fig 6.1, we begin by deriving some dependencies of various term upon P_i, $\overline{\eta}_i$ and $\overline{\rho}_i$. Since P, $\overline{\eta}$, and $\overline{\rho}$ are considered primary dependent variables (as defined earlier), only $H_i = \frac{X_i^2}{2}$ needs to be considered as

a secondary dependent variable. Hence

$$\frac{\partial H_i}{\partial P_j} = \frac{\partial H_i}{\partial \overline{\eta}_j} = \frac{\partial H_i}{\partial \overline{\rho}_j} = 0,$$

however

$$\frac{\partial H_i}{\partial H_0} = 1, \quad \text{and} \quad \frac{\partial H_i}{\partial X_c} = X_i.$$

This final equality follows from the fact that X_i is defined as $X_c - D + i \times \Delta X$ (where D is the domain size), and so $\frac{\partial X_i}{\partial X_c} = 1$. Also, given ε_i defined above, when $i = j$ it follows that:

$$\frac{\partial \varepsilon_i}{\partial P_j} = 0,$$

$$\frac{\partial \varepsilon_i}{\partial \overline{\eta}_j} = -\frac{\overline{\rho}_i H_i^3}{\lambda \overline{\eta}_i^2},$$

$$\frac{\partial \varepsilon_i}{\partial \overline{\rho}_j} = \frac{H_i^3}{\lambda \overline{\eta}_i}.$$

When $j \neq i$ these terms are zero, with

$$\frac{\partial \varepsilon_i}{\partial H_0} = \frac{3\overline{\rho}_i H_i^2}{\lambda \overline{\eta}_i},$$

$$\frac{\partial \varepsilon_i}{\partial X_c} = \frac{3X_i \overline{\rho}_i H_i^2}{\lambda \overline{\eta}_i}.$$

Hence, we see that

$$\frac{\partial \varepsilon_{i\pm\frac{1}{2}}}{\partial P_i} = \frac{\partial}{\partial P_i}\left(\frac{\varepsilon_{i\pm1} + \varepsilon_i}{2}\right) = 0,$$

and similarly,

$$\frac{\partial \varepsilon_{i\pm\frac{1}{2}}}{\partial \overline{\eta}_i} = -\frac{1}{2}\frac{\overline{\rho}_i H_i^3}{\lambda \overline{\eta}_i^2}, \qquad \frac{\partial \varepsilon_{i\pm\frac{1}{2}}}{\partial \overline{\eta}_{i\pm1}} = -\frac{1}{2}\frac{\overline{\rho}_{i\pm1} H_{i\pm1}^3}{\lambda \overline{\eta}_{i\pm1}^2}, \tag{6.17}$$

$$\frac{\partial \varepsilon_{i\pm\frac{1}{2}}}{\partial \overline{\rho}_i} = \frac{1}{2}\frac{H_i^3}{\lambda \overline{\eta}_i}, \qquad \frac{\partial \varepsilon_{i\pm\frac{1}{2}}}{\partial \overline{\rho}_{i\pm1}} = \frac{1}{2}\frac{H_{i\pm1}^3}{\lambda \overline{\eta}_{i\pm1}}, \tag{6.18}$$

$$\frac{\partial \varepsilon_{i\pm\frac{1}{2}}}{\partial H_0} = \frac{1}{2\lambda}\left(\frac{3\overline{\rho}_i H_i^2}{\overline{\eta}_i} + \frac{3\overline{\rho}_{i\pm1} H_{i\pm1}^2}{\overline{\eta}_{i\pm1}}\right), \tag{6.19}$$

$$\frac{\partial \varepsilon_{i\pm\frac{1}{2}}}{\partial X_c} = \frac{1}{2\lambda}\left(\frac{3X_i\overline{\rho}_i H_i^2}{\overline{\eta}_i} + \frac{3X_{i\pm1}\overline{\rho}_{i\pm1} H_{i\pm1}^2}{\overline{\eta}_{i\pm1}}\right). \tag{6.20}$$

These expressions are now used in the evaluation of the Jacobian itself.

6.3.2 Differentiating the R_i residual equations

Using (6.12),

$$\frac{\partial R_i}{\partial P_i} = \left(\frac{\varepsilon_{i+\frac{1}{2}} + \varepsilon_{i-\frac{1}{2}}}{\Delta X}\right), \quad \frac{\partial R_i}{\partial P_{i+1}} = -\left(\frac{\varepsilon_{i+\frac{1}{2}}}{\Delta X}\right), \quad \frac{\partial R_i}{\partial P_{i-1}} = -\left(\frac{\varepsilon_{i-\frac{1}{2}}}{\Delta X}\right).$$

Otherwise $\frac{\partial R_i}{\partial P_j} = 0$. Also, using (6.11) and (6.17),

$$\begin{aligned}\frac{\partial R_i}{\partial \overline{\eta}_i} &= -\left(\left(\frac{P_{i+1}-P_i}{\Delta X}\right)\left(-\frac{\overline{\rho}_i H_i^3}{2\lambda\overline{\eta}_i^2}\right) - \left(\frac{P_i - P_{i-1}}{\Delta X}\right)\left(-\frac{\overline{\rho}_i H_i^3}{2\lambda\overline{\eta}_i^2}\right)\right) \\ &= \left(\frac{\overline{\rho}_i H_i^3}{2\lambda\overline{\eta}_i^2}\right)\left(\frac{P_{i+1}-2P_i+P_{i-1}}{\Delta X}\right), \qquad (6.21)\end{aligned}$$

$$\frac{\partial R_i}{\partial \overline{\eta}_{i+1}} = \left(\frac{\overline{\rho}_{i+1} H_{i+1}^3}{2\lambda\overline{\eta}_{i+1}^2}\right)\left(\frac{P_{i+1}-P_i}{\Delta X}\right),$$

$$\frac{\partial R_i}{\partial \overline{\eta}_{i-1}} = -\left(\frac{\overline{\rho}_{i-1} H_{i-1}^3}{2\lambda\overline{\eta}_{i-1}^2}\right)\left(\frac{P_i - P_{i-1}}{\Delta X}\right).$$

Otherwise $\frac{\partial R_i}{\partial \overline{\eta}_j} = 0$. Using (6.11) and (6.18),

$$\begin{aligned}\frac{\partial R_i}{\partial \overline{\rho}_i} &= H_i - \left(\left(\frac{P_{i+1}-P_i}{\Delta X}\right)\left(\frac{H_i^3}{2\lambda\overline{\eta}_i}\right) - \left(\frac{P_i - P_{i-1}}{\Delta X}\right)\left(\frac{H_i^3}{2\lambda\overline{\eta}_i}\right)\right) \\ &= H_i - \left(\frac{H_i^3}{2\lambda\overline{\eta}_i}\right)\left(\frac{P_{i+1}-2P_i+P_{i-1}}{\Delta X}\right), \qquad (6.22)\end{aligned}$$

$$\frac{\partial R_i}{\partial \overline{\rho}_{i+1}} = -\left(\frac{H_{i+1}^3}{2\lambda\overline{\eta}_{i+1}}\right)\left(\frac{P_{i+1}-P_i}{\Delta X}\right),$$

$$\frac{\partial R_i}{\partial \overline{\rho}_{i-1}} = -H_{i-1} + \left(\frac{H_{i-1}^3}{2\lambda\overline{\eta}_{i-1}}\right)\left(\frac{P_i - P_{i-1}}{\Delta X}\right).$$

Otherwise $\frac{\partial R_i}{\partial \overline{\rho}_j} = 0$. Finally, using (6.11) and (6.19),

$$\frac{\partial R_i}{\partial H_0} = (\overline{\rho}_i - \overline{\rho}_{i-1})$$

$$
\begin{aligned}
&- \frac{1}{2\lambda}\left[\left(\frac{P_{i+1}-P_i}{\Delta X}\right)\left(\frac{3H_i^2\overline{\rho}_i}{\overline{\eta}_i}+\frac{3H_{i+1}^2\overline{\rho}_{i+1}}{\overline{\eta}_{i+1}}\right)\right.\\
&\left.- \left(\frac{P_i-P_{i-1}}{\Delta X}\right)\left(\frac{3H_i^2\overline{\rho}_i}{\overline{\eta}_i}+\frac{3H_{i-1}^2\overline{\rho}_{i-1}}{\overline{\eta}_{i-1}}\right)\right], \qquad (6.23)
\end{aligned}
$$

and, using (6.11) and (6.20),

$$
\begin{aligned}
\frac{\partial R_i}{\partial X_c} &= (X_i\overline{\rho}_i - X_{i-1}\overline{\rho}_{i-1})\\
&- \frac{1}{2\lambda}\left[\left(\frac{P_{i+1}-P_i}{\Delta X}\right)\left(\frac{3X_iH_i^2\overline{\rho}_i}{\overline{\eta}_i}+\frac{3X_{i+1}H_{i+1}^2\overline{\rho}_{i+1}}{\overline{\eta}_{i+1}}\right)\right.\\
&\left.- \left(\frac{P_i-P_{i-1}}{\Delta X}\right)\left(\frac{3X_iH_i^2\overline{\rho}_i}{\overline{\eta}_i}+\frac{3X_{i-1}H_{i-1}^2\overline{\rho}_{i-1}}{\overline{\eta}_{i-1}}\right)\right]. \qquad (6.24)
\end{aligned}
$$

6.3.3 Differentiating the $R_{\overline{\eta}_i}$ equations

The derivatives of (6.15) are straight forward to evaluate:

$$
\frac{\partial R_{\overline{\eta}_i}}{\partial P_i} = \Delta X\left(\overline{\alpha}e^{\overline{\alpha}P_i}\right), \quad \frac{\partial R_{\overline{\eta}_i}}{\partial P_j} = 0(i\neq j),
$$

$$
\frac{\partial R_{\overline{\eta}_i}}{\partial \overline{\eta}_i} = -\Delta X, \quad \frac{\partial R_{\overline{\eta}_i}}{\partial \overline{\eta}_i} = 0(i\neq j),
$$

$$
\frac{\partial R_{\overline{\eta}_i}}{\partial \overline{\rho}_j} = \frac{\partial R_{\overline{\eta}_i}}{\partial H_0} = \frac{\partial R_{\overline{\eta}_i}}{\partial X_c} = 0.
$$

6.3.4 Differentiating the $R_{\overline{\rho}_i}$ equations

Similarly, the derivatives of (6.16) are relatively straightforward:

$$
\begin{aligned}
\frac{\partial R_{\overline{\rho}_i}}{\partial P_i} &= \Delta X\left(\frac{(0.59\times10^9+P_ip_h)1.34p_h-(0.59\times10^9+1.34P_ip_h)p_h}{(0.59\times10^9+P_ip_h)^2}\right)\\
&= \Delta X\left(\frac{(0.59\times10^9\times1.34p_h)+(1.34p_h^2P_i)-(0.59\times10^9p_h)-(1.34p_h^2P_i)}{(0.59\times10^9+P_ip_h)^2}\right)\\
&= \Delta X\left(\frac{(1.34-1.0)0.59\times10^9p_h}{(0.59\times10^9+P_ip_h)^2}\right)\\
&= \Delta X\left(\frac{0.34\times0.59\times10^9p_h}{(0.59\times10^9+P_ip_h)^2}\right),
\end{aligned}
$$

$$\frac{\partial R_{\overline{\rho}_i}}{\partial P_j} = 0 (i \neq j),$$

$$\frac{\partial R_{\overline{\rho}_i}}{\partial \overline{\eta}_i} = 0,$$

$$\frac{\partial R_{\overline{\rho}_i}}{\partial \overline{\rho}_i} = -\Delta X, \qquad \frac{\partial R_{\overline{\rho}_i}}{\partial \overline{\rho}_i} = 0 (i \neq j),$$

$$\frac{\partial R_{\overline{\rho}_i}}{\partial H_0} = \frac{\partial R_{\overline{\rho}_i}}{\partial X_c} = 0$$

6.3.5 Differentiating the R_{H_0} and R_{X_c} equations

The final two equations in the system are also easy to differentiate. For the force balance residual:

$$\frac{\partial R_{H_0}}{\partial P_j} = -\Delta X, \qquad \text{for } \; j = 1, \ldots, n-2, \tag{6.25}$$

and

$$\frac{\partial R_{H_0}}{\partial \overline{\eta}_j} = \frac{\partial R_{H_0}}{\partial \overline{\rho}_j} = \frac{\partial R_{H_0}}{\partial H_0} = \frac{\partial R_{H_0}}{\partial X_c} = 0.$$

For the free boundary residual:

$$\frac{\partial R_{X_c}}{\partial P_{n-3}} = -\frac{1}{2\Delta X}, \qquad \frac{\partial R_{X_c}}{\partial P_{n-2}} = \frac{2}{\Delta X}, \tag{6.26}$$

$$\frac{\partial R_{X_c}}{\partial P_j} = 0 \;\; (j < n-3), \tag{6.27}$$

and

$$\frac{\partial R_{X_c}}{\partial \overline{\eta}_j} = \frac{\partial R_{X_c}}{\partial \overline{\rho}_j} = \frac{\partial R_{X_c}}{\partial H_0} = \frac{\partial R_{X_c}}{\partial X_c} = 0.$$

6.3.6 The right-hand side of the adjoint system

Recall from the previous chapter that the right-hand side of the discrete adjoint system is the derivative of the quantity of interest with respect to the dependent variables. In this example, dimensional friction is considered, where m_1 and m_2 are the dimensionalising parameters multiplying the non-dimensional variables.

Let $m_1 = \frac{b}{2R_x}$ and $m_2 = \frac{\eta_0 R_x}{b}$. The friction is then given by:

$$F = \int_{X_{in}}^{X_c} \left(-m_1 \frac{\partial P}{\partial X} \frac{H}{2} + m_2 \frac{\overline{\eta}}{H} (u_b - u_a) \right) \mathrm{d}X.$$

In discrete form, this quantity may be expressed as

$$F = \sum_{i=0}^{n-2} \left(-m_1 \left(\frac{P_{i+1} - P_i}{\Delta X} \right) \left(\frac{H_{i+1} + H_i}{4} \right) + m_2 \left(\frac{\overline{\eta}_{i+1} + \overline{\eta}_i}{H_{i+1} + H_i} \right) (u_b - u_a) \right) \Delta X.$$

Hence it is possible to differentiate with respect to each of the primary dependent variables:

$$\frac{\partial F}{\partial P_j} = m_1 \left(\frac{H_{j+1} + H_j}{4} - \frac{H_j + H_{j-1}}{4} \right),$$

$$\frac{\partial F}{\partial \overline{\eta}_j} = m_2 \left(\frac{u_b - u_a}{H_{j+1} + H_j} + \frac{u_b - u_a}{H_j + H_{j-1}} \right) \Delta X,$$

$$\frac{\partial F}{\partial \overline{\rho}_j} = 0,$$

$$\begin{aligned} \frac{\partial F}{\partial H_0} = & - m_1 \sum_{i=0}^{n-2} \frac{P_{i+1} - P_i}{2} \\ & - 2m_2 \sum_{i=0}^{n-2} \left(\frac{\overline{\eta}_{i+1} + \overline{\eta}_i}{(H_{i+1} + H_i)^2} \right) (u_b - u_a) \Delta X, \end{aligned} \tag{6.28}$$

and

$$\begin{aligned} \frac{\partial F}{\partial X_c} = & - m_1 \sum_{i=0}^{n-2} (P_{i+1} - P_i) \left(\frac{X_{i+1} + X_i}{4} \right) \\ & - m_2 \sum_{i=0}^{n-2} \left(\frac{(\overline{\eta}_{i+1} + \overline{\eta}_i)(X_{i+1} + X_i)}{(H_{i+1} + H_i)^2} \right) (u_b - u_a) \Delta X. \end{aligned}$$

The adjoint system of equations consists of the transpose of the Jacobian matrix with the above terms forming the right-hand side vector.

6.4 Jacobian sparsity for the compact system

We continue to consider a mesh with n node points, however we now eliminate $\overline{\eta}$ and $\overline{\rho}$ by expressing them explicitly in terms of P. Figure 6.2 shows the sparsity pattern for

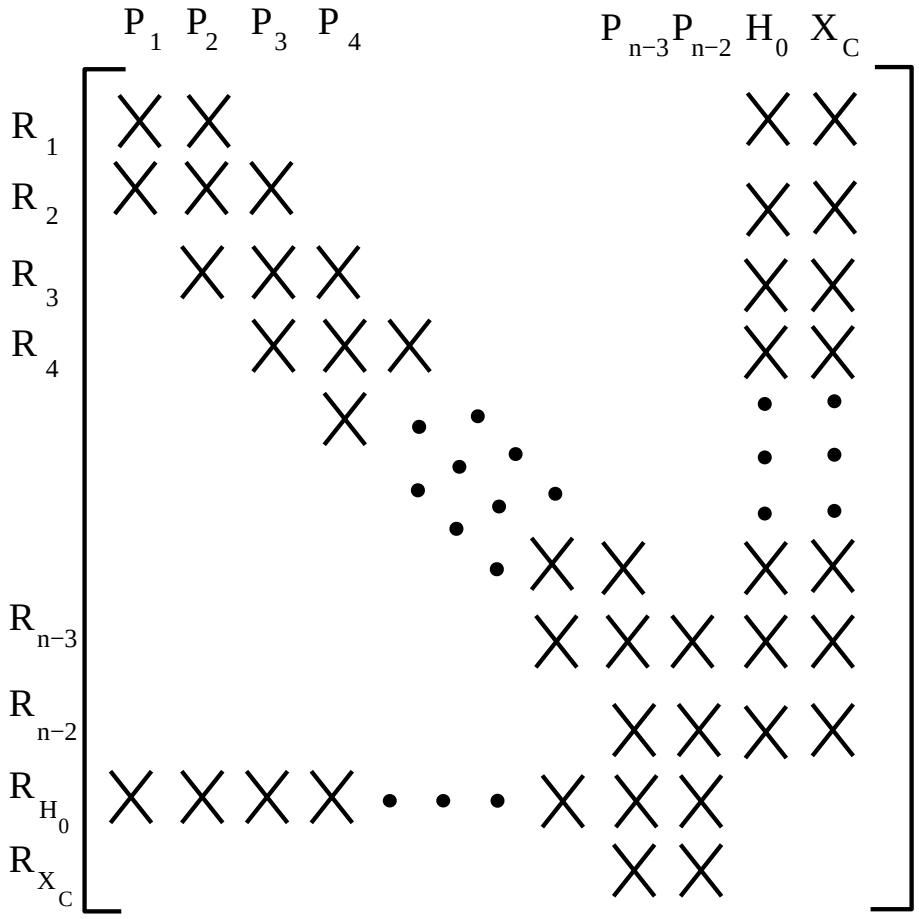

Figure 6.2: Compact Jacobian sparsity pattern for the hydrodynamic line contact problem

the resulting Jacobian of this compact system. It has the same pattern for the $R_i \times P_j$ block as in Figure 6.1, however this block is augmented with just two additional rows and columns. The non-zero entries for the main tri-diagonal block are more complicated to evaluate than before so we begin by writing the residuals out in full.

The Reynolds residuals, for $i = 1 \ldots n-2$, are given by

$$\begin{aligned} R_i &= \Delta X \left(\left(\frac{\overline{\rho}_i H_i - \overline{\rho}_{i-1} H_{i-1}}{\Delta X} \right) - \left(\frac{(P_{i+1} - P_i)\varepsilon_{i+\frac{1}{2}} - (P_i - P_{i-1})\varepsilon_{i-\frac{1}{2}}}{(\Delta X)^2} \right) \right) \\ &= \left(\overline{\rho}_i H_i - \overline{\rho}_{i-1} H_{i-1}\right) - \left(\frac{(P_{i+1} - P_i)\varepsilon_{i+\frac{1}{2}} - (P_i - P_{i-1})\varepsilon_{i-\frac{1}{2}}}{\Delta X} \right) \qquad (6.29) \\ &= \left(\overline{\rho}_i H_i - \overline{\rho}_{i-1} H_{i-1}\right) - \left(\frac{\varepsilon_{i+\frac{1}{2}} P_{i+1} - (\varepsilon_{i+\frac{1}{2}} + \varepsilon_{i-\frac{1}{2}}) P_i + \varepsilon_{i-\frac{1}{2}} P_{i-1}}{\Delta X} \right), \qquad (6.30) \end{aligned}$$

where $\varepsilon_i = \frac{H_i^3 \overline{\rho}_i}{\lambda \overline{\eta}_i}$ and $\varepsilon_{i\pm\frac{1}{2}} = (\varepsilon_i + \varepsilon_{i\pm1})/2$. Also, H_i, $\overline{\eta}_i$, and $\overline{\rho}_i$ are given respectively by

$$H_i = H_0 + \frac{X_i^2}{2}, \qquad \overline{\eta}_i = e^{\overline{\alpha} P_i}, \qquad \overline{\rho}_i = \frac{0.59 \times 10^9 + 1.34 P_i p_h}{0.59 \times 10^9 + P_i p_h}.$$

The boundary conditions are imposed by requiring $R_0 = R_{n-1} = 0$. The force balance and free boundary residuals are as before:

$$R_{H_0} = \frac{\pi}{2} - \sum_{i=0}^{n-2} \frac{P_i + P_{i+1}}{2} \Delta X, \tag{6.31}$$

and

$$R_{X_c} = \frac{3P_{n-1} - 4P_{n-2} + P_{n-3}}{2\Delta X}. \tag{6.32}$$

6.4.1 Compact Jacobian derivation

In order to simplify the Jacobian calculation, we first differentiate the secondary dependent variables dependent variables H_i, $\overline{\eta}_i$ and $\overline{\rho}_i$ with respect to the primary dependent variables P_j, H_0 and X_c. When $j = i$,

$$\frac{\partial H_i}{\partial P_j} = 0, \qquad \frac{\partial H_i}{\partial H_0} = 1, \qquad \frac{\partial H_i}{\partial X_c} = X_i;$$

$$\frac{\partial \overline{\eta}_i}{\partial P_j} = \frac{\partial}{\partial P_i} e^{\overline{\alpha} P_i} = \overline{\alpha} e^{\overline{\alpha} P_i} = \overline{\alpha \eta}_i, \qquad \frac{\partial \overline{\eta}_i}{\partial H_0} = \frac{\partial \overline{\eta}_i}{\partial X_c} = 0;$$

$$\begin{aligned}
\frac{\partial \overline{\rho}_i}{\partial P_j} &= \frac{(0.59 \times 10^9 + P_i p_h) 1.34 p_h - (0.59 \times 10^9 + 1.34 P_i p_h) p_h}{(0.59 \times 10^9 + P_i p_h)^2} \\
&= \frac{(0.59 \times 10^9 \times 1.34 p_h) + (1.34 p_h^2 P_i) - (0.59 \times 10^9 p_h) - (1.34 p_h^2 P_i)}{(0.59 \times 10^9 + P_i p_h)^2} \\
&= \left(\frac{(1.34 - 1.0) 0.59 \times 10^9 p_h}{(0.59 \times 10^9 + P_i p_h)^2} \right) \\
&= \left(\frac{0.34 \times 0.59 \times 10^9 p_h}{(0.59 \times 10^9 + P_i p_h)^2} \right),
\end{aligned}$$

$$\frac{\partial \overline{\rho}_i}{\partial H_0} = \frac{\partial \overline{\rho}_i}{\partial X_c} = 0.$$

When $j \neq i$,

$$\frac{\partial H_i}{\partial P_j} = \frac{\partial \overline{\eta}_i}{\partial P_j} = \frac{\partial \overline{\rho}_i}{\partial P_j} = 0.$$

Next, we consider differentiating ε_i with respect to the independent variables. When $j = i$,

$$\begin{aligned}
\frac{\partial \varepsilon_i}{\partial P_j} &= \frac{\partial}{\partial P_i}\left(\frac{\overline{\rho}_i H_i^3}{\lambda \overline{\eta}_i}\right) \\
&= \frac{1}{\lambda}\left(\frac{H_i^3}{\overline{\eta}_i}\frac{\partial \overline{\rho}_i}{\partial P_i} + \frac{\overline{\rho}_i}{\overline{\eta}_i}\frac{\partial (H_i^3)}{\partial P_i} + \overline{\rho}_i H_i^3 \frac{\partial}{\partial P_i}\left(\frac{1}{\overline{\eta}_i}\right)\right) \\
&= \frac{1}{\lambda}\left(\frac{H_i^3}{\overline{\eta}_i}\left(\frac{0.34 \times 0.59 \times 10^9 p_h}{(0.59 \times 10^9 + P_i p_h)^2}\right) + 0 + \overline{\rho}_i H_i^3 \frac{-\overline{\alpha}}{\overline{\eta}_i}\right) \\
&= \frac{H_i^3}{\lambda \overline{\eta}_i}\left(\frac{0.34 \times 0.59 \times 10^9 p_h}{(0.59 \times 10^9 + P_i p_h)^2}\right) - \overline{\alpha}\varepsilon_i, \qquad (6.33)
\end{aligned}$$

otherwise

$$\frac{\partial \varepsilon_i}{\partial P_j} = 0.$$

Following on from this, we consider $\varepsilon_{i\pm\frac{1}{2}}$:

$$\frac{\partial \varepsilon_{i\pm\frac{1}{2}}}{\partial P_i} = \frac{\partial}{\partial P_i}\left(\frac{\varepsilon_i + \varepsilon_{i\pm1}}{2}\right) = \frac{\partial}{\partial P_i}\left(\frac{\varepsilon_i}{2}\right) = \frac{1}{2}\frac{\partial \varepsilon_i}{\partial P_i}, \qquad (6.34)$$

and similarly

$$\frac{\partial \varepsilon_{i\pm\frac{1}{2}}}{\partial P_{i\pm1}} = \frac{1}{2}\frac{\partial \varepsilon_{i\pm1}}{\partial P_{i\pm1}}. \qquad (6.35)$$

The final expressions that are useful to us at this stage are obtained from (6.29). Considering differentiating the first part of (6.29) with respect to P:

$$\frac{\partial}{\partial P_i}\left(\overline{\rho}_i H_i - \overline{\rho}_{i-1} H_{i-1}\right) = H_i \frac{\partial \overline{\rho}_i}{\partial P_i} \qquad (6.36)$$

and

$$\frac{\partial}{\partial P_{i-1}}\left(\overline{\rho}_i H_i - \overline{\rho}_{i-1} H_{i-1}\right) = -H_{i-1}\frac{\partial \overline{\rho}_{i-1}}{\partial P_{i-1}}. \qquad (6.37)$$

Considering differentiating the second part of (6.29):

$$\begin{aligned}
&\frac{\partial}{\partial P_i}\left(\frac{(P_{i+1} - P_i)\varepsilon_{i+\frac{1}{2}} - (P_i - P_{i-1})\varepsilon_{i-\frac{1}{2}}}{\Delta X}\right) \qquad (6.38) \\
= \; &-\left(\frac{\varepsilon_{i+\frac{1}{2}} + \varepsilon_{i-\frac{1}{2}}}{\Delta X}\right) + \left(\frac{P_{i+1} - P_i}{\Delta X}\right)\frac{\partial \varepsilon_{i+\frac{1}{2}}}{\partial P_i} - \left(\frac{P_i - P_{i-1}}{\Delta X}\right)\frac{\partial \varepsilon_{i-\frac{1}{2}}}{\partial P_i}
\end{aligned}$$

$$
\begin{aligned}
&= -\left(\frac{\varepsilon_{i+\frac{1}{2}}+\varepsilon_{i-\frac{1}{2}}}{\Delta X}\right)+\left(\frac{P_{i+1}-P_i}{\Delta X}\right)\frac{1}{2}\frac{\partial \varepsilon_i}{\partial P_i}-\left(\frac{P_i-P_{i-1}}{\Delta X}\right)\frac{1}{2}\frac{\partial \varepsilon_i}{\partial P_i}\\
&= -\left(\frac{\varepsilon_{i+\frac{1}{2}}+\varepsilon_{i-\frac{1}{2}}}{\Delta X}\right)+\frac{1}{2}\frac{\partial \varepsilon_i}{\partial P_i}\left(\frac{P_{i+1}-2P_i+P_{i-1}}{\Delta X}\right); \qquad (6.39)
\end{aligned}
$$

whereas

$$
\begin{aligned}
&\frac{\partial}{\partial P_{i+1}}\left(\frac{(P_{i+1}-P_i)\varepsilon_{i+\frac{1}{2}}-(P_i-P_{i-1})\varepsilon_{i-\frac{1}{2}}}{\Delta X}\right) \qquad (6.40)\\
&= \left(\frac{\varepsilon_{i+\frac{1}{2}}}{\Delta X}\right)+\left(\frac{P_{i+1}-P_i}{\Delta X}\right)\frac{\partial \varepsilon_{i+\frac{1}{2}}}{\partial P_{i+1}}\\
&= \left(\frac{\varepsilon_{i+\frac{1}{2}}}{\Delta X}\right)+\left(\frac{P_{i+1}-P_i}{\Delta X}\right)\frac{1}{2}\frac{\partial \varepsilon_{i+1}}{\partial P_{i+1}}\\
&= \left(\frac{\varepsilon_{i+\frac{1}{2}}}{\Delta X}\right)+\frac{1}{2}\frac{\partial \varepsilon_{i+1}}{\partial P_{i+1}}\left(\frac{P_{i+1}-P_i}{\Delta X}\right); \qquad (6.41)
\end{aligned}
$$

and similarly

$$
\begin{aligned}
&\frac{\partial}{\partial P_{i-1}}\left(\frac{(P_{i+1}-P_i)\varepsilon_{i+\frac{1}{2}}-(P_i-P_{i-1})\varepsilon_{i-\frac{1}{2}}}{\Delta X}\right) \qquad (6.42)\\
&= \left(\frac{\varepsilon_{i-\frac{1}{2}}}{\Delta X}\right)-\left(\frac{P_i-P_{i-1}}{\Delta X}\right)\frac{\partial \varepsilon_{i-\frac{1}{2}}}{\partial P_{i-1}}\\
&= \left(\frac{\varepsilon_{i-\frac{1}{2}}}{\Delta X}\right)-\left(\frac{P_i-P_{i-1}}{\Delta X}\right)\frac{1}{2}\frac{\partial \varepsilon_{i-1}}{\partial P_{i-1}}\\
&= \left(\frac{\varepsilon_{i-\frac{1}{2}}}{\Delta X}\right)-\frac{1}{2}\frac{\partial \varepsilon_{i-1}}{\partial P_{i-1}}\left(\frac{P_i-P_{i-1}}{\Delta X}\right). \qquad (6.43)
\end{aligned}
$$

These expressions will now be used in the evaluation of the Jacobian itself.

6.4.2 Evaluation of $\frac{\partial R_i}{\partial P_j}$

Using (6.30), (6.36), (6.37), (6.39), (6.41) and (6.43),

$$
\begin{aligned}
\frac{\partial R_i}{\partial P_i} &= H_i\frac{\partial \overline{\rho}_i}{\partial P_i}-\left(-\left(\frac{\varepsilon_{i+\frac{1}{2}}+\varepsilon_{i-\frac{1}{2}}}{\Delta X}\right)+\frac{1}{2}\frac{\partial \varepsilon_i}{\partial P_i}\left(\frac{P_{i+1}-2P_i+P_{i-1}}{\Delta X}\right)\right)\\
&= H_i\left(\frac{0.34\times 0.59\times 10^9 p_h}{(0.59\times 10^9+P_i p_h)^2}\right)+\left(\frac{\varepsilon_{i+\frac{1}{2}}+\varepsilon_{i-\frac{1}{2}}}{\Delta X}\right)\\
&\quad -\frac{1}{2}\left(\frac{H_i^3}{\lambda\overline{\eta}_i}\left(\frac{0.34\times 0.59\times 10^9 p_h}{(0.59\times 10^9+P_i p_h)^2}\right)-\overline{\alpha}\varepsilon_i\right)\left(\frac{P_{i+1}-2P_i+P_{i-1}}{\Delta X}\right).
\end{aligned}
$$

Similarly,

$$\begin{aligned}\frac{\partial R_i}{\partial P_{i+1}} &= -\left(\left(\frac{\varepsilon_{i+\frac{1}{2}}}{\Delta X}\right)+\frac{1}{2}\frac{\partial \varepsilon_{i+1}}{\partial P_{i+1}}\left(\frac{P_{i+1}-P_i}{\Delta X}\right)\right)\\ &= -\left(\frac{\varepsilon_{i+\frac{1}{2}}}{\Delta X}\right)\\ &\quad -\frac{1}{2}\left(\frac{H_{i+1}^3}{\lambda\overline{\eta}_{i+1}}\left(\frac{0.34\times 0.59\times 10^9 p_h}{(0.59\times 10^9+P_{i+1}p_h)^2}\right)-\overline{\alpha}\varepsilon_{i+1}\right)\left(\frac{P_{i+1}-P_i}{\Delta X}\right),\end{aligned}$$

and

$$\begin{aligned}\frac{\partial R_i}{\partial P_{i-1}} &= -H_{i-1}\frac{\partial \overline{\rho}_{i-1}}{\partial P_{i-1}}-\left(\left(\frac{\varepsilon_{i-\frac{1}{2}}}{\Delta X}\right)-\frac{1}{2}\frac{\partial \varepsilon_{i-1}}{\partial P_{i-1}}\left(\frac{P_i-P_{i-1}}{\Delta X}\right)\right)\\ &= -H_{i-1}\left(\frac{0.34\times 0.59\times 10^9 p_h}{(0.59\times 10^9+P_{i-1}p_h)^2}\right)-\left(\frac{\varepsilon_{i-\frac{1}{2}}}{\Delta X}\right)\\ &\quad +\frac{1}{2}\left(\frac{H_{i-1}^3}{\lambda\overline{\eta}_{i-1}}\left(\frac{0.34\times 0.59\times 10^9 p_h}{(0.59\times 10^9+P_{i-1}p_h)^2}\right)-\overline{\alpha}\varepsilon_{i-1}\right)\left(\frac{P_i-P_{i-1}}{\Delta X}\right).\end{aligned}$$

6.4.3 Evaluation of $\frac{\partial R_i}{\partial H_0}$

Recalling that $H_i = H_0 + \frac{1}{2}X_i^2$, it is trivial to show that

$$\frac{\partial H_i}{\partial H_0} = 1.$$

Hence,

$$\frac{\partial \varepsilon_i}{\partial H_0} = \frac{\partial}{\partial H_0}\left(\frac{H_i^3\overline{\rho}_i}{\lambda\overline{\eta}_i}\right) = \frac{3H_i^2\overline{\rho}_i}{\lambda\overline{\eta}_i},$$

and

$$\frac{\partial \varepsilon_{i\pm\frac{1}{2}}}{\partial H_0} = \frac{1}{2}\left(\frac{\partial \varepsilon_i}{\partial H_0}+\frac{\partial \varepsilon_{i\pm1}}{\partial H_0}\right).$$

Hence, from (6.29),

$$\begin{aligned}\frac{\partial R_i}{\partial H_0} &= (\overline{\rho}_i-\overline{\rho}_{i-1})-\left(\left(\frac{P_{i+1}-P_i}{\Delta X}\right)\frac{\partial \varepsilon_{i+\frac{1}{2}}}{\partial H_0}-\left(\frac{P_i-P_{i-1}}{\Delta X}\right)\frac{\partial \varepsilon_{i-\frac{1}{2}}}{\partial H_0}\right)\\ &= (\overline{\rho}_i-\overline{\rho}_{i-1})\\ &- \left(\left(\frac{P_{i+1}-P_i}{\Delta X}\right)\frac{1}{2}\left(\frac{\partial \varepsilon_i}{\partial H_0}+\frac{\partial \varepsilon_{i+1}}{\partial H_0}\right)-\left(\frac{P_i-P_{i-1}}{\Delta X}\right)\frac{1}{2}\left(\frac{\partial \varepsilon_i}{\partial H_0}+\frac{\partial \varepsilon_{i-1}}{\partial H_0}\right)\right)\end{aligned}$$

$$
\begin{aligned}
&= (\overline{\rho}_i - \overline{\rho}_{i-1}) - \frac{1}{2\lambda}\left(\left(\frac{P_{i+1}-P_i}{\Delta X}\right)\left(\frac{3H_i^2\overline{\rho}_i}{\overline{\eta}_i} + \frac{3H_{i+1}^2\overline{\rho}_{i+1}}{\overline{\eta}_{i+1}}\right)\right. \\
&- \left.\left(\frac{P_i - P_{i-1}}{\Delta X}\right)\left(\frac{3H_i^2\overline{\rho}_i}{\overline{\eta}_i} + \frac{3H_{i-1}^2\overline{\rho}_{i-1}}{\overline{\eta}_{i-1}}\right)\right). \qquad (6.44)
\end{aligned}
$$

6.4.4 Evaluation of $\frac{\partial R_i}{\partial X_c}$

Recalling that $X_i = X_c - D + i \times \Delta X$ and $H_i = H_0 + \frac{1}{2}X_i^2$, it is clear that

$$\frac{\partial H_i}{\partial X_c} = X_i.$$

Hence,

$$\frac{\partial \varepsilon_i}{\partial X_c} = \frac{\partial}{\partial X_c}\left(\frac{H_i^3\overline{\rho}_i}{\lambda\overline{\eta}_i}\right) = \frac{3X_iH_i^2\overline{\rho}_i}{\lambda\overline{\eta}_i}$$

and

$$\frac{\partial \varepsilon_{i\pm\frac{1}{2}}}{\partial X_c} = \frac{1}{2}\left(\frac{\partial \varepsilon_i}{\partial X_c} + \frac{\partial \varepsilon_{i\pm1}}{\partial X_c}\right).$$

Thus, from (6.29),

$$
\begin{aligned}
\frac{\partial R_i}{\partial X_c} &= (X_i\overline{\rho}_i - X_{i-1}\overline{\rho}_{i-1}) - \left(\left(\frac{P_{i+1}-P_i}{\Delta X}\right)\frac{\partial \varepsilon_{i+\frac{1}{2}}}{\partial X_c} - \left(\frac{P_i - P_{i-1}}{\Delta X}\right)\frac{\partial \varepsilon_{i-\frac{1}{2}}}{\partial X_c}\right) \qquad (6.45)\\
&= (X_i\overline{\rho}_i - X_{i-1}\overline{\rho}_{i-1}) \\
&\quad - \left(\left(\frac{P_{i+1}-P_i}{\Delta X}\right)\frac{1}{2}\left(\frac{\partial \varepsilon_i}{\partial X_c} + \frac{\partial \varepsilon_{i+1}}{\partial X_c}\right)\right. \\
&\quad - \left.\left(\frac{P_i - P_{i-1}}{\Delta X}\right)\frac{1}{2}\left(\frac{\partial \varepsilon_i}{\partial X_c} + \frac{\partial \varepsilon_{i-1}}{\partial X_c}\right)\right) \\
&= (X_i\overline{\rho}_i - X_{i-1}\overline{\rho}_{i-1}) \\
&\quad - \frac{1}{2\lambda}\left(\left(\frac{P_{i+1}-P_i}{\Delta X}\right)\left(\frac{3X_iH_i^2\overline{\rho}_i}{\overline{\eta}_i} + \frac{3X_{i+1}H_{i+1}^2\overline{\rho}_{i+1}}{\overline{\eta}_{i+1}}\right)\right. \\
&\quad - \left.\left(\frac{P_i - P_{i-1}}{\Delta X}\right)\left(\frac{3X_iH_i^2\overline{\rho}_i}{\overline{\eta}_i} + \frac{3X_{i-1}H_{i-1}^2\overline{\rho}_{i-1}}{\overline{\eta}_{i-1}}\right)\right).
\end{aligned}
$$

6.4.5 Differentiating the R_{H_0} and R_{X_c} equations

The remaining contributions to the Jacobian for this problem are all relatively straightforward to evaluate:

$$\frac{\partial R_{H_0}}{\partial P_j} = -\Delta X, \quad (-\frac{\Delta X}{2} for j = 0, j = n-1),$$

$$\frac{\partial R_{H_0}}{\partial H_0} = 0, \quad \frac{\partial R_{H_0}}{\partial X_c} = 0;$$

and,

$$\frac{\partial R_{X_c}}{\partial P_{n-3}} = \frac{1}{2\Delta X}, \qquad \frac{\partial R_{X_c}}{\partial P_{n-2}} = -\frac{2}{\Delta X}, \qquad \frac{\partial R_{X_c}}{\partial H_0} = 0, \qquad \frac{\partial R_{X_c}}{\partial X_c} = 0. \tag{6.46}$$

6.4.6 The right-hand side of the adjoint system

As with the expanded discretisation, if the discrete adjoint approach is to be used to approximate the error in a quantity of interest then the derivative of this quantity must feature on the right-hand side of the adjoint system. As in the previous section, the dimensional friction is used as the quantity of interest:

$$F = \int_{X_{in}}^{X_c} \left(-m_1 \frac{\partial P}{\partial X} \frac{H}{2} + m_2 \frac{\overline{\eta}}{H} (u_b - u_a) \right) \mathrm{d}X.$$

In discrete form this quantity may be expressed as

$$F = \sum_{i=0}^{n-2} \left(-m_1 \left(\frac{P_{i+1} - P_i}{\Delta X} \right) \left(\frac{H_{i+1} + H_i}{4} \right) + m_2 \left(\frac{\overline{\eta}_{i+1} + \overline{\eta}_i}{H_{i+1} + H_i} \right) (u_b - u_a) \right) \Delta X,$$

hence differentiation with respect to P_j, H_0 and X_c yields:

$$\frac{\partial F}{\partial P_j} = -m_1 \left(\frac{H_{j+1} + H_j}{4} - \frac{H_j + H_{j-1}}{4} \right) + m_2 \overline{\alpha\eta}_j \left(\frac{u_b - u_a}{H_{j+1} + H_j} + \frac{u_b - u_a}{H_j + H_{j-1}} \right) \Delta X,$$

$$\frac{\partial F}{\partial H_0} = -m_1 \sum_{i=0}^{n-2} \frac{P_{i+1} - P_i}{2} - 2m_2 \sum_{i=0}^{n-2} \left(\frac{\overline{\eta}_{i+1} + \overline{\eta}_i}{(H_{i+1} + H_i)^2} \right) (u_b - u_a) \Delta X$$

and

$$\frac{\partial F}{\partial X_c} = -m_1 \sum_{i=0}^{n-2} (P_{i+1} - P_i) \left(\frac{X_{i+1} + X_i}{4} \right) - m_2 \sum_{i=0}^{n-2} \left(\frac{(\overline{\eta}_{i+1} - \overline{\eta}_i)(X_{i+1} + X_i)}{(H_{i+1} + H_i)^2} \right) (u_b - u_a) \Delta X.$$

6.5 Adjoint solution method and results

Having defined the adjoint equation system for both the "compact" and "expanded" Jacobians in the previous section, attention is turned to their solution. Since both of the Jacobians are still sparse, the same numerical package is used as in Chapter 5, SPARSKIT. Again, the specific method used is GMRES.

In the rest of this section it is demonstrated, via numerical examples, that the implementations of both the "compact" and "expanded" Jacobians, used within the adjoint system, give excellent error estimates for the given quantity of interest. Since this hydrodynamic problem is only intended as a step toward the full EHL problem, local mesh refinement is not considered here: it is sufficient to demonstrate the quality of the results on a sequence of uniform refinements. Local mesh refinement will be considered again in the following chapter.

All of the numerical results presented in this chapter are for a hydrodynamic case with load $L = 1309$. Two different sets of different surface speeds are considered, namely $u_a = u_b = 0.5$ and $u_a = 0.1$, $u_b = 0.9$. These corresponds to a case with pure rolling, and one with a slide-roll ratio of 0.8, respectively.

6.5.1 Expanded Jacobian

The first thing to notice about a hydrodynamic pressure solution is how much less complicated the pressure profile is than for the EHL problem. This can be seen by comparing Figures 4.1 and 6.3. Looking at Figures 6.3 and 6.4, the solutions for viscosity and density are very similar in shape to the pressure solution. In contrast to this, Figure 6.5 shows how different the three computed adjoint solutions (relating to P, $\overline{\eta}$ and $\overline{\rho}$) are from each other. Looking at Figure 6.5, apart from being fairly influential in broadly the same region (around the contact region), it is clear that they are really quite different. This is shown more clearly in Figure 6.6 which uses a different vertical scale for the density adjoint. From this observation alone, one might be tempted to conclude that the adjoint equations are all important and as such all adjoint variables are equally important in the adjoint method. However, a look at the residuals for each of the three variables (P, $\overline{\eta}$ and $\overline{\rho}$) shows that this is not the case. Figure 6.7 shows that only the pressure residuals are actually non-negligible. This is because the residual equations for viscosity and density (equations (6.15) and (6.16)) are only trivial pointwise calculations. As a result of this,

mesh points which are coincident between the coarse and fine meshes have identically zero residuals, and the very small residual at the non-coincident points is due primarily to interpolation error. This means that the adjoint solutions for viscosity and density do not make any significant contribution to the correction calculated for the quantity of interest. These vectors can be seen in Figure 6.8. It is perhaps to be expected therefore that the compact approximation, using just P as a primary variable, will provide equally good results.

The most persuasive evidence of this is shown next where the tables showing convergence of the adjoint error estimates are presented.

6.5.2 Tables

Tables 6.1 to 6.4 show how accurately the adjoint error estimation predicts the inter-grid friction error in all four cases. Those case are sliding and rolling friction for both the compact and expanded Jacobians introduced earlier. As with the tables in Chapter 5, the grid shows the effectivity index converging to 1.0 with increased mesh resolution. Column 2 shows the friction as calculated on the fine mesh using values interpolated from the coarse mesh solution, while column 3 shows the correction as calculated using the adjoint error estimation. Column 4 combines these two values to get the corrected friction, which can then be directly compared to the actual friction as solved for and calculated on the fine grid, shown in column 5. The measured error, given in column 6, is calculated as the difference between columns 2 and 5. The ratio of the actual measured error to that predicted is known as the effectivity index, and is given in column 7.

As mentioned above, it can be seen that in all four cases the effectivity index gets closer to 1.0 with increasing mesh resolution. This shows that the adjoint error estimation is extremely effective at predicting the inter-grid error for hydrodynamic lubrication. More importantly in this instance, though, is the fact that both the expanded and the compact Jacobians have been demonstrated to be accurate as part of the adjoint solution process. This is an important conclusion going forwards, as it shows that when applying adjoint error estimation to elastohydrodynamic lubrication in the following chapter, only a compact Jacobian need be considered, allowing for the increased efficiency described earlier. In a wider context, it sheds light on how complex systems of equations can be solved, in particular problems of real engineering interest which use iterative techniques to solve them.

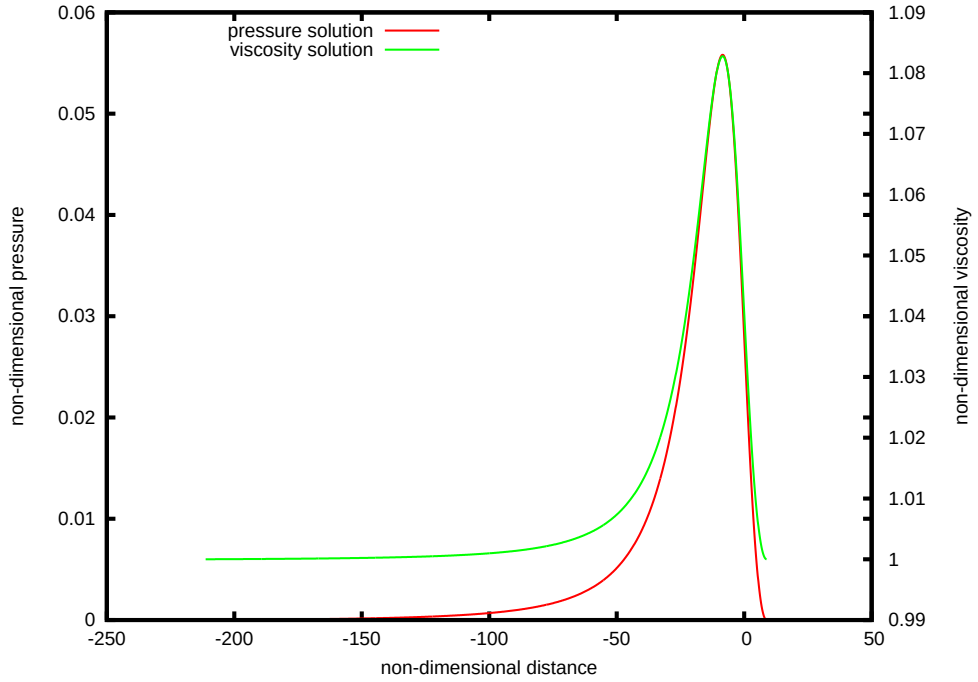

Figure 6.3: Pressure and viscosity solutions for the hydrodynamic problem; $L = 1309$

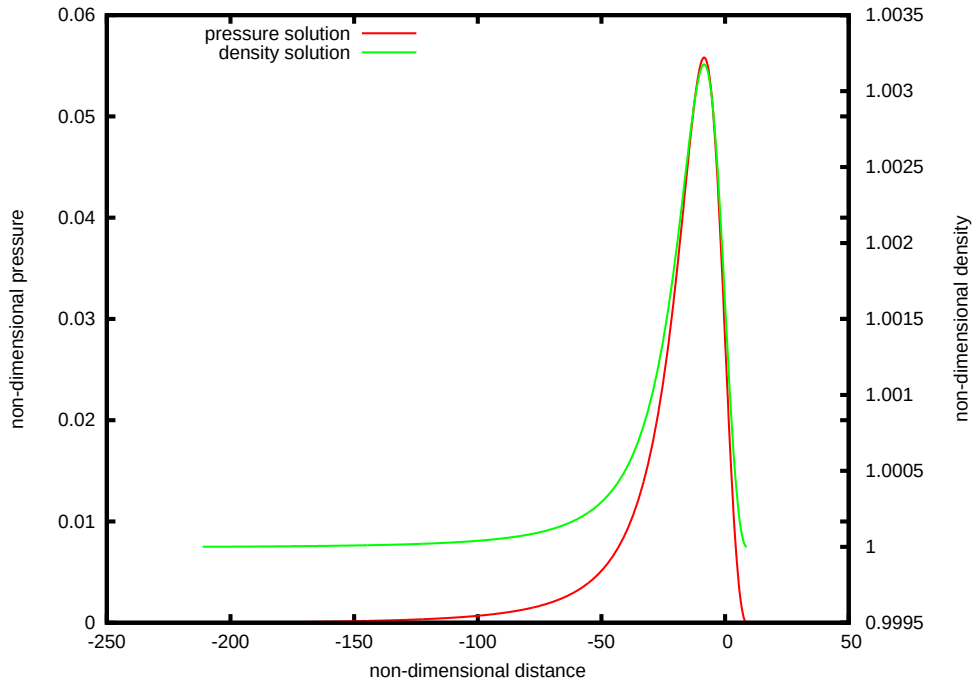

Figure 6.4: Pressure and density solutions for the hydrodynamic problem; $L = 1309$

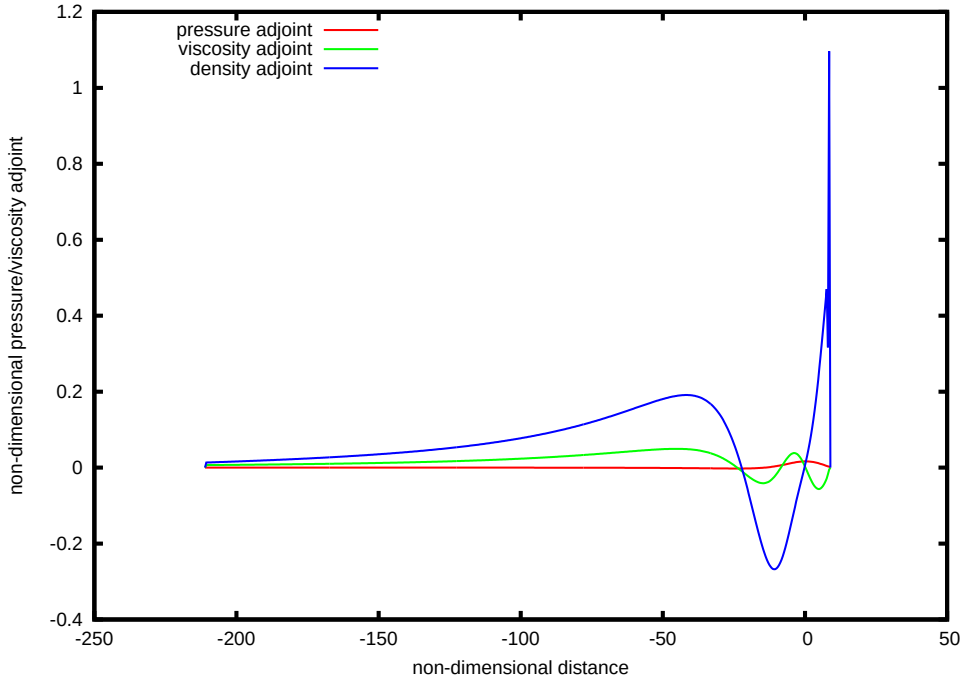

Figure 6.5: Adjoint solutions for the hydrodynamic problem; $L = 1309$, slide-roll ratio = 0.0 (pure rolling)

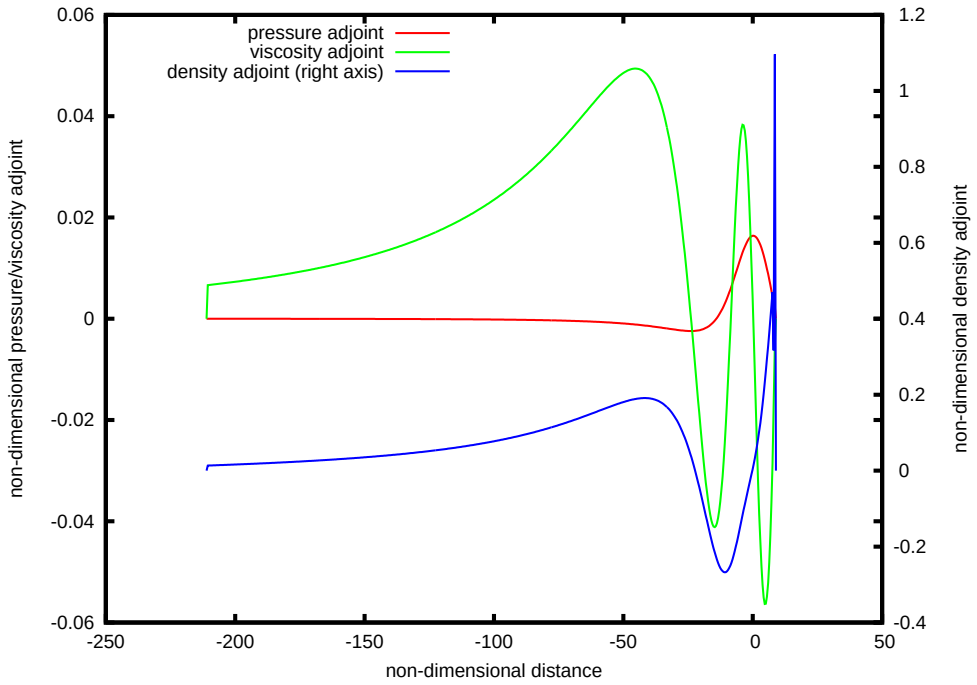

Figure 6.6: Adjoint solutions for the hydrodynamic problem; $L = 1309$, slide-roll ratio = 0.0 (pure rolling)

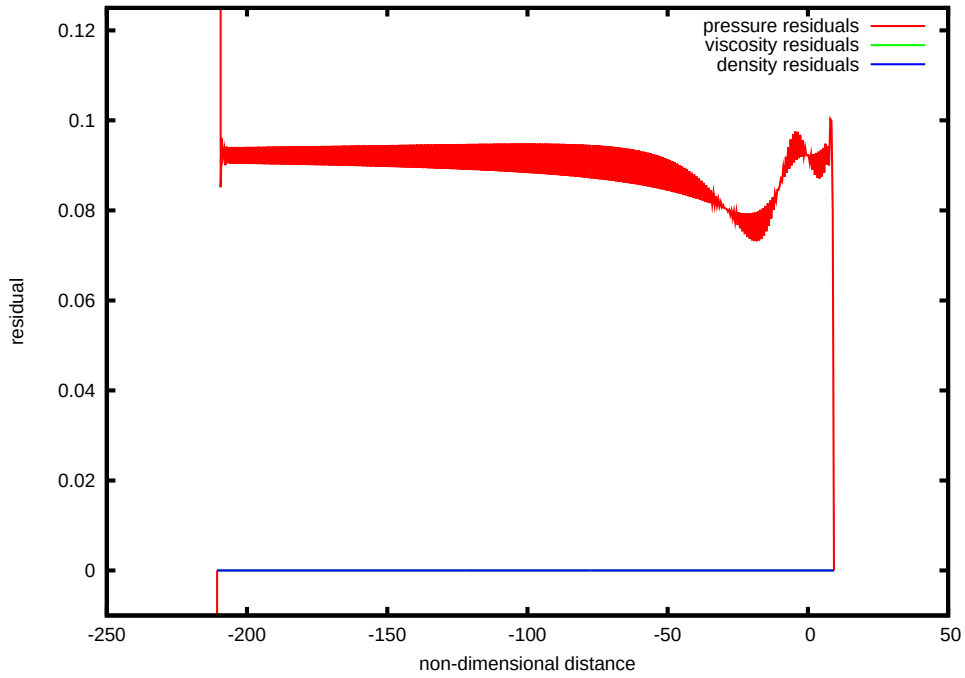

Figure 6.7: Comparison of solution residuals for P, $\overline{\eta}$, and $\overline{\rho}$ for the hydrodynamic problem; $L = 1309$, slide-roll ratio = 0.0 (pure rolling)

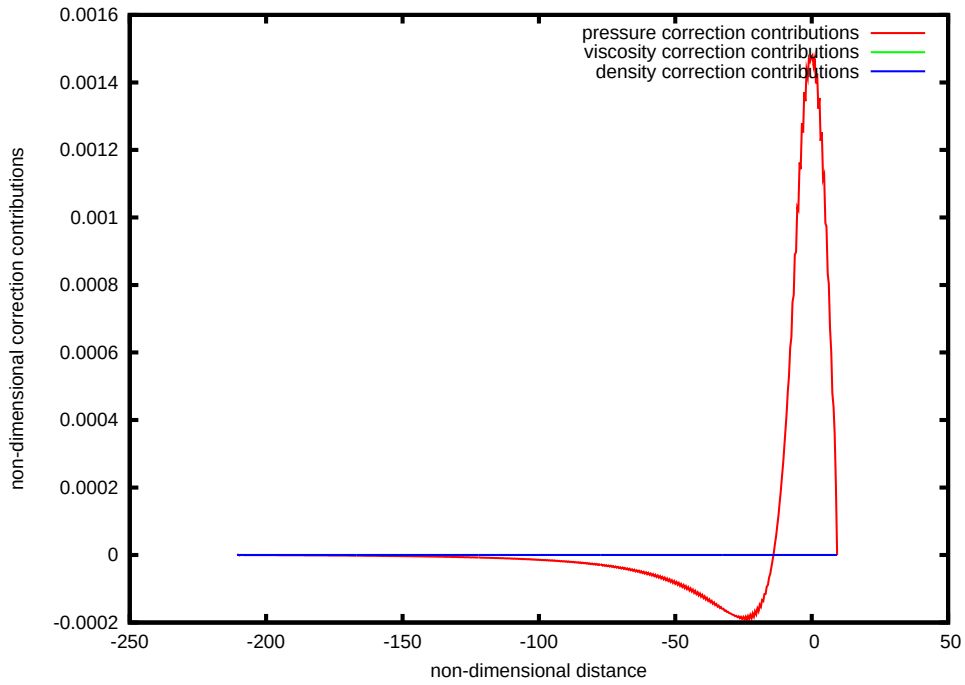

Figure 6.8: Comparison of correction contributions for P, $\overline{\eta}$, and $\overline{\rho}$ for the hydrodynamic problem with the expanded Jacobian system; $L = 1309$, slide-roll ratio = 0.0 (pure rolling)

Grid (g)	Interpolated Fric. (g)	Calculated correction	Corrected Fric. (g)	Friction ($g+1$)	Measured Error	Effectiv. Index
5	-8.52510	0.11986	-8.64496	-8.64753	0.12242	1.02139
6	-8.64751	0.05886	-8.70637	-8.70663	0.05912	1.00442
7	-8.70663	0.02876	-8.73539	-8.73545	0.02882	1.00195
8	-8.73545	0.01417	-8.74962	-8.74964	0.01419	1.00098
9	-8.74964	0.00703	-8.75667	-8.75667	0.00703	1.00035
10	-8.75667	0.00350	-8.76017	-8.76017	0.00350	0.99997
11	-8.76017	0.00175	-8.76192	-8.76192	0.00175	0.99986

Table 6.1: Adjoint based inter-grid friction error on uniform meshes using compact Jacobian; $L = 1309$, slide-roll ratio = 0.0 (pure rolling)

Grid (g)	Interpolated Fric. (g)	Calculated correction	Corrected Fric. (g)	Friction ($g+1$)	Measured Error	Effectiv. Index
5	-8.52510	0.11986	-8.64496	-8.64753	0.12242	1.02140
6	-8.64751	0.05883	-8.70634	-8.70663	0.05912	1.00491
7	-8.70663	0.02875	-8.73538	-8.73545	0.02882	1.00250
8	-8.73545	0.01417	-8.74962	-8.74964	0.01419	1.00154
9	-8.74964	0.00703	-8.75666	-8.75667	0.00703	1.00091
10	-8.75667	0.00350	-8.76017	-8.76017	0.00350	1.00055
11	-8.76017	0.00175	-8.76192	-8.76192	0.00175	1.00044

Table 6.2: Adjoint based inter-grid friction error on uniform meshes using expanded Jacobian; $L = 1309$, slide-roll ratio = 0.0 (pure rolling)

Grid (g)	Interpolated Fric. (g)	Calculated correction	Corrected Fric. (g)	Friction ($g+1$)	Measured Error	Effectiv. Index
5	-18.22851	0.27258	-18.50109	-18.51682	0.28831	1.05770
6	-18.52599	0.15056	-18.67656	-18.68449	0.15850	1.05270
7	-18.68689	0.07824	-18.76513	-18.76743	0.08054	1.02942
8	-18.76804	0.03973	-18.80777	-18.80834	0.04030	1.01438
9	-18.80850	0.02003	-18.82853	-18.82870	0.02020	1.00876
10	-18.82874	0.01001	-18.83875	-18.83882	0.01007	1.00664
11	-18.83883	0.00500	-18.84382	-18.84384	0.00502	1.00462

Table 6.3: Adjoint based inter-grid friction error on uniform meshes using compact Jacobian; $L = 1309$ slide-roll ratio = 0.8 (sliding)

Grid (g)	Interpolated Fric. (g)	Calculated correction	Corrected Fric. (g)	Friction ($g+1$)	Measured Error	Effectiv. Index
5	-18.22852	0.27322	-18.50173	-18.51682	0.28831	1.05523
6	-18.52599	0.15074	-18.67673	-18.68449	0.15850	1.05148
7	-18.68689	0.07833	-18.76522	-18.76743	0.08054	1.02823
8	-18.76804	0.03977	-18.80782	-18.80834	0.04030	1.01316
9	-18.80850	0.02005	-18.82855	-18.82870	0.02020	1.00751
10	-18.82874	0.01002	-18.83876	-18.83882	0.01007	1.00537
11	-18.83883	0.00500	-18.84383	-18.84384	0.00502	1.00333

Table 6.4: Adjoint based inter-grid friction error on uniform meshes using expanded Jacobian; $L = 1309$ slide-roll ratio = 0.8 (sliding)

6.6 Summary

Adjoint error estimation has been applied to a compressible piezo-viscous hydrodynamic lubrication problem. The additional non-linearities introduced by the viscosity and density equations have been shown to cause no difficulty to the adjoint error estimation procedure, which still gives accurate predictions of the inter-grid error in the friction, as demonstrated by Tables 6.1 to 6.4. This shows that the adjoint error estimation procedure can be carried out using either the compact or expanded Jacobians, which will be useful going forward. In the next chapter, the application of the adjoint error estimation will be further extended to a full steady-state elastohydrodynamic lubrication problem, by introducing the deformation calculation within the film thickness equation.

Chapter 7

EHL Line Contact Problems

In the previous chapter, adjoint error estimation was successfully applied to a hydrodynamic problem. This was achieved for the residual equations posed in two different ways and it was shown that both were equally accurate when attempting to predict the inter-grid functional error. In this chapter, adjoint error estimation is used on an elastohydrodynamic problem. It will be shown that, again, adjoint error estimation provides good predictions of the inter-grid functional error.

Having highlighted the efficacy of this approach on uniform meshes, spatial mesh adaptation will be introduced. The exact nature of the forward problem will be discussed, including the suitability of performing a global mesh calculation on an adaptive multi-grid problem. Following a short discussion on the correct form of the Jacobian for this problem, and the approximation used, results of spatial mesh adaptation carried out using the size of the correction components will be presented. Additional functionals will be introduced to further illustrate adjoint error estimation as applied to EHL, as well as to highlight some apparent limitations of this approach.

7.1 Uniform mesh EHL

In this section, the full EHL system is defined by including the elastic deformation term into the film thickness equation. There is also a change to the viscosity model used, in that the Barus equation (2.6), used for all of the previous work, has been replaced by the more accurate Roelands equation (2.5). Not only is the latter model more physically realistic but it also has computational advantages since the exponential growth of viscosity is not unbounded, as in the Barus case.

7.2 Forward problem

7.2.1 Continuous mathematical model

In Section 2.2, the equations and parameters for the non-dimensional EHL model were defined. The following set of equations in the unknowns P, H, $\overline{\eta}$, $\overline{\rho}$, and X_c are repeated below.

The Reynolds equation for the full line contact is given by

$$\frac{\partial}{\partial X}\left(\varepsilon\frac{\partial P}{\partial X}\right)-\frac{\partial(\overline{\rho}H)}{\partial X}=0, \tag{7.1}$$

with the film thickness equation, now including the deformation term, written as

$$H=H_0+\frac{X^2}{2}+\frac{1}{\pi}\int_{-\infty}^{\infty}\ln|X-X'|P(X')\mathrm{d}X'. \tag{7.2}$$

The viscosity model is now provided by Roelands [62],

$$\overline{\eta}=\exp\left\{\left(\frac{\alpha p_0}{z}\right)\left(-1+\left[1+\frac{Pp_h}{p_0}\right]^z\right)\right\}, \tag{7.3}$$

with justification for this change explained in Section 7.4. The density, as before, is given by [17],

$$\overline{\rho}=\frac{0.59\times10^9+1.34Pp_h}{0.59\times10^9+Pp_h}. \tag{7.4}$$

Note that the cavitation boundary position, X_c, must be found such that the boundary

conditions

$$P(X_{-\infty}) = P(X_c) = P'(X_c) = 0 \tag{7.5}$$

are satisfied, and H_0 must be found such that the sum of the pressure is equal to the applied load. This is shown here as

$$\int_{-\infty}^{\infty} P \, \mathrm{d}X = \frac{\pi}{2}. \tag{7.6}$$

7.2.2 Residual equations

Once discretised, equations (7.1) to (7.6) can be written as residual equations. As in previous chapters, these residual equations will be used in the derivation of the Jacobian matrix for the calculation of the adjoint solution. For a uniform mesh with n nodes, labelled 0 to $n-1$, we have the following. The residuals for the Reynolds equation (7.1) for points $i = 1 \ldots n-2$, are given by

$$\begin{aligned} R_i &= \Delta X \left(\left(\frac{\overline{\rho}_i H_i - \overline{\rho}_{i-1} H_{i-1}}{\Delta X} \right) - \left(\frac{(P_{i+1} - P_i)\varepsilon_{i+\frac{1}{2}} - (P_i - P_{i-1})\varepsilon_{i-\frac{1}{2}}}{(\Delta X)^2} \right) \right) \\ &= \left(\overline{\rho}_i H_i - \overline{\rho}_{i-1} H_{i-1}\right) - \left(\frac{(P_{i+1} - P_i)\varepsilon_{i+\frac{1}{2}} - (P_i - P_{i-1})\varepsilon_{i-\frac{1}{2}}}{\Delta X} \right) \qquad (7.7) \\ &= \left(\overline{\rho}_i H_i - \overline{\rho}_{i-1} H_{i-1}\right) - \left(\frac{\varepsilon_{i+\frac{1}{2}} P_{i+1} - (\varepsilon_{i+\frac{1}{2}} + \varepsilon_{i-\frac{1}{2}}) P_i + \varepsilon_{i-\frac{1}{2}} P_{i-1}}{\Delta X} \right), \qquad (7.8) \end{aligned}$$

and for the two end points are given by

$$R_0 = 0 - P_0,$$

and

$$R_{n-1} = 0 - P_{n-1},$$

where $\varepsilon_i = \frac{H_i^3 \overline{\rho}_i}{\lambda \overline{\eta}_i}$, and $\varepsilon_{i\pm\frac{1}{2}} = (\varepsilon_i + \varepsilon_{i\pm1})/2$. The discrete form of H_i, $\overline{\eta}_i$, and $\overline{\rho}_i$ are given respectively by

$$H_i = H_0 + \frac{X_i^2}{2} + \frac{1}{\pi} \sum_{j=0}^{n-1} K_{ij} P_j, \tag{7.9}$$

$$\overline{\eta}_i = \exp\left\{ \left(\frac{\alpha p_0}{z} \right) \left(-1 + \left[1 + \frac{P_i p_h}{p_0} \right]^z \right) \right\}, \tag{7.10}$$

$$\overline{\rho}_i = \frac{0.59 \times 10^9 + 1.34 P_i p_h}{0.59 \times 10^9 + P_i p_h}. \tag{7.11}$$

Note that in (7.9) the terms K_{ij} result from the application of quadrature to (7.2), see Section 2.3. The discrete cavitation position residual is gained through a second order upwind finite difference approximation, $\frac{\partial P_i}{\partial X} = \frac{3P_i - 4P_{i-1} + P_{i-2}}{2\Delta X}$. By evaluating this at the boundary point $i = n-1$, and noting that $P_{n-1} = 0$, this residual can be expressed as

$$R_{X_c} = \frac{4P_{n-2} - P_{n-3}}{2\Delta X}. \tag{7.12}$$

The final condition that must be satisfied in the forward solve is the discrete force balance equation, used to update H_0. The residual for this discrete equation is

$$R_{H_0} = \frac{\pi}{2} - \sum_{i=0}^{n-2} \frac{P_i + P_{i+1}}{2} \Delta X. \tag{7.13}$$

7.2.3 Solution method: Newton-Raphson boundary solve

In order to solve the EHL problem, the Carmehl solver [71] developed for Shell Global Solutions is being used. This is being treated as a 'black-box' in order to provide a guaranteed level of accuracy and reliability from the solver. The solver operates as described in [26] and is summarised in Chapter 2, specifically Figure 2.2. Note that the multilevel multi-integration (MLMI) capability within Carmehl is not used in this work since it is only applicable on uniform spatial discretisations and we wish the work here to be applicable on locally refined, as well as uniform, meshes. One of the inputs to the solver is the computational domain range. Note that as part of our new "sliding grid" process to satisfy the cavitation condition (7.12) (see Section 7.2), this domain may be shifted by up to half a grid cell. Moreover, since the EHL solver is relatively computationally expensive, a more efficient approach to finding the correct boundary position is needed than was previously employed in Chapter 5. Two new approaches have been implemented; a secant-type method, and a Newton-Raphson-type method. Both give similar increases in performance and so it is the secant method that is used throughout this chapter.

7.3 Jacobian for adjoint solution

In this section the residual equations shown above are differentiated with respect to each of the degrees of freedom. As was shown in Chapter 6, the adjoint error estimation procedure is equally applicable for both the "expanded" and "dense" Jacobian formulations.

In this Chapter, the dense Jacobian is used throughout. This is because a fully formed expanded Jacobian would now have approximately four times as many rows as the equivalent dense Jacobian, leading to longer solution times for no benefit. Although much of the expanded Jacobian would be sparse (block tri-diagonal) there would still be a dense block the size of the dense Jacobian eliminating the possibility of a faster iterative solution procedure.

7.3.1 Preliminaries

First, we consider differentiating the secondary dependent variables H_i, $\overline{\eta}_i$ and $\overline{\rho}_i$ with respect to the primary dependent variables P_j, H_0 and X_c. These results will be used to compute derivatives of $\varepsilon_{i+\frac{1}{2}}$. These preliminary results will simplify the Jacobian evaluation in the next subsection. Where appropriate, the Kronecker delta will be used. This discrete function is a special case of the generalised Kronecker delta symbol, and is defined to be

$$\delta_{ij} = \begin{cases} 1 & i = j \\ 0 & i \neq j \end{cases} .$$

Note that the distance through the domain, X_i, given by

$$X_i = X_c + (i-n)\Delta X,$$

depends on X_c which is one of the degrees of freedom. This is therefore another contributing complication into the discrete film thickness equation (7.9). This film thickness equation can be differentiated with respect to the n pressure values, the cavitation position and H_0, to give

$$\frac{\partial H_i}{\partial P_j} = \frac{1}{\pi} K_{ij}, \qquad \frac{\partial H_i}{\partial H_0} = 1, \qquad \frac{\partial H_i}{\partial X_c} = X_i. \tag{7.14}$$

The non-dimensional viscosity, given in equation (7.10), is differentiated with respect to the pressures as

$$\begin{aligned} \frac{\partial \overline{\eta}_i}{\partial P_j} &= \frac{\partial}{\partial P_j}\left(\exp\left\{\left(\frac{\alpha p_0}{z_0}\right)\left(-1+\left[1+\frac{P_i p_h}{p_0}\right]^z\right)\right\}\right) \\ &= \delta_{ij}\left(z\frac{\alpha p_0}{z_0}\frac{p_h}{p_0}\left[1+\frac{P_i p_h}{p_0}\right]^{z-1}\exp\left\{\left(\frac{\alpha p_0}{z_0}\right)\left(-1+\left[1+\frac{P_i p_h}{p_0}\right]^z\right)\right\}\right) \\ &= \delta_{ij}\left(\frac{z\alpha p_h}{z_0}\left[1+\frac{P_i p_h}{p_0}\right]^{z-1}\exp\left\{\left(\frac{\alpha p_0}{z_0}\right)\left(-1+\left[1+\frac{P_i p_h}{p_0}\right]^z\right)\right\}\right), \end{aligned} \tag{7.15}$$

and with respect to H_0 and X_c as

$$\frac{\partial \overline{\eta}_i}{\partial H_0} = \frac{\partial \overline{\eta}_i}{\partial X_c} = 0.$$

The non-dimensional density, (7.11), similarly, gives

$$\begin{aligned}
\frac{\partial \overline{\rho}_i}{\partial P_j} &= \delta_{ij}\left(\frac{(0.59\times10^9 + P_i p_h)1.34p_h - (0.59\times10^9 + 1.34P_i p_h)p_h}{(0.59\times10^9 + P_i p_h)^2}\right) \\
&= \delta_{ij}\left(\frac{(0.59\times10^9\times1.34p_h) + (1.34p_h^2P_i) - (0.59\times10^9 p_h) - (1.34p_h^2P_i)}{(0.59\times10^9 + P_i p_h)^2}\right) \\
&= \delta_{ij}\left(\frac{(1.34-1.0)0.59\times10^9 p_h}{(0.59\times10^9 + P_i p_h)^2}\right) \\
&= \delta_{ij}\left(\frac{0.34\times0.59\times10^9 p_h}{(0.59\times10^9 + P_i p_h)^2}\right), \qquad (7.16)
\end{aligned}$$

and

$$\frac{\partial \overline{\rho}_i}{\partial H_0} = \frac{\partial \overline{\rho}_i}{\partial X_c} = 0. \qquad (7.17)$$

Next, differentiation of ε_i with respect to the primary dependent variables is considered. This is defined above as

$$\varepsilon_i = \frac{H_i^3 \overline{\rho}_i}{\lambda \overline{\eta}_i},$$

which means that differentiation with respect to P_j requires use of the chain rule. Hence

$$\begin{aligned}
\frac{\partial(\varepsilon_i)}{\partial P_j} &= \frac{\partial(\varepsilon_i)}{\partial H_i}\frac{\partial H_i}{\partial P_j} + \frac{\partial(\varepsilon_i)}{\partial \overline{\rho}_i}\frac{\partial \overline{\rho}_i}{\partial P_j} + \frac{\partial(\varepsilon_i)}{\partial \overline{\eta}_i}\frac{\partial \overline{\eta}_i}{\partial P_j} \qquad (7.18) \\
&= \frac{1}{\pi}K_{ij}\frac{3H_i^2\overline{\rho}_i}{\lambda\overline{\eta}_i} + \delta_{ij}\left(\frac{0.34\times0.59\times10^9 p_h}{(0.59\times10^9 + P_i p_h)^2}\right)\frac{H_i^3}{\lambda\overline{\eta}_i} \\
&\quad -\delta_{ij}\left(p_h\alpha\left[1+\frac{P_i p_h}{p_0}\right]^{z-1}\overline{\eta}_i\right)\frac{H_i^3\overline{\rho}_i}{\lambda(\overline{\eta}_i)^2} \qquad (7.19) \\
&= \frac{K_{ij}}{\pi}\frac{3\varepsilon_i}{H_i} + \delta_{ij}\left(\frac{0.34\times0.59\times10^9 p_h}{(0.59\times10^9 + P_i p_h)^2}\frac{\varepsilon_i}{\overline{\rho}_i} - p_h\alpha\varepsilon_i\left[1+\frac{P_i p_h}{p_0}\right]^{z-1}\right). \qquad (7.20)
\end{aligned}$$

Similarly,

$$\frac{\partial(\varepsilon_i)}{\partial H_0} = \frac{3H_i^2\overline{\rho}_i}{\lambda\overline{\eta}_i} = \frac{3\varepsilon_i}{H_i} \qquad (7.21)$$

and

$$\frac{\partial(\varepsilon_i)}{\partial X_c} = \frac{3X_i H_i^2\overline{\rho}_i}{\lambda\overline{\eta}_i} = \frac{3X_i\varepsilon_i}{H_i}. \qquad (7.22)$$

Following on from this, $\varepsilon_{i\pm\frac{1}{2}}$ is considered:

$$\frac{\partial \varepsilon_{i\pm\frac{1}{2}}}{\partial P_j} = \frac{\partial}{\partial P_j}\left(\frac{\varepsilon_i + \varepsilon_{i\pm1}}{2}\right) \tag{7.23}$$

$$= \frac{1}{2}\frac{\partial \varepsilon_i}{\partial P_j} + \frac{1}{2}\frac{\partial \varepsilon_{i\pm1}}{\partial P_j} \tag{7.24}$$

$$\begin{aligned} = {} & \frac{1}{2}\frac{K_{ij}}{\pi}\frac{3\varepsilon_i}{H_i} + \frac{1}{2}\frac{K_{i\pm1,j}}{\pi}\frac{3\varepsilon_{i\pm1}}{H_{i\pm1}} \\ & + \frac{1}{2}\delta_{ij}\left(\frac{0.34\times0.59\times10^9 p_h}{(0.59\times10^9 + P_i p_h)^2}\frac{\varepsilon_i}{\overline{\rho}_i} - \overline{\alpha}\varepsilon_i\left[1+\frac{P_i p_h}{p_0}\right]^{z-1}\right) \\ & + \frac{1}{2}\delta_{i\pm1,j}\left(\frac{0.34\times0.59\times10^9 p_h}{(0.59\times10^9 + P_{i\pm1} p_h)^2}\frac{\varepsilon_{i\pm1}}{\overline{\rho}_{i\pm1}} - \overline{\alpha}\varepsilon_{i\pm1}\left[1+\frac{P_{i\pm1} p_h}{p_0}\right]^{z-1}\right) \end{aligned} \tag{7.25}$$

where for this problem $z = z_0$, and hence $z/z_0 = 1$.

7.3.2 Residual equation differentiation

Having obtained some helpful preliminary expressions, the terms of the Jacobian are now derived. In certain places, superfluous use of the δ notation will be used to make dependencies more immediately obvious.

First, the discrete Reynolds residual, equation (7.7), is restated,

$$R_i = \left(\overline{\rho}_i H_i - \overline{\rho}_{i-1} H_{i-1}\right) - \left(\frac{(P_{i+1}-P_i)\varepsilon_{i+\frac{1}{2}} - (P_i - P_{i-1})\varepsilon_{i-\frac{1}{2}}}{\Delta X}\right). \tag{7.26}$$

Considering the first part of the equation above, $\left(\overline{\rho}_i H_i - \overline{\rho}_{i-1} H_{i-1}\right)$,

$$\begin{aligned} \frac{\partial}{\partial P_j}\left(\left(\overline{\rho}_i H_i - \overline{\rho}_{i-1} H_{i-1}\right)\right) = {} & \overline{\rho}_i \frac{\partial H_i}{\partial P_j} + \delta_{ij}\left(H_i \frac{\partial \overline{\rho}_i}{\partial P_j}\right) \\ & - \overline{\rho}_{i-1}\frac{\partial H_{i-1}}{\partial P_j} - \delta_{i-1,j}\left(H_{i-1}\frac{\partial \overline{\rho}_{i-1}}{\partial P_j}\right) \end{aligned} \tag{7.27}$$

Now, considering the second part of the above equation, $\left(\frac{(P_{i+1}-P_i)\varepsilon_{i+\frac{1}{2}} - (P_i - P_{i-1})\varepsilon_{i-\frac{1}{2}}}{\Delta X}\right)$,

$$\frac{\partial}{\partial P_j}\left(\frac{(P_{i+1}-P_i)\varepsilon_{i+\frac{1}{2}} - (P_i - P_{i-1})\varepsilon_{i-\frac{1}{2}}}{(\Delta X)}\right)$$

$$
\begin{aligned}
&= -\delta_{ij}\left(\frac{\varepsilon_{i+\frac{1}{2}}+\varepsilon_{i-\frac{1}{2}}}{\Delta X}\right) \\
&\quad +\delta_{i-1,j}\left(\frac{\varepsilon_{i-\frac{1}{2}}}{\Delta X}\right)+\delta_{i+1,j}\left(\frac{\varepsilon_{i+\frac{1}{2}}}{\Delta X}\right) \\
&\quad +\left(\frac{P_{i+1}-P_i}{\Delta X}\right)\frac{\partial \varepsilon_{i+\frac{1}{2}}}{\partial P_j}-\left(\frac{P_i-P_{i-1}}{\Delta X}\right)\frac{\partial \varepsilon_{i-\frac{1}{2}}}{\partial P_j}
\end{aligned} \tag{7.28}
$$

Combining these two results, it is possible to obtain

$$
\begin{aligned}
\frac{\partial R_i}{\partial P_j} &= \overline{\rho}_i\frac{\partial H_i}{\partial P_j}+\delta_{ij}\left(H_i\frac{\partial \overline{\rho}_i}{\partial P_j}\right)-\overline{\rho}_{i-1}\frac{\partial H_{i-1}}{\partial P_j}-\delta_{i-1,j}\left(H_{i-1}\frac{\partial \overline{\rho}_{i-1}}{\partial P_j}\right) \\
&- \left[-\delta_{ij}\left(\frac{\varepsilon_{i+\frac{1}{2}}+\varepsilon_{i-\frac{1}{2}}}{\Delta X}\right)+\delta_{i-1,j}\left(\frac{\varepsilon_{i-\frac{1}{2}}}{\Delta X}\right)+\delta_{i+1,j}\left(\frac{\varepsilon_{i+\frac{1}{2}}}{\Delta X}\right)\right. \\
&\quad \left. +\left(\frac{P_{i+1}-P_i}{\Delta X}\right)\frac{\partial \varepsilon_{i+\frac{1}{2}}}{\partial P_j}-\left(\frac{P_i-P_{i-1}}{\Delta X}\right)\frac{\partial \varepsilon_{i-\frac{1}{2}}}{\partial P_j}\right]
\end{aligned} \tag{7.29}
$$

$$
\begin{aligned}
&= \overline{\rho}_i\frac{\partial H_i}{\partial P_j}-\overline{\rho}_{i-1}\frac{\partial H_{i-1}}{\partial P_j}+\delta_{ij}\left(H_i\frac{\partial \overline{\rho}_i}{\partial P_j}\right)-\delta_{i-1,j}\left(H_{i-1}\frac{\partial \overline{\rho}_{i-1}}{\partial P_j}\right) \\
&\quad +\delta_{ij}\left(\frac{\varepsilon_{i+\frac{1}{2}}+\varepsilon_{i-\frac{1}{2}}}{\Delta X}\right)-\delta_{i-1,j}\left(\frac{\varepsilon_{i-\frac{1}{2}}}{\Delta X}\right)-\delta_{i+1,j}\left(\frac{\varepsilon_{i+\frac{1}{2}}}{\Delta X}\right) \\
&\quad -\left(\frac{P_{i+1}-P_i}{\Delta X}\right)\frac{\partial \varepsilon_{i+\frac{1}{2}}}{\partial P_j}+\left(\frac{P_i-P_{i-1}}{\Delta X}\right)\frac{\partial \varepsilon_{i-\frac{1}{2}}}{\partial P_j}.
\end{aligned} \tag{7.30}
$$

Note that this expression, whilst still quite complex, is simplified by the use of the sub-expressions derived in the previous subsection. Similarly, differentiating equation (7.26) with respect to H_0, gives

$$
\frac{\partial R_i}{\partial H_0} = (\overline{\rho}_i-\overline{\rho}_{i-1})-\left[\left(\frac{P_{i+1}-P_i}{\Delta X}\right)\frac{\partial \varepsilon_{i+\frac{1}{2}}}{\partial H_0}-\left(\frac{P_i-P_{i-1}}{\Delta X}\right)\frac{\partial \varepsilon_{i-\frac{1}{2}}}{\partial H_0}\right], \tag{7.31}
$$

and, with respect to X_c,

$$
\frac{\partial R_i}{\partial X_c} = (\overline{\rho}_i X_i-\overline{\rho}_{i-1}X_{i-1})-\left[\left(\frac{P_{i+1}-P_i}{\Delta X}\right)\frac{\partial \varepsilon_{i+\frac{1}{2}}}{\partial X_c}-\left(\frac{P_i-P_{i-1}}{\Delta X}\right)\frac{\partial \varepsilon_{i-\frac{1}{2}}}{\partial X_c}\right]. \tag{7.32}
$$

Having finished deriving the terms of the Jacobian related to the Reynolds residual equations, attention is turned to equation (7.13) the force balance residual, given again here as

$$
R_{H_0} = \frac{\pi}{2}-\sum_{i=0}^{n-2}\frac{P_i+P_{i+1}}{2}\Delta X.
$$

It is straightforward to see that for each P_j for $j = 1$ to $n-2$

$$\frac{\partial R_{H_0}}{\partial P_j} = -\Delta X.$$

With no dependence on H or X, clearly

$$\frac{\partial R_{H_0}}{\partial H_0} = \frac{\partial R_{H_0}}{\partial X_c} = 0.$$

Finally, given the discrete residual equation for the cavitation boundary condition (7.12) as

$$R_{X_c} = \frac{4P_{n-2} - P_{n-3}}{2\Delta X},$$

it follows that

$$\frac{\partial R_{X_c}}{\partial P_{n-3}} = -\frac{1}{2\Delta X}, \qquad \frac{\partial R_{X_c}}{\partial P_{n-2}} = \frac{2}{\Delta X}$$

and that

$$\frac{\partial R_{X_c}}{\partial H_0} = \frac{\partial R_{X_c}}{\partial X_c} = 0.$$

Having obtained expressions for all of the terms which appear in the dense form of the Jacobian matrix associated with the full EHL problem, we are now in a position to consider generalisation of our adjoint techniques to this problem.

7.4 Choice of viscosity model

In this section, the reason for the change of viscosity model to Roelands from Barus is outlined. Initially, work was completed to make adjoint error estimation work for an expanded Jacobian for the full EHL, as well as for a compact Jacobian. This was largely successful, although the best accuracy that could be gained by the adjoint error estimation had around a 6% error in it, and the effectivity index reliably converged to a value of about 1.06. The move to Roelands viscosity has eliminated this inaccuracy, and the effectivity index now converges to 1.0 again. There are two possible reasons that have been identified as to why the previous model may not have been completely successful.

The first refers to the shape of the pressure spike. The shape of the pressure spike generated with the Barus viscosity is “sharp”, i.e. there is a distinct singularity in the pressure gradient at that point. The reason that this might be a problem is to do with the interpolation of these values and the consistency between the different mesh levels. When

interpolating the pressure solution to move it to the fine grid, this sharp spike becomes rounded by the cubic spline interpolation. This is not an issue for the Roelands viscosity, as the spike is smooth to begin with. A summary of the argument is as follows:

- The coarse grid Jacobian uses the coarse grid "sharp" pressure solution
- The fine grid interpolation of the pressure has a smooth, or rounded spike
- The residuals calculated on the fine mesh use the smooth spike
- The adjoint solved on the coarse grid as an approximation to the fine grid uses the sharp spike
- Now there is an inconsistency between the Jacobian and the residuals calculated on the fine grid.

It is this inconsistency which is likely to be responsible for the slight discrepancy between the solutions.

There are two potential methods that could be explored in order to avoid this. The first is to try to calculate the adjoint solution on the fine mesh using the interpolated pressure values, so that the residuals and Jacobian are consistent. The other is to use an interpolation method which preserves the shape of the spike. However, since we are interested in more realistic rheological models such as Roelands, resolving this issue is not of paramount importance.

The second potential reason that has been identified is to do with the behaviour of the pressure spike with increased mesh resolution. Using the Roelands viscosity, the pressure spike of the resultant solution can be resolved, and it converges with increasing mesh points [4, 31]. Using the Barus viscosity, this is not the case, and adding more points merely adds to the size and sharpness of the pressure spike. The adjoint error estimation method has at its core the idea that, given sufficient mesh resolution, the first order approximation from the Jacobian will be sufficient, and that the higher order terms will be negligible. This may not be true for a solution that has a clear singularity which appears not to converge.

7.5 Uniform mesh results

We begin our assessment of the adjoint-based error estimate by assessing its performance on a sequence of uniformly refined grids. The following sections will then discuss the application with adaptivity and results on non-uniformly refined meshes.

7.5.1 Forward-solution profiles

In this section, results are presented for the adjoint error estimation procedure as applied to the full EHL problem on a series of uniform meshes. Results are shown for five different loadings on each of a purely rolling case and a sliding case. The non-dimensional solution profiles for pressure, film thickness, and viscosity are shown in Figures 7.1-7.3 respectively. These results were calculated using a uniform mesh of 257 points. The five solutions go through the range from being almost entirely hydrodynamic for the most lightly loaded case, though to a relatively highly loaded EHL case for the largest load. Figure 7.1 clearly illustrates the pressure spike moving towards the outlet with increasing load, with the main pressure bump becoming increasingly rounded. The non-dimensional film thickness, shown in Figure 7.2, is reduced overall with increased load, but also becomes thinner in the contact area, which is itself wider. Figure 7.3 shows the non-dimensional viscosity which increases dramatically with load. To understand this, consider for simplicity the non-dimensional Barus viscosity equation (2.16),

$$\overline{\eta} = e^{\overline{\alpha} P}, \tag{7.33}$$

as an example, where P is the non-dimensional pressure, and $\overline{\alpha} = \alpha p_h$. As shown in Figure 7.1, although the solution profile changes shape, the non-dimensionalised P values are broadly similar with increasing load. However, because $\overline{\alpha}$ contains the dimensional quantity p_h (the maximum Hertzian pressure), the viscosity, whilst non-dimensional, is not scaled to a range with maximum value around unity. A similar argument can be applied for the Roelands viscosity shown in Figure 7.3.

Next, results are presented for a rolling EHL case, followed by a case with sliding.

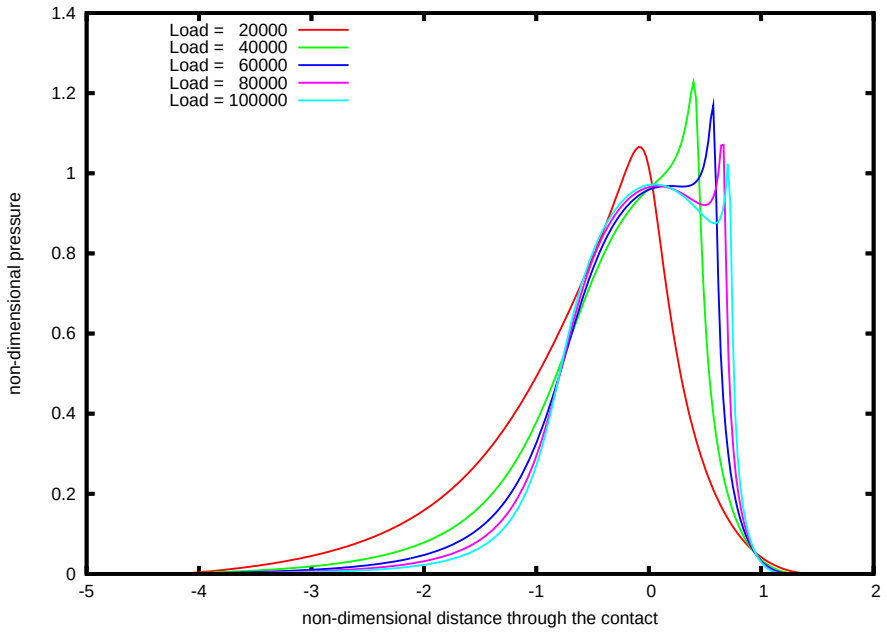

Figure 7.1: EHL pressure profiles for a series of loadings; $L = 20000$, 40000, 60000, 80000 and 100000

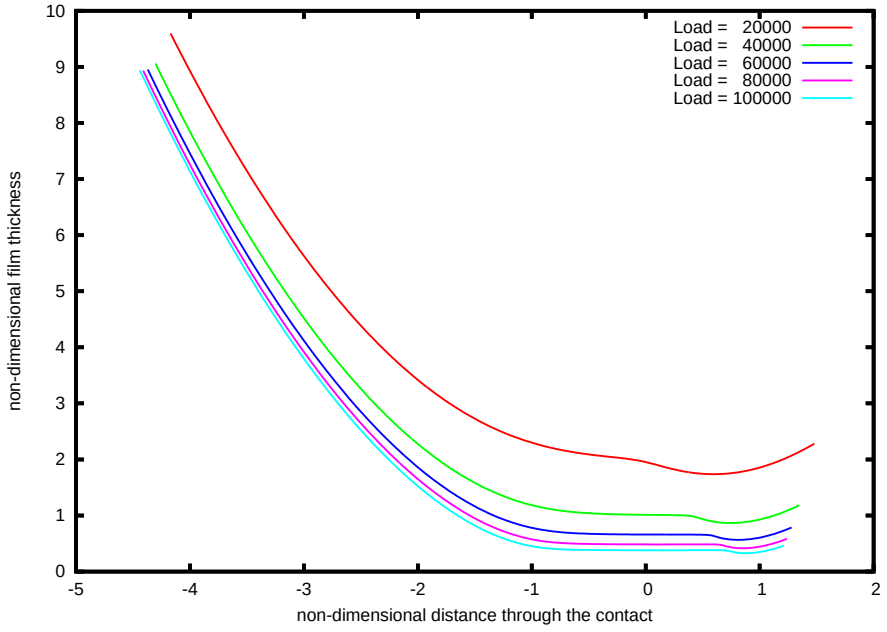

Figure 7.2: EHL film thickness profiles for a series of loadings; $L = 20000$, 40000, 60000, 80000 and 100000

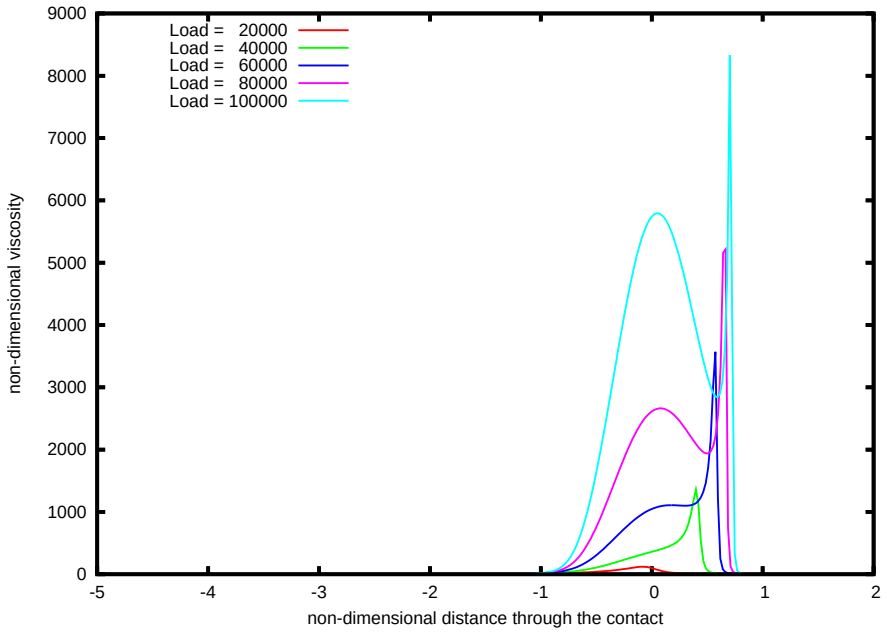

Figure 7.3: EHL viscosity profiles for a series of loadings; $L = 20000$, 40000, 60000, 80000 and 100000

7.5.2 Pure rolling

The dimensional friction, derived from that shown in Chapter 4, is given by

$$\overline{F} = \int_{-\infty}^{\infty} \left(-m_1 \frac{\partial P}{\partial X} \frac{H}{2} + m_2 \frac{\overline{\eta}}{H} (u_b - u_a) \right) \mathrm{d}X, \tag{7.34}$$

where the re-dimensionalising factors $m_1 = \frac{p_h b^2}{R_x}$ and $m_2 = \frac{\eta_0 R_x}{b}$. Pure rolling is the case where the two surface speeds, u_b and u_a, are moving at the same speed in the same direction, and hence the second term of the friction is zero. For the case where the surface speeds are $u_a = u_b = 0.5$, results for five different non-dimensional loads are presented. With no relative motion of the surfaces, the resistance to motion is purely that generated by trying to squeeze the fluid into the contact against the pressure gradient. The adjoint for each of the five solutions is shown in Figure 7.4. The solution profile of each of these adjoints is remarkably smooth, with little influence seen from the pressure spike. Tables 7.1 to 7.5 show the usual measures of success, including the effectivity index, for these typically loaded cases. This is the ratio of the measured error to the predicted error. In addition, there is an extra column. This, the last column in the table, shows the difference between the effectivity index and unity. Clearly, as the effectivity index approaches a value of 1.0 with increasing mesh refinement, the difference should become increasingly

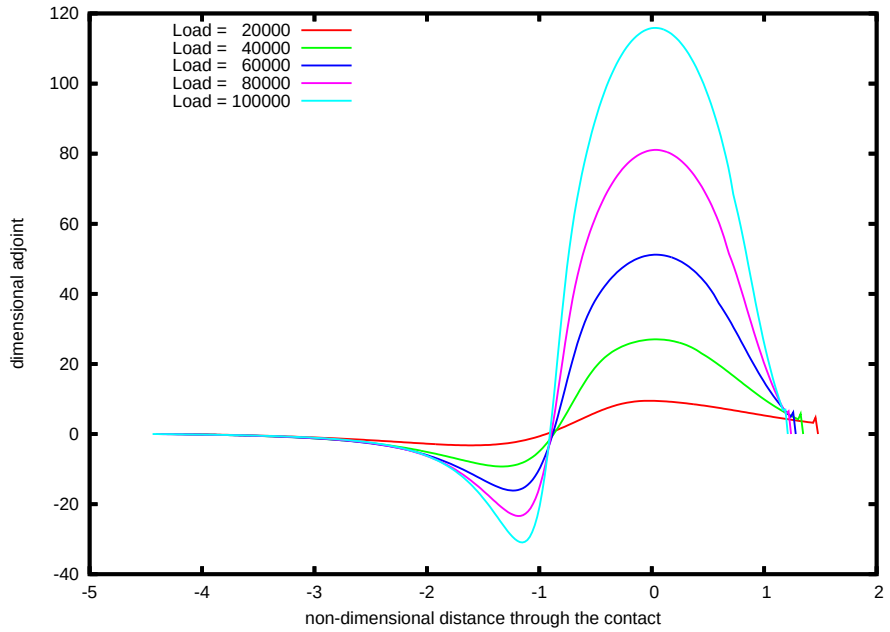

Figure 7.4: Adjoint solutions for pure rolling EHL cases; $L = 20000$, 40000, 60000, 80000 and 100000, $u_a = u_b = 0.5$

small. It is clear to see that all of the tables exhibit excellent convergence of the effectivity index. In other words, the adjoint error estimation can predict the inter-grid friction error, in cases of pure rolling, extremely accurately for EHL. Furthermore, this estimate appears to be equally effective over the range of loads.

Grid (g)	Interpolated Fric. (g)	Calculated correction	Corrected Fric. (g)	Friction ($g+1$)	Measured Error	Effectiv. Index	$\mid$ 1.0 - effct. $\mid$
5	-15.72099	0.02302	-15.74401	-15.73426	0.01327	0.57623	0.42377
6	-15.73444	0.01190	-15.74634	-15.74391	0.00947	0.79602	0.20398
7	-15.74395	0.00596	-15.74991	-15.74931	0.00535	0.89922	0.10078
8	-15.74932	0.00297	-15.75230	-15.75215	0.00283	0.95001	0.04999
9	-15.75215	0.00149	-15.75364	-15.75360	0.00145	0.97512	0.02488
10	-15.75360	0.00074	-15.75434	-15.75433	0.00073	0.98772	0.01228
11	-15.75433	0.00037	-15.75471	-15.75470	0.00037	0.99347	0.00653
12	-15.75470	0.00019	-15.75489	-15.75489	0.00019	0.99720	0.00280

Table 7.1: Adjoint based inter-grid friction error on uniform meshes; $L = 20000$, $u_a = u_b = 0.5$, slide-roll ratio = 0.0 (pure rolling)

Grid (g)	Interpolated Fric. (g)	Calculated correction	Corrected Fric. (g)	Friction ($g+1$)	Measured Error	Effectiv. Index	| 1.0 - effct. |
5	-23.46751	-0.24336	-23.22415	-23.20372	-0.26379	1.08397	0.08397
6	-23.20388	-0.10870	-23.09518	-23.08984	-0.11404	1.04908	0.04908
7	-23.08988	-0.05025	-23.03964	-23.03834	-0.05154	1.02578	0.02578
8	-23.03835	-0.02372	-23.01463	-23.01435	-0.02401	1.01194	0.01194
9	-23.01435	-0.01141	-23.00294	-23.00288	-0.01147	1.00510	0.00510
10	-23.00288	-0.00557	-22.99731	-22.99730	-0.00558	1.00216	0.00216
11	-22.99730	-0.00275	-22.99455	-22.99455	-0.00275	1.00092	0.00092
12	-22.99455	-0.00136	-22.99319	-22.99319	-0.00136	1.00071	0.00071

Table 7.2: Adjoint based inter-grid friction error on uniform meshes; $L = 40000$, $u_a = u_b = 0.5$, slide-roll ratio = 0.0 (pure rolling)

Grid (g)	Interpolated Fric. (g)	Calculated correction	Corrected Fric. (g)	Friction ($g+1$)	Measured Error	Effectiv. Index	| 1.0 - effct. |
5	-27.55984	-0.52940	-27.03044	-26.99802	-0.56182	1.06125	0.06125
6	-26.99814	-0.23267	-26.76547	-26.75316	-0.24498	1.05291	0.05291
7	-26.75319	-0.10732	-26.64588	-26.64236	-0.11083	1.03278	0.03278
8	-26.64237	-0.05046	-26.59191	-26.59097	-0.05140	1.01866	0.01866
9	-26.59097	-0.02410	-26.56687	-26.56665	-0.02432	1.00911	0.00911
10	-26.56665	-0.01166	-26.55500	-26.55495	-0.01170	1.00375	0.00375
11	-26.55495	-0.00571	-26.54925	-26.54924	-0.00571	1.00137	0.00137
12	-26.54924	-0.00282	-26.54642	-26.54642	-0.00282	1.00043	0.00043

Table 7.3: Adjoint based inter-grid friction error on uniform meshes; $L = 60000$, $u_a = u_b = 0.5$, slide-roll ratio = 0.0 (pure rolling)

Grid (g)	Interpolated Fric. (g)	Calculated correction	Corrected Fric. (g)	Friction ($g+1$)	Measured Error	Effectiv. Index	| 1.0 - effct. |
5	-30.19587	-0.81428	-29.38159	-29.32429	-0.87158	1.07037	0.07037
6	-29.32437	-0.35367	-28.97070	-28.95105	-0.37332	1.05556	0.05556
7	-28.95108	-0.16250	-28.78858	-28.78296	-0.16812	1.03454	0.03454
8	-28.78297	-0.07577	-28.70720	-28.70528	-0.07769	1.02545	0.02545
9	-28.70528	-0.03599	-28.66929	-28.66871	-0.03657	1.01608	0.01608
10	-28.66871	-0.01734	-28.65138	-28.65123	-0.01748	1.00817	0.00817
11	-28.65123	-0.00844	-28.64280	-28.64277	-0.00847	1.00348	0.00348
12	-28.64277	-0.00414	-28.63862	-28.63862	-0.00415	1.00125	0.00125

Table 7.4: Adjoint based inter-grid friction error on uniform meshes; $L = 80000$, $u_a = u_b = 0.5$, slide-roll ratio = 0.0 (pure rolling)

Grid (g)	Interpolated Fric. (g)	Calculated correction	Corrected Fric. (g)	Friction ($g+1$)	Measured Error	Effectiv. Index	| 1.0 - effct. |
5	-32.11875	-1.11456	-31.00419	-30.92962	-1.18913	1.06690	0.06690
6	-30.92962	-0.47488	-30.45474	-30.43133	-0.49829	1.04930	0.04930
7	-30.43135	-0.21507	-30.21628	-30.20711	-0.22424	1.04262	0.04262
8	-30.20712	-0.09973	-30.10739	-30.10431	-0.10281	1.03087	0.03087
9	-30.10431	-0.04722	-30.05709	-30.05607	-0.04824	1.02162	0.02162
10	-30.05607	-0.02268	-30.03340	-30.03309	-0.02298	1.01349	0.01349
11	-30.03309	-0.01101	-30.02208	-30.02201	-0.01108	1.00691	0.00691
12	-30.02201	-0.00538	-30.01662	-30.01661	-0.00540	1.00279	0.00279

Table 7.5: Adjoint based inter-grid friction error on uniform meshes; $L = 100000$, $u_a = u_b = 0.5$, slide-roll ratio = 0.0 (pure rolling)

7.5.3 Sliding

Using the same five non-dimensional loads used for the rolling case, results are presented here for the case where the non-dimensional surface speeds are $u_a = 0.1$, $u_b = 0.9$. In addition to the friction generated by having to force fluid against the pressure gradient, there is now an extra source of friction. Since the surfaces move at different speeds, there is shear in the fluid between them. With viscosity being the resistance to fluid shear, the friction is then the product of the two. This term is typically dominant, as evidenced by the fact that the friction value for the most heavily loaded rolling case is still an order of magnitude smaller than the most lightly loaded case with both sliding and rolling. Figure 7.5 shows the adjoint solutions for the five loads. In contrast to the adjoint solutions for the rolling case in Figure 7.4, there is significant activity in and around the pressure spike region. Tables 7.6 to 7.10 show the effectivity index for this problem. For the two lightest loads, the method again shows its effectiveness at predicting the inter-grid friction error where the effectivity index is close to unity by grid 6 (129 points), and gets increasingly close with further refinement. The middle load of the five starts off with an error estimate on grid 5 (65 points) which is nearly 80% wrong, with the estimate on grid 6 just under 50% out. However, after that the error in the estimate falls to an acceptable level. The two most heavily loaded cases provide rather less accurate predictions for the coarse grids, but even here, once the mesh becomes sufficiently refined, the inter-grid error estimates are again very good. There is clearly a trend of worsening accuracy with increasing load, which is likely due to the large increases in the viscosity. Nevertheless, convergence of the estimate to the true error is observed in all cases.

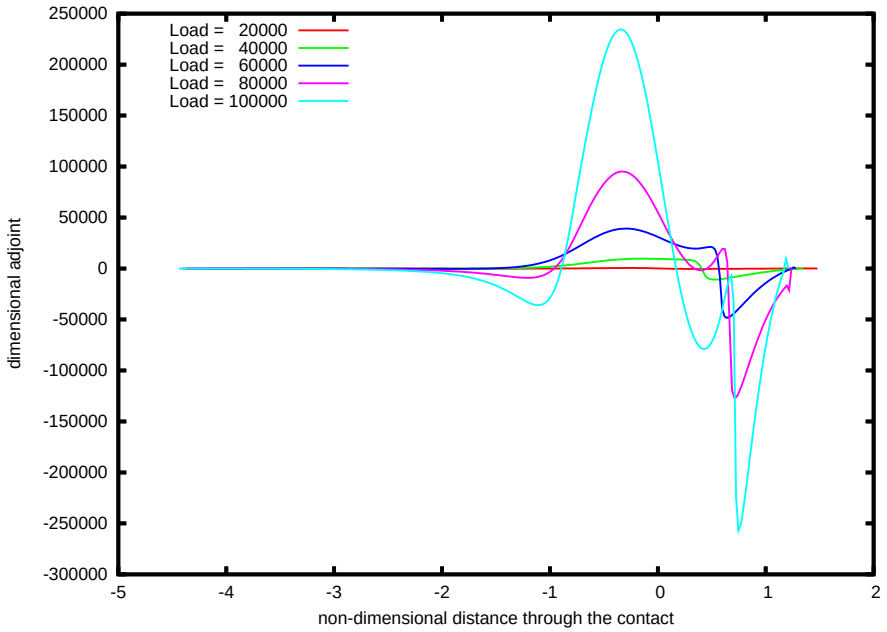

Figure 7.5: Adjoint solutions for EHL cases with sliding; $L = 20000$, 40000, 60000, 80000 and 100000, $u_a = 0.1$, $u_b = 0.9$

Grid (g)	Interpolated Fric. (g)	Calculated correction	Corrected Fric. (g)	Friction ($g+1$)	Measured Error	Effectiv. Index	| 1.0 - effct. |
5	381.16185	-13.24747	394.40933	395.29655	-14.13469	1.06697	0.06697
6	395.26199	-7.77855	403.04054	403.33739	-8.07540	1.03816	0.03816
7	403.32754	-4.25516	407.58269	407.67011	-4.34258	1.02054	0.02054
8	407.66746	-2.23175	409.89921	409.92306	-2.25560	1.01069	0.01069
9	409.92237	-1.14377	411.06615	411.07239	-1.15001	1.00545	0.00545
10	411.07221	-0.57911	411.65133	411.65292	-0.58071	1.00275	0.00275
11	411.65288	-0.29140	411.94428	411.94467	-0.29180	1.00136	0.00136
12	411.94466	-0.14617	412.09083	412.09093	-0.14627	1.00067	0.00067

Table 7.6: Adjoint based inter-grid friction error on uniform meshes; $L = 20000$, $u_a = 0.1$, $u_b = 0.9$, slide-roll ratio = 0.8 (sliding)

Grid (g)	Interpolated Fric. (g)	Calculated correction	Corrected Fric. (g)	Friction ($g+1$)	Measured Error	Effectiv. Index	| 1.0 - effct. |
5	3345.49389	-80.14426	3425.63815	3451.10255	-105.60866	1.31773	0.31773
6	3448.33170	-83.26708	3531.59878	3542.09648	-93.76478	1.12607	0.12607
7	3541.39335	-61.49194	3602.88529	3610.58244	-69.18908	1.12517	0.12517
8	3610.39035	-40.27333	3650.66369	3653.83995	-43.44960	1.07887	0.07887
9	3653.78827	-23.57142	3677.35969	3678.37504	-24.58677	1.04308	0.04308
10	3678.36143	-12.81609	3691.17752	3691.46376	-13.10233	1.02233	0.02233
11	3691.46025	-6.68934	3698.14959	3698.22543	-6.76519	1.01134	0.01134
12	3698.22456	-3.41806	3701.64262	3701.66221	-3.43765	1.00573	0.00573

Table 7.7: Adjoint based inter-grid friction error on uniform meshes; $L = 40000$, $u_a = 0.1$, $u_b = 0.9$, slide-roll ratio = 0.8 (sliding)

Grid (g)	Interpolated Fric. (g)	Calculated correction	Corrected Fric. (g)	Friction ($g+1$)	Measured Error	Effectiv. Index	| 1.0 - effct. |
5	12205.96611	-375.30052	12581.26663	12278.18194	-72.21583	0.19242	0.80758
6	12255.02955	-144.91328	12399.94283	12469.84738	-214.81783	1.48239	0.48239
7	12462.70119	-188.24168	12650.94287	12700.28466	-237.58347	1.26212	0.26212
8	12698.50913	-162.15862	12860.66775	12892.64558	-194.13645	1.19720	0.19720
9	12892.20697	-116.43783	13008.64481	13022.62082	-130.41385	1.12003	0.12003
10	13022.50895	-72.05889	13094.56784	13099.34594	-76.83699	1.06631	0.06631
11	13099.31731	-40.41668	13139.73399	13141.12181	-41.80450	1.03434	0.03434
12	13141.11457	-21.42438	13162.53895	13162.90936	-21.79478	1.01729	0.01729

Table 7.8: Adjoint based inter-grid friction error on uniform meshes; $L = 60000$, $u_a = 0.1$, $u_b = 0.9$, slide-roll ratio = 0.8 (sliding)

Grid (g)	Interpolated Fric. (g)	Calculated correction	Corrected Fric. (g)	Friction ($g+1$)	Measured Error	Effectiv. Index	| 1.0 - effct. |
5	32847.90292	717.87994	32130.02299	32667.90099	180.00194	0.25074	0.74926
6	32582.36697	-518.46131	33100.82828	32846.97578	-264.60881	0.51037	0.48963
7	32824.63259	-559.14829	33383.78088	33305.84795	-481.21536	0.86062	0.13938
8	33301.04221	-383.39286	33684.43507	33784.93053	-483.88832	1.26212	0.26212
9	33782.59231	-305.36009	34087.95240	34151.60976	-369.01745	1.20847	0.20847
10	34151.05130	-216.58757	34367.63887	34393.64885	-242.59756	1.12009	0.12009
11	34393.51454	-132.54454	34526.05908	34534.96140	-141.44687	1.06716	0.06716
12	34534.92943	-73.90874	34608.83817	34611.39598	-76.46655	1.03461	0.03461

Table 7.9: Adjoint based inter-grid friction error on uniform meshes; $L = 80000$, $u_a = 0.1$, $u_b = 0.9$, slide-roll ratio = 0.8 (sliding)

Grid (g)	Interpolated Fric. (g)	Calculated correction	Corrected Fric. (g)	Friction ($g+1$)	Measured Error	Effectiv. Index	| 1.0 - effct. |
5	75942.44786	1514.05197	74428.39590	74961.63818	980.80968	0.64780	0.35220
6	74829.35179	-1429.76015	76259.11195	75076.18903	-246.83723	0.17264	0.82736
7	75062.32454	-447.54805	75509.87259	76036.19337	-973.86883	2.17601	1.17601
8	76004.98630	-884.18078	76889.16708	76898.72841	-893.74211	1.01081	0.01081
9	76888.36623	-662.51809	77550.88431	77645.73835	-757.37213	1.14317	0.14317
10	77643.20345	-468.41145	78111.61490	78188.36713	-545.16368	1.16386	0.16386
11	78187.85170	-309.36932	78497.22102	78529.37180	-341.52011	1.10392	0.10392
12	78529.25738	-182.68070	78711.93808	78722.30232	-193.04495	1.05673	0.05673

Table 7.10: Adjoint based inter-grid friction error on uniform meshes; $L = 100000$, $u_a = 0.1$, $u_b = 0.9$, slide-roll ratio = 0.8 (sliding)

7.6 Adaptive EHL

In the previous section it has been seen how the adjoint solution can be used to predict the error in a given functional for elastohydrodynamic lubrication cases. The aim is now to establish how this solution can be used to guide adaptive refinement of the domain. The aim is, as explained in Chapter 3, to give the value of the functional, rather than the full solution profile, as accurately as possible.

In this section, the adaptation method used in the industrial code is explained. This uses multigrid patches for the non-uniform mesh discretisation as mentioned in Section 2.4.3. Then in Section 7.6.2, the overall adjoint mesh refinement algorithm is detailed. The rest of the section is devoted to discussing how the solution from the multigrid patches for the EHL cases is not as consistent as is normally expected.

7.6.1 Adaptive solution process

The following algorithm provides an overview of the adaptive solution process that is used in this chapter.

1. Solve forward problem on the current non-uniform mesh (the coarse mesh).
2. Solve adjoint problem on the same mesh.
3. Interpolate the above solutions onto a uniformly refined version of the coarse mesh (the fine mesh).

4. Evaluate the residuals on the fine mesh.
5. Calculate the error correction value (i.e. the scalar product of the residuals and the interpolated adjoint solution).
6. Define an error correction vector to be a vector of the contributions to the above scalar product ($v_i = r_i.a_i$, where r_i is the residual and a_i is the adjoint solution at mesh point i).
7. Use the error correction vector to identify where the current coarse mesh needs refining (i.e. around those nodes with the greatest contribution to this vector).
8. Write out the new refined mesh and use the interpolated solution as continuation input to next iteration.
9. Repeat the above process until a satisfactory solution is obtained: return to step 1.

7.6.2 Mesh refinement

The above algorithm provides a means of identifying which part of the current solution is contributing the most to the error in the functional of interest. The specific details of the refinement are described according to the following algorithm:

1. Identify the grid points where the error correction component associated with that point is above a prescribed tolerance ($1e^{-6}$).
2. Add a "safety layer" either side of all such points.
3. Sweep over the grid and identify areas not marked for refinement which are too small, and mark these for refinement too.
4. If the coarse mesh is already non-uniform, take care around the interfaces between different mesh levels. This means that if further refinement is required at these points, the current level of adaptivity should be extended outwards into the coarse region.

7.6.3 Film thickness

There is a slight complication with how the film thickness is solved for on a non-uniform mesh. As previously described in Chapter 2, the forward solve is obtained by solving

using multigrid with adaptive patches [26, 70]. One test to see if the residual equations which have been defined for use in the adjoint error procedure are consistent with the solutions obtained from the forward solve is to check that the residuals produced using these solutions are small. In other words, there should be a single non-uniform grid on which the solution P is equivalent to the multi-level solution. Clearly the P value to be used at any given point can just be obtained from the finest level mesh, since any points which were solved on coarser meshes have already been interpolated to the fine level so that the film thickness can be calculated. Equally, the viscosity and density are calculated from these pointwise values so there is no confusion as to the values to use. However, any film thickness value is calculated from the P values at all of the other mesh points. This is why the finest mesh must be fine everywhere even though large sections may not be used in the actual solution of the Reynolds equation.

This however leads to a dilemma. Should H values in coarse regions be calculated using the interpolated P values (on the uniformly fine mesh), or should the H value calculated during the solution on the coarse level be used? The best answer is that the coarse values should be used since it was those that were used when solving for the P values at those points. However, this is not perfect, since at least some of the pressure values would have been calculated with the FAS right-hand side being non-zero. The main problem comes from the interface points. When the adaptive patch is refined, the ends are taken to be Dirichlet points using the values from the coarser mesh. So the H values used in the residual equation for either of those points should use the coarse H values. However, the point inside of the fine region is solved for using fine grid H values. Since the residual for any point uses values from either side, the points either side should have fine H values too. However, it has already been said that the interface point should have coarse H values. So in order for the H value at the interface to be consistent with the residuals used to calculate the P values around it, two values are required at the same point. The same is also true for the first point inside the interface on the fine mesh side. This means that there are two points, the interface and the first point inside on the fine side, which need two film thickness values at the same point to satisfy the equations as solved in the multi-level solution.

This clearly casts some doubt over the exact formulation of the multi-level solution as it stands. However, in practice, as demonstrated by the results in the next section, this has little or no discernible effect on the solution or the adjoint error estimation method.

We conclude this section by noting that the evaluation of the Jacobian is made slightly more complex by the inclusion of a non-uniform spatial mesh. Hence these modifications

must not be overlooked when moving from a uniform to a non-uniform grid.

7.7 Non-uniform mesh results

In order to illustrate adjoint error estimation and spatial mesh adaptivity, an EHL case is presented with a load of 120000. In this section, attention is focused on a typical highly loaded example, similar to those presented in the previous section. The main difference here is that rather than the usual dimensional rolling friction used for the majority of the work presented, a new "friction-like" functional is introduced. This is basically the same as the rolling term from friction from the standard friction equation (7.34):

$$\overline{F}_1 = \int_{X_c-D}^{X_c} H \frac{\partial P}{\partial X} \, \mathrm{d}X. \tag{7.35}$$

This can be discretised in the usual manner to give

$$\overline{F}_1 = \sum_{i=0}^{n-2} 0.5(H_{i+1}+H_i)\frac{P_{i+1}-P_i}{X_{i+1}-X_i}(X_{i+1}-X_i). \tag{7.36}$$

It is harder to assess the quality of our error approximation on non-uniform meshes than on uniform meshes since the effectivity index is not likely to tend to unity in this case (the grid is only refined where the contributions to the error estimate are large not where the error in the estimate itself is large!). Furthermore, in addition to the need for a reliable error estimate the proposed adaptation procedure also requires that the regions that contribute most to this error estimate are the most suitable ones in which to perform local mesh refinement. Fortunately, the results in Figure 7.6 suggest that the error estimate and the adaptive strategy are both robust for the purposes of controlling local adaptivity.

Figure 7.6 shows the estimated error based upon a comparison of various computed solutions against a "numerical truth solution" that is calculated using an excessively refined uniform mesh (level 14, 32769 points). Clearly the most desirable area of this figure is in the bottom left-hand corner, where there is greater accuracy for fewer points! However, there is a trade-off between the desirable quantity (increased accuracy) and that which it costs to achieve (increased mesh points). This is clearly shown by all three lines, which illustrate the error in the solutions when compared to a "truth solution". The top line on the graph shows the error in the friction for a series of uniform grid solutions. This is the benchmark against which a comparison of the adaptivity can be made. The second

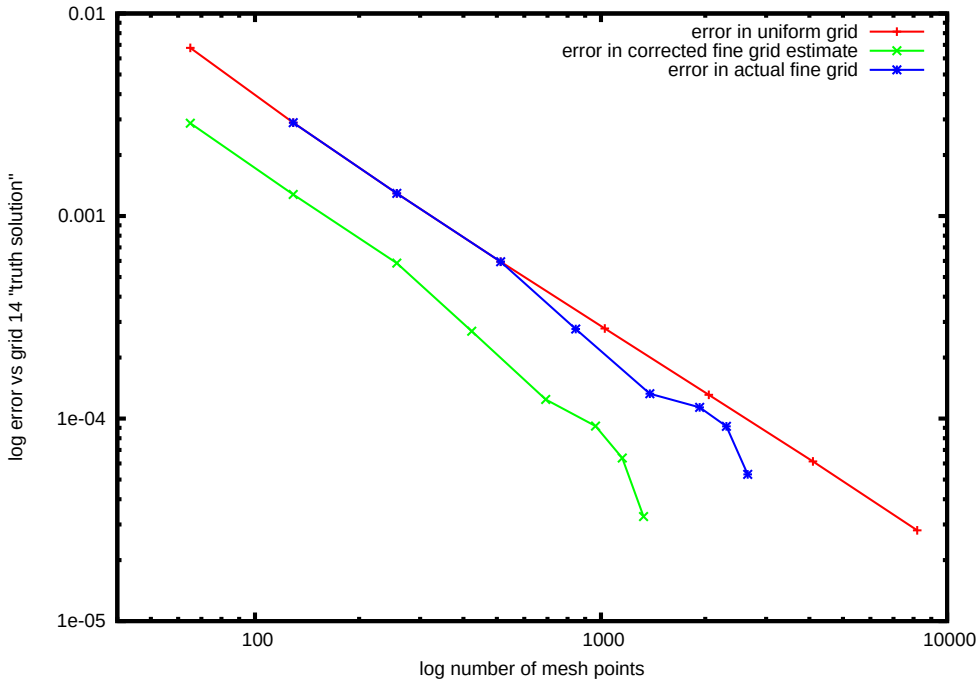

Figure 7.6: Friction error compared against a grid 14 “truth” solution

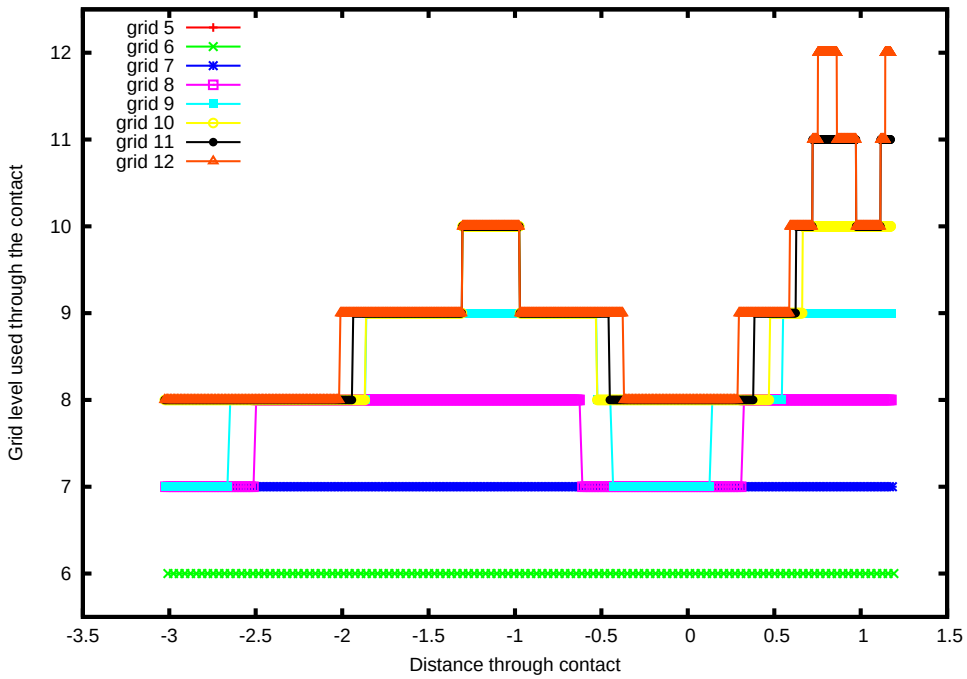

Figure 7.7: Multigrid patch refinement pattern shown for adaptive refinement of an EHL case ($L = 120000$) for finest meshes from grids 6 to 12

line shows the resulting error using local adaptivity based upon the adjoint correction procedure applied to the coarse grid solution. This is where the coarse grid solution has been refined based on the components of the error correction vector (as described earlier). Once the solution has been obtained on this coarse grid, it is interpolated onto a uniformly refined version, where an estimate of the friction can be calculated as if it had been on that fine grid. The value shown on this second graph is that of the aforementioned estimate as corrected by the adjoint method. The third graph shows the friction calculated from solutions obtained directly once on the uniformly refined adaptive mesh.

Initially, the error is reduced in line with the uniform solutions. This is simply because only global refinement has taken place at this stage, i.e. the components of the error correction vector are all sufficiently large to warrant refinement (this may not quite be true to the extent that it is the buffer regions introduced around components which are larger than the tolerance which mean that all of the mesh points become refined). As previously seen, where the adjoint error estimation is applied to these uniform solutions, the error is reduced to that of a uniformly refined version, but with the majority of the calculation performed only on the original coarse mesh. As the mesh is further refined, the contribution to the error is primarily found to be in certain regions. Here Figure 7.6 clearly shows the value of the local versus the global mesh refinement.

In Figure 7.7 the meshes used on each multigrid level are shown. This shows, as stated above, that the first few levels (up to the blue line) have only global refinement. At this stage the gradient of both of the adaptive error lines sharpens, indicating that the adaptive meshing is actually working. In other words, by refining the regions where the components of the error vector are large the error in the friction can be reduced by an amount roughly comparable to that achieved by uniform refinement, but with far fewer grid points. This trend continues with further local refinement. By noting in Figure 7.6 that the adaptive solution on the fine grid stays to the left of the uniform line, it is clear that adaptivity is effective at reducing the number of grid points needed to calculate friction to a specific accuracy. Further, by correcting this value according to the adjoint error estimate, the line can be moved further left, clearly demonstrating the efficacy of this method.

We conclude this section by presenting the results in the same tabular form as used for demonstrating the accuracy of the error estimate on uniform meshes. Table 7.11 shows the data corresponding to the calculations in Figures 7.6 and 7.7. As already predicted, the effectivity index is no longer tending to unity, however the estimate always remains within about 20% of the true error and its variation is very much in line with that of the

Grid (g)	No. Points	Interpolated Fric. (g)	Calculated correction	Corrected Fric. (g)	Friction ($g+1$)	Measured Error	Effectiv. Index
5	65	0.11423	0.00359	0.11064	0.11036	0.00387	1.07787
6	129	0.11036	0.00148	0.10888	0.10876	0.00160	1.07955
7	257	0.10876	0.00066	0.10809	0.10806	0.00070	1.05185
8	423	0.10800	0.00024	0.10775	0.10774	0.00026	1.04994
9	692	0.10788	0.00031	0.10757	0.10760	0.00028	0.90484
10	964	0.10761	0.00004	0.10757	0.10758	0.00003	0.68463
11	1152	0.10771	0.00019	0.10751	0.10756	0.00015	0.76009
12	1327	0.10775	0.00029	0.10746	0.10752	0.00023	0.79639

Table 7.11: Adjoint based inter-grid friction error on adaptive non-uniform meshes; $L = 120000$, slide-roll ratio = 0.0 (pure rolling)

true error.

7.8 Summary

In this chapter, adjoint error estimation procedures have been successfully applied to full elastohydrodynamic lubrication problems. First, several differently loaded cases were considered on uniform meshes. Adjoint error estimation was shown to give excellent predictions of the inter-grid error estimate in the case of purely rolling friction, and also for moderately loaded sliding friction. For high loads, very good predictions for the sliding friction error estimate were also achieved after sufficient grid resolution had been achieved. Finally, adjoint error estimation for EHL has been shown to be useful for driving spatial mesh adaptation. By adaptively refining the grid in regions where the contribution to the adjoint error estimation was large, and then correcting the friction with the error estimate, significant savings in the number of points used in the calculation were made over the uniform grids. However, it is clear that there are limitations to this approach as implemented for this work. Two areas which may benefit from further attention are now discussed.

As mentioned above, the accuracy of the adjoint error estimation procedure described above worsens for highly loaded EHL cases where the friction contains a sliding component. Preliminary investigations suggest that this is due to the exponential term within the viscosity equation, which is a multiplier in the second term of equation (7.34). These investigations centred around choosing the functional of interest to be each of the terms from the friction calculation in turn to see the accuracy of each. The precise mechanism

which causes the degradation in accuracy compared to purely rolling friction is as yet unclear. One possibility is that the linear approximations used in the derivation of the method are only valid for meshes with medium to high levels of refinement when dealing with exponential values. In this sense, the asymptotic range is further away with increasing load, and it may be possible to derive some empirical way of deciding the coarsest level possible. It is also the case that since the derivative of an exponential is another exponential, the right hand side of the adjoint system to be solved will contain exponential terms. It may be possible to mitigate the effect of these large values by using a different non-dimensionalisation for the viscosity equation which uses $\overline{\alpha}$ to reduce the maximum value of the viscosity to approximately unity.

The adaptive mesh refinement here is straight-forward to implement. A mesh point is marked for refinement wherever the contribution to the error correction for that point is above some prescribed tolerance. After a fresh solution is calculated on the refined mesh, the process is repeated until the inter-grid friction error is below some other prescribed tolerance. There are therefore two tolerances which need to be specified, the first is used to decided where to refine, and the second to decide when sufficient accuracy has been obtained. While the second of the two can be chosen with the goal of the overall accuracy in mind, the first tolerance requires an arbitrary choice based on previous experience to determine a suitable value. A more sophisticated method, which would avoid this problem, would involve identifying the points with the largest error, and then refining those. This means that only the second of the two tolerance values need be supplied, and as before this process can continue until the inter-grid friction error is below the prescribed value.

Chapter 8

Discussion

This final chapter of the thesis provides a brief overview of the research that has been undertaken and then presents a short discussion of some of the main extensions of this work that should be undertaken.

8.1 Overview

In this thesis, adjoint error estimation techniques have been applied to complex EHL problems. A functional has been introduced, the friction, and justification has been provided as to why this quantity, and hence its accuracy, is important. An iterative approach has been taken to understanding the mechanisms at work, starting with a model problem, and culminating with the full EHL line contact problem.

In Chapter 4, friction has been introduced as a quantity of interest. Here it has been demonstrated that resolution of the pressure spike is key in accurately capturing the friction through the contact. A model free-boundary problem resembling EHL in certain key features has been formulated in Chapter 5. With this, a novel way of solving for the free boundary allowing for the exact capture of the cavitation position has been shown, and a new functional introduced analogous to the friction in Chapter 4. Non-uniform grids have been introduced, with the adjoint error estimate used as the basis for refinement,

again showing the prediction of the estimate to be accurate. The successful application of adjoint error estimation to this free-boundary problem has been published in [34, 35]. In Chapter 6, hydrodynamic lubrication was introduced via the addition of non-linear viscosity and density models. The formulation of the adjoint system of equations for this more complicated engineering problem has been considered, with two possible alternatives explored. The "expanded" and "dense" Jacobians have been shown to be similar, with both predicting the inter-grid friction error accurately. This informed the choice of system for the following chapter, Chapter 7. The final part of this work is presented in Chapter 7, where adjoint error estimation theory has been applied to the complicated real-world engineering problem of elastohydrodynamic lubrication. Results have been presented showing this to give reliable estimates of the inter-grid friction error. Non-uniform meshes have been used with adaptivity driven automatically by the size of the components of the adjoint correction, and this has been shown to dramatically reduce the number of points needed in order to achieve a given accuracy of friction.

8.2 Future Work

In this section, a number of areas of work are discussed with regard to extending the current research.

8.2.1 Overall speed and efficiency

The work in this thesis is very much a proof of concept for the application of adjoint error estimation to EHL, and in that sense it has been shown to be effective. However, in order for the method to become more attractive from a user's perspective, MLMI must be incorporated into the forward solve. This would mean investigating efficient techniques for MLMI implementation on non-uniform meshes (a topic that has received little attention in the literature [9, 10]), as well as considering the implications for the formulation of the adjoint system.

In addition to this, faster ways of solving the adjoint system must be found. In the work of Chapter 7, a direct solver is used to get a solution to the adjoint system as the Jacobian is almost entirely dense due to the film thickness calculation. The solution of this takes $O(n^3)$ operations, so quickly becomes prohibitively expensive on even a moderately refined mesh. There is potential for some kind of multigrid type approach to be applied

to the adjoint error estimation process, since the residual terms in the FAS right-hand side for the forward problem are not dissimilar to the interpolated residuals in the adjoint error estimation approach. In this work the full system Jacobian was used in formulating the adjoint system. It may be that sufficient accuracy can be gained using an approximate Jacobian, such as that used in the Newton iteration which forms part of the smoothing process in the multigrid solve. Finally, by realising the equivalence of the expanded and dense Jacobians shown in Chapter 6, it would be possible to derive something between the two, where P, H_0 and X_c were primary dependent variables, but also H. The sparsity pattern for this Jacobian would then have four main blocks, with one of them dense, due to the film thickness kernel K. If this could be solved in a de-coupled way, MLMI may become applicable which could potentially speed up the solution process enormously.

8.2.2 2D point contact EHL

The most obvious extension to the work carried out in this thesis would be the extension to the 2D point contact problem, introduced briefly in Chapter 2 as equation (2.1). As this problem is now 2D, the work involved in solving on a uniformly refined grid jumps by at least a factor of four (and by a larger factor if a non-optimal solver is employed). This should clearly indicate the potential benefit for solving two systems on a coarse grid rather than one system on a fine grid. In a similar fashion, non-uniform meshes have greater potential for saving in 2D than in 1D. Consider, for example, a 1D mesh which is refined by one extra level over half of the domain. In this case, approximately a quarter of the total points of the fine mesh are saved by only refining where necessary. If the same were true in 2D, and half of the domain in each direction was refined by one extra level (so a quarter of the domain), three eighths of the equivalent fine mesh could be saved.

The main obstacle to the immediate application of the work presented here to a 2D case is the treatment of the cavitation condition. In this work, the 1D solver was augmented by an outer-iteration which solved for the cavitation condition though the use of a sliding grid. This allowed X_c to be a continuous variable, facilitating the direct implementation of the adjoint error estimation. However, it should be clear that this is no longer an option in 2D for a sliding rectangular grid. Rather than one cavitation point, there is now a cavitation line, represented by a set of cavitation points, one for each row of mesh points parallel to the x-axis. Satisfaction of the cavitation condition at one point would almost certainly guarantee that the cavitation condition would not hold at most of the rest of the points. If each row of mesh points parallel to the x-axis were allowed to slide,

the cavitation condition could be satisfied at all of the points, but this would come at the expense of the rectangular grid, and would make finite differences, and multigrid with the MLAT scheme, a significant challenge to implement. This could perhaps be overcome by mapping to a rectangular reference grid to perform the solution.

One obvious alternative to using finite differences would be to move to a finite element solution. Since finite elements can be used on non-regular domains far more naturally, exact capture of the cavitation condition with a moving mesh method may be possible. However, any move away from regular grids comes at the price of not using multilevel multi-integration.

One method for dealing with the cavitation region not considered in this work, is the penalty method [47, 90]. As mentioned in Chapter 2, rather than explicitly finding the cavitation region, in this method all negative pressures are forced to be zero (or negligibly small) by a penalty term in the residual equations. Since the exact boundary no longer needs including in the formulation, there would be no need to find X_c and hence no need to include it as a free and continuous variable. This method also has the advantage that it can be applied to both finite difference and finite element methods. It is not yet clear however exactly how the adjoint system would be formulated in this case.

The final suggestion for overcoming the cavitation boundary condition in 2D is to treat each X_c as a continuous variable on a fixed grid, but then only allow them to move to the discrete grid points. In this way, the adjoint system could still be formed, including any sensitivities to the cavitation condition, and a residual calculated. However, the correction may not be as reliable as a sliding grid, since the change in friction due to a change in the mesh position predicted by a cavitation residual may not correspond to the actual change on the fine grid if the position predicted does not fall on or very near a grid point. This method may still be sufficiently accurate for practical solution purposes, and would also remove the need for resolving the solution every time the mesh moves.

8.2.3 Advanced constitutive models

Two potential augmentations to the model used here are thermal EHL, and non-Newtonian fluid behaviour. Thermal EHL arises due to the temperature dependence of the lubricant viscosity. When sliding is present, the heat generated in the lubricant through the contact region can no longer be ignored, as it has a significant thinning effect on the lubricant. A model for this is presented in [22]. Any behaviour of a fluid where the shear-rate is

not proportional to the applied strain is deemed non-Newtonian. Two such fluid models are the Ree-Eyring fluid model [60] and the more complicated White-Metzner model [65, 86]. The second of these is visco-elastic, and hence the fluid viscosity is time-dependent. Either of these would increase the number of adjoint variables to be solved for, potentially making the solution with even moderately refined grids challenging.

8.2.4 Transient EHL

Adjoint sensitivity analysis for time-dependent PDEs is still relatively poorly understood [69]. However spatial mesh refinement could take place in order to reduce the growth of errors in the friction over time. Also, with transient EHL, surface roughness becomes a possibility, with refinement only around those areas which would adversely affect the friction. In order to capture the roughness profile accurately, very fine meshes are likely to be needed. While this may be achievable for 1D line contact cases, in 2D parallel solutions on the grid become a necessity [32].

Bibliography

[1] M. Alsaad, S. Bair, D. M. Sanborn, and W. O. Winer. Glass transitions in lubricants: Its relation to elastohydrodynamic lubrication/EHD. *American Society of Mechanical Engineers Transactions*, 100:404–417, 1978.

[2] C. Barus. Isothermals, isopiestics and isometrics relative to viscosity. *American Journal of Science*, 45:87–96, 1893.

[3] R. Becker and R. Rannacher. An optimal control approach to a posteriori error estimation in finite element methods. *Acta Numerica*, 37:1–225, 2001.

[4] E. J. Bissett and D. W. Glander. A highly accurate approach that resolves the pressure spike of elastohydrodynamic lubrication. *J. Tribology*, 110:241–246, 1988.

[5] P. J. Blau. *Friction Science and Technology*. Dekker, 1996.

[6] K. A. Blencoe, G. W. Roper, and J. A. Williams. The influence of lubricant rheology and surface topography in modelling friction at concentrated contacts. *Proceedings of the Institution of Mechanical Engineers Part J, Journal of Engineering Tribology*, 212(6):391–400, 1998.

[7] C. Bovington. Elastohydrodynamic lubrication: a lubricant industry perspective. *Proc. Instn. Mech. Engrs.*, 213:417–426, 1999.

[8] A. Brandt and A. A. Lubrecht. Multilevel matrix multiplication and fast solution of integral equations. *Journal of Computational Physics*, 90(2):348–370, 1990.

[9] A. Brandt and C. H. Venner. Multilevel evaluation of integral transforms with asymptotically smooth kernels. *SIAM Journal of Scientific Computing*, 19(2):468–492, 1998.

[10] A. Brandt and C. H. Venner. Fast evaluation of integral transforms on adaptive grids. In W. Hackbusch and G. Wittum, editors, *Multigrid Methods V, Lecture Notes*

in Computer Science and Engineering, Vol. 3, pages 20–44. Springer-Verlag, Berlin, 1999.

[11] W. L. Briggs. *A Multigrid Tutorial, second edition.* SIAM, 2000.

[12] R.L. Burden and J.D. Faires. *Numerical analysis, 7th ed.* Pacific Grove, CA: Brooks/Cole, 2001.

[13] G. Carpentieri, B. Koren, and M. J. L. van Tooren. Adjoint-based aerodynamic shape optimization on unstructured meshes. *Journal of Computational Physics*, 224(1):267–287, 2007.

[14] L. S. H. Chow and H. S. Cheng. The effect of surface roughness on the average film thickness between lubricated rollers. *J. Lubrication Technology*, pages 117–124, 1976.

[15] D. Dowson. Elastohydrodynamic and micro-elastohydrodynamic lubrication. *WEAR*, 190:125–138, 1995.

[16] D. Dowson and P. Ehret. Past, present and future studies in elastohydrodynamics. *Proc. Instn. Mech. Engrs.*, 213:317–333, 1999.

[17] D. Dowson and G. R. Higginson. *Elasto-hydrodynamic Lubrication, The Fundamentals of Roller and Gear Lubrication*. Permagon Press, Oxford, Great Britain, 1966.

[18] D. Dowson and C. M. Taylor. Cavitation in bearings. *Annual Review of Fluid Mechanics*, 11:35–65, 1979.

[19] J. Durany, G. Garcia, and C. Vazquez. Numerical computation of free boundary problems in elastohydrodynamic lubrication. *Appl. Math. Modelling*, 20:104–113, 1996.

[20] J. Durany, G. Garcia, and C. Vazquez. Numerical simulation of a lubricated Hertzian contact problem under imposed load. *Finite Elements in Analysis and Design*, 38:645–658, 2002.

[21] H. P. Evans and R. W. Snidle. Analysis of micro-elastohydrodynamic lubrication for engineering contacts. *Tribology International*, 29(8):659–667, 1996.

[22] R. Fairlie, C. E. Goodyer, M. Berzins, and L. E. Scales. Numerical modelling of thermal effects in elastohydrodynamic lubrication solvers. In D. Dowson *et al.*, editor, *Tribological Research and Design for Engineering Systems, Proceedings of the 29th Leeds-Lyon Symposium on Tribology*, pages 675–683. Elsevier, 2003.

[23] N. Fang, L. Chang, and G.J. Johnston. Some insights into micro-EHL pressures. *J. Tribology*, 121(3):473–480, 1999.

[24] K.J. Fidkowski and D.L. Darmofal. Development of a higher-order solver for aerodynamic applications. *42nd AIAA Aerospace Sciences Meeting and Exhibit, AIAA Paper*, 436:2004, 2004.

[25] M. B. Giles and E. Süli. Adjoint methods for PDEs: *a posteriori* error analysis and postprocessing by duality. Acta Numerica , 11:145–236, 2002.

[26] C. E. Goodyer. *Adaptive Numerical Methods for Elastohydrodynamic Lubrication*. PhD thesis, School of Computing, University of Leeds, 2001.

[27] C. E. Goodyer and M. Berzins. Adaptive timestepping for elastohydrodynamic lubrication solvers. *SIAM Journal on Scientific Computing*, 28:626–650, 2006.

[28] C. E. Goodyer and M. Berzins. Efficient parallelisation of a multilevel elastohydrodynamic lubrication solver. *Concurrency and Computation: Practice and Experience*, 19(4):369–396, 2007.

[29] C. E. Goodyer, M. Berzins, P. K. Jimack, and L. E. Scales. Grid-based numerical optimisation in a problem solving environment. In S. Cox, editor, *Proceedings of the All Hands Meeting 2003*, pages 854–861. EPSRC, 2003. ISBN: 1-904425-11-9.

[30] C. E. Goodyer, R. Fairlie, M. Berzins, and L. E. Scales. Adaptive mesh methods for elastohydrodynamic lubrication. In *ECCOMAS CFD 2001 : Computational Fluid Dynamics Conference Proceedings*. Institute of Mathematics and its Applications, 2001. ISBN 0-905-091-12-4.

[31] C. E. Goodyer, R. Fairlie, D. E. Hart, M. Berzins, and L. E. Scales. Calculation of friction in steady-state and transient EHL simulations. In A.A. Lubrecht and G. Dalmaz, editors, *Transient Processes in Tribology: Proceedings of the 30th Leeds-Lyon Symposium on Tribology*, pages 579–590. Elsevier, 2004.

[32] C. E. Goodyer, J. Wood, and M. Berzins. A parallel Grid based PSE for EHL problems. In J. Fagerholm, J. Haataja, J. Järvinen, M. Lyly, P. Råback, and V. Savolainen,

editors, *Applied Parallel Computing, Proceedings of PARA '02, Lecture Notes in Computer Science*, volume 2367, pages 523–532. Springer, 2002.

[33] R. W. Hall. Pressure spikes in elastohydrodynamics - some elastic considerations. *WEAR*, 131(1):151–161, 1988.

[34] D. E. Hart, C. E. Goodyer, M. Berzins, P. K. Jimack, and L. E. Scales. Adjoint error estimation for EHL-like models. *International Journal for Numerical Methods in Fluids*, 47:1069–1075, 2005.

[35] D. E. Hart, C. E. Goodyer, M. Berzins, P. K. Jimack, and L. E. Scales. Adjoint error estimation and spatial adaptivity for EHL-like models. *IUTAM Symposium on Elastohydrodynamics And Micro-elastohydrodynamics: Proceedings of the IUTAM Symposium Held in Cardiff, UK, 1-3 September 2004*, pages 47–58, 2006.

[36] H. Hertz. The contact of elastic solids. *Journal für die reine angew. Math.*, 92:156–171, 1881.

[37] M. J. A. Holmes, H. P. Evans, and R. W. Snidle. Transient effects in EHL point contacts with transverse surface finish. In A.A. Lubrecht and G. Dalmaz, editors, *Transient Processes in Tribology: Proceedings of the 30^{th} Leeds-Lyon Symposium on Tribology*. Elsevier, 2004.

[38] C. J. Hooke and K. Y. Li. An inverse approach to the validation of pressure predictions in rough elastohydrodynamic contacts. *J. Tribology*, 124:103–108, 2002.

[39] B. Jacobson. Thin film lubrication of real surfaces. *Tribology International*, 33:205–210, 2000.

[40] D. Jalali-Vahid, Z. M. Jin, and D. Dowson. Prediction of lubricating film thickness in a ball-in-socket model with a soft lining representing human natural and artificial hip joints. *Proc. Instn. Mech. Engrs.*, 215:363–372, 2001.

[41] K. L. Johnson. *Contact Mechanics*. Cambridge University Press, 2001.

[42] C. C. Kweh, H. P. Evans, and R. W. Snidle. Micro-elastohydrodynamic lubrication of an elliptical contact with transverse and three-dimensional sinusoidal roughness. *J. Tribology*, 111:577–584, 1989.

[43] R.-T. Lee and C.-H. Hsu. A fast method for the analysis of thermal-elastohydrodynamic lubrication of rolling/sliding line contacts. *WEAR*, 166(1):107–117, 1993.

[44] K. Y. Li and C. J. Hooke. Use of the inverse approach to investigate the stresses in rough elastohydrodynamic contacts. *J. Tribology*, 124:109–113, 2002.

[45] S. Li and L. Petzold. Adjoint sensitivity analysis for time-dependent partial differential equations with adaptive mesh refinement. *J. Comput. Phys.*, 198(1):310–325, 2004.

[46] H. Lu. *High Order Finite Element Solutions of Elastohydrodynamic Lubrication Problems*. PhD thesis, School of Computing, University of Leeds, 2006.

[47] H. Lu, M. Berzins, C. E. Goodyer, P. K. Jimack, and M. A. Walkley. Adaptive high-order finite element solutions of transient elastohydrodynamic lubrication problems. *Proceedings of the Institution of Mechanical Engineers Part J, Journal of Engineering Tribology*, 220(3):215–225, 2006.

[48] H. Lu, Berzins M., Goodyer C. E., and Jimack P. K. High order discontinuous galerkin method for ehl line contact problems. *Communication in Numerical Methods in Engineering*, 21(11):643–650, 2005.

[49] A. A. Lubrecht. *Numerical solution of the EHL line and point contact problem using multigrid techniques*. PhD thesis, University of Twente, Endschende, The Netherlands, 1987. ISBN 90-9001583-3.

[50] A. A. Lubrecht, W. E. ten Napel, and R. Bosma. Multigrid, an alternative method of calculating film thicknesses and pressure profiles in elastohydrodynamically lubricated line contacts. *Trans. ASME, Journal of Tribology*, 108(4):551–556, 1986.

[51] A. A. Lubrecht, W. E. ten Napel, and R. Bosma. The influence of longitudinal and transverse roughness on the elastohydrodynamic lubrication of circular contacts. *J. Tribology*, 110:421–426, 1988.

[52] A. A. Lubrecht and C. H. Venner. Elastohydrodynamic lubrication of rough surfaces. *Proc. Instn. Mech. Engrs.*, 213:397–404, 1999.

[53] S. Nadarajah and A. Jameson. A comparison of the continuous and discrete adjoint approach to automatic aerodynamic optimization. In *Proceedings of the 38th Aerospace Sciences Meeting and Exhibit, Reno, NV*, number AIAA-200-0667, 2000.

[54] E. Nurgat, M. Berzins, and L. E. Scales. Solving EHL problems using iterative, multigrid and homotopy methods. *Trans. ASME, Journal of Tribology*, 121(1):28–34, 1999.

[55] E. G. Nurgat. *Numerical Methods in Lubrication Modelling.* PhD thesis, School of Computer Studies, University of Leeds, 1997.

[56] K. P. Oh. The numerical solution of dynamically loaded elastohydrodynamic contact as a nonlinear complementarity problem. *J. Tribology*, 106:88–95, 1984.

[57] A. I. Petrusevich. Fundamental conclusions from the contact-hydrodynamic theory of lubrication. *Izv. Akad. Nauk. SSSR (OTN)*, 2:209, 1951.

[58] N. A. Pierce and M. B. Giles. Adjoint recovery of superconvergent functionals from PDE approximations. *SIAM Review*, 42(2):247–264, 2000.

[59] W.H. Press, S.A. Teukolsky, W.T. Vetterling, and B.P. Flannery. *Numerical recipes in C.* Cambridge University Press Cambridge, 1992.

[60] T. Ree and H. Eyring. Theory of non-Newtonian flow. I. solid plastic system. *Journal of Applied Physics*, 26(7):793–800, 1955.

[61] O. Reynolds. On the theory of lubrication and its application to Mr Beauchamp Tower's experiments, including an experimental determination of the viscosity of olive oil. *Philosophical Transactions of the Royal Society of London*, 177:157–234, 1886.

[62] C. J. A. Roelands. *Correlational Aspects of the viscosity-temperature-pressure relationship of lubricating oils*. PhD thesis, Technische Hogeschool Delft, The Netherlands, 1966.

[63] C. N. Rowe. Specific Film Thickness: A Closer Examination of the Effects of EHL Film Thickness and Surface Roughness on Bearing Fatigue. *Tribology Transactions*, 24(4):423–430, 1981.

[64] Y. Saad. *Iterative Methods for Sparse Linear Systems*. SIAM, 2003.

[65] L. E. Scales. Quantifying the rheological basis of traction fluid performance. In *Proceedings of the SAE International Fuels and Lubricants Meeting, Toronto, Canada*. Society of Automotive Engineers, 1999.

[66] M. Smeeth and H. A. Spikes. Central and minimum elastohydrodynamic film thickness at high contact pressure. *Journal of Tribology*, 119(2):291–296, 1997.

[67] G. D. Smith. *Numerical Solution of Partial Differential Equations.* Oxford University Press, 1999.

[68] I. Taylor. Car lubricants: fact and friction. *Physics World*, February 2002.

[69] L-T. Tran, C. E. Goodyer, and M. Berzins. Adaptive methods for time-dependent problems using classical and adjoint methods. Presentation at SIAM Conference on Computer Science and Engineering, Costa Mesa, California, USA, 19–23rd February, 2007.

[70] U. Trottenberg, C. Oosterlee, and A. Schüller. *Multigrid*. Academic Press, 2001.

[71] University of Leeds, CPDE Unit. *Carmehl, EHL Lubrication software for Shell Global Solutions*, 1996-2007.

[72] D. A. Venditti and D. L. Darmofal. A multilevel error estimation and grid adaptive strategy for improving the accuracy of integral outputs. In *14th Computational Fluid Dynamics Conference*. American Institute of Aeronautics and Astronautics, 1999.

[73] D. A. Venditti and D. L. Darmofal. Adjoint error estimation and grid adaptation for functional outputs: application to quasi-one-dimensional flow. *Journal of Computational Physics*, 164:204–227, 2000.

[74] D. A. Venditti and D. L. Darmofal. Adjoint error estimation and grid adaptation for functional outputs: Application to quasi-one-dimensional flow. *Journal of Computational Physics*, 164:204–227, 2000.

[75] D. A. Venditti and D. L. Darmofal. A grid adaptive methodology for functional outputs of compressible flow simulations. In *15th Computational Fluid Dynamics Conference*. American Institute of Aeronautics and Astronautics, 2001.

[76] D. A. Venditti and D. L. Darmofal. Adjoint recovery of superconvergent functionals from pde approximations. *SIAM Review*, 42(2):247–264, 2002.

[77] D. A. Venditti and D. L. Darmofal. Grid adaptation for functional outputs: Application to two-dimensional inviscid flows. *Journal of Computational Physics*, 176:40–69, 2002.

[78] D. A. Venditti and D. L. Darmofal. Output-based error estimation and adaptation for aerodynamics. In H. A. Mang and F. G. Rammerstorfer, editors, *Fifth World Congress on Computational Mechanics*, 2002.

[79] D.A. Venditti and D.L. Darmofal. Grid adaptation for functional outputs: Application to two-dimensional inviscid flows. *Journal of Computational Physics*, 176:40–69, 2002.

[80] C. H. Venner. *Multilevel solution of the EHL line and point contact problems*. PhD thesis, School of Mech. Eng., University of Twente, Enschede, the Netherlands, 1991.

[81] C. H. Venner and A. A. Lubrecht. Transient analysis of surface features in an EHL line contact in the case of sliding. *J. Tribology*, 116:186–193, 1994.

[82] C. H. Venner and A. A. Lubrecht. Numerical analysis of the influence of waviness on the film thickness of a circular EHL contact. *J. Tribology*, 118:153–161, 1996.

[83] C. H. Venner and A. A. Lubrecht. *Multilevel Methods in Lubrication*. Elsevier, 2000.

[84] Webpage. *http://www.engineersedge.com/lubrication/friction_knowledge_menu.shtml*. January 2008.

[85] Webpage. *http://www.chevrontexacoursa.com/glossary/l.html*. September 2005.

[86] J. L. White and A. B. Metzner. Development of constitutive equations for polymeric melts and solutions. *Journal of Applied Polymeric Science*, 7:1867–1889, 1963.

[87] Y. Wijnant. *Contacts Dynamics in the field of Elastohydrodynamic Lubrication*. PhD thesis, School of Mech. Eng., University of Twente, Enschede, the Netherlands, 1998.

[88] M. F. Workel, D. Dowson, P. Ehret, and C. M. Taylor. The influence of mean contact pressure on the friction coefficient of a traction fluid at high pressure. *Proceedings of the Institute of Mechanical Engineers Part C, Journal of Mechanical Engineering Science*, 214:309–312, 2000.

[89] M.F. Workel, D. Dowson, P. Ehret, and C.M. Taylor. Measurements of the coefficients of friction of different lubricants during impact under high pressure and shear. *Proceedings of the Institution of Mechanical Engineers, Part J: Journal of Engineering Tribology*, 217(2):115–124, 2003.

[90] S. R. Wu. A penalty formulation and numerical approximation of the Reynolds-Hertz problem of elastohydrodynamic lubrication. *Int. J. Engng. Sci.*, 24(6):1001–1013, 1986.

[91] S. R. Wu and J. T. Oden. Convergence and error estimates for finite element solutions of elastohydrodynamic lubrication. *Comput. Math. Applic.*, 13(7):583–593, 1987.

[92] S. R. Wu and J. T. Oden. A note on applications of adaptive finite elements to elastohydrodynamic lubrication problems. *Communications in Applied Numerical Methods*, 3:485–494, 1987.

[93] S. R. Wu and J. T. Oden. A note on some mathematical studies on elastohydrodynamic lubrication. *Int. J. Engng. Sci.*, 25(6):681–690, 1987.

[94] P. Yang and J. Shen. On the theory of time-dependant micro-TEHL for a non-Newtonian lubricant in line contacts. *Lubrication Science*, 8(3):297–312, 1996.

[95] P. Yang and S. Wen. A forward iterative numerical method for steady-state elastohydrodynamically lubricated contacts at high loads. *J. Tribology*, 108:411–420, 1986.

[96] D. Zhu. Effect of surface roughness on mixed EHD lubrication characteristics. *Tribology Transactions*, 46(1):44–48, 2003.

Appendix

In this appendix are copies of the previously published papers of the candidate.